Colloidal Interactions in Aquatic Environments: Effect of Charge Heterogeneity and Charge Asymmetry

A Thesis
Presented to
The Academic Faculty

by

Patricia L. Taboada-Serrano

In Partial Fulfillment
of the Requirements for the Degree
Doctor in Philosophy in the
School of Civil and Environmental Engineering

Georgia Institute of Technology
December 2005

Colloidal Interactions in Aquatic Environments: Effect of Charge Heterogeneity and Charge Asymmetry

Approved:

Dr. Sotira Yiacoumi, Advisor
School of Civil and Environmental Engineering
Georgia Institute of Technology

Dr. Costas Tsouris, Co-advisor
School of Civil and Environmental Engineering
Georgia Institute of Technology

Dr. Spyros Pavlostathis
School of Civil and Environmental Engineering
Georgia Institute of Technology

Dr. Rina Tannenbaum
School of Materials Science and Engineering
Georgia Institute of Technology

Dr. David Sherrill
School of Chemistry and Biochemistry
Georgia Institute of Technology

Date approved: November 10, 2005

To Bolivia

ACKNOWLEDGMENTS

I would like to express my gratitude to the following persons who contributed in a direct or indirect way to the completion of this work:

- To my advisors, Prof. Sotira Yiacoumi and Prof. Costas Tsouris, for their support, encouragement and friendship, and to Iris for her sweetness.
- To my Committee members: Prof. Spyros Pavlostathis, Prof. Rina Tannenbaum, and Prof. David Sherrill, for their patience, critique, and valuable input. I am especially grateful to Prof. Sherrill and his research group for unveiling the beauty of quantum mechanics to me inside and outside the classroom.
- To my lab mates, Monica, Kun-Lin, Thorben, Jeremy, Chia-Hung and Viriya for the encouragement, help and friendship. Dee and Chia-Hung, thank you!
- To Dr. Muhammed Shaikh, for the patience, advice, and valuable help with the high performance computers.
- To all my professors and colleagues at Georgia Tech for providing me with a nice environment for learning and developing this work.
- To Andrea and Therese, for all the support and friendship during these past four years.
- To Dr. Zhu for all the assistance with the logistics of research.
- To my parents, Carmen and Gonzalo, and to my brother, Eduardo, because they always believe in me and support me in anything I want to accomplish.
- To my husband, Ketan, for encouraging me through the hardest and last part of this work and for serving as a source of inspiration.
- To my little brother, Eduardo, for his friendship and encouragement.
- To my many friends at Georgia Tech, especially to Rebeca, Yan, Rahul, Devon, Anup, Nidhi, Amit, Efrat, Ana, Dida, Estelle, Gelsy, Lucia, Alfredo, Camilo, and Mo-Han, for creating a piece of home for me in Atlanta.
- To the Fulbright Fellowship, to the Molecular Design Institute and to the Oak Ridge National Laboratory for the economic support and the many opportunities to improve this research work.
- To the High Performance Computing Center at Georgia Tech for the computational resources.
- To Dr. Ronanth Zavaleta Mercado for starting me in the art of research and for encouraging me to pursue a Ph.D. degree.
- To my extended family members, my new family and my many friends for always being there for me.

TABLE OF CONTENTS

DEDICATION…..……. iii

ACKNOWLEDGMENTS...……. iv

LIST OF TABLES…… ix

LIST OF FIGURES……... x

LIST OF SYMBOLS OR ABBREVIATIONS…...……. xvii

SUMMARY...…… xxi

CHAPTER 1 INTRODUCTION…….. 1

CHAPTER 2 INTERPARTICLE INTERACTIONS: MEASUREMENT AND MODELING…….. 11

2.1 Introduction…….. 11

2.2 Interparticle interactions……... 12

2.2.1 Van der Waals or dispersion forces……. 13

2.2.2 Electrostatic or EDL forces……. 14

2.3 Classical theory on electrical double layer and electrostatic interactions……... 17

2.3.1 The Gouy-Chapman theory: solving the Poisson-Boltzmann equation…… 17

2.3.2 Modeling EDL interactions…… 21

2.4 Molecular modeling of electrolytes and electrostatic interactions……... 23

2.4.1 Modeling systems at a microscopic scale……... 23

2.4.2 Calculating thermodynamic properties: averaging procedures and ensembles……... 26

2.4.3 Monte Carlo methods and molecular modeling……. 28

2.4.4 Canonical Monte Carlo simulations of electrolyte solutions…….. 35

2.4.5 Monte Carlo modeling of the electrical double layer and the interactions between charged surfaces……... 36

2.5 Experimental determination of the interactions between charged surfaces: the atomic force microscope…….. 40

2.5.1 Operating principle of AFM……... 41

2.5.2 The AFM force curve……. 44

2.5.3 Force-volume AFM…… 46

2.6 Conclusions……. 48

CHAPTER 3 ELECTRICAL DOUBLE LAYER STRUCTURE WITH ASYMMETRIC INDIFFERENT ELECTROLYTES…….. 50
3.1 Introduction……. 50
3.2 CMC simulations of the EDL structure…….. 54
3.2.1 Simulation box…… 54
3.2.2 Potential energy of the EDL……... 55
3.2.3 Simulation Parameters…… 59
3.3 EDL structure in the presence of a single electrolyte……. 62
3.3.1 EDL structure in the presence of a 1:1 electrolyte: CMC simulations versus MGC theory predictions…… 63
3.3.2 EDL structure in the presence of asymmetric electrolytes…….. 66
3.4 EDL structure in mixtures of symmetric and asymmetric electrolytes……... 68
3.4.1 Mixtures of symmetric and asymmetric electrolytes: charge versus size…… 68
3.4.2 Surface charge and EDL structure in mixtures of symmetric and asymmetric electrolytes……. 73
3.5 Conclusions……. 77
3.6 Summary……. 80

CHAPTER 4 ELECTRICAL DOUBLE LAYER INTERACTIONS: A SPHERICAL PARTICLE AND A PLANAR SURFACE…… 81
4.1 Introduction……. 81
4.2 CMC simulations of the interaction of a spherical particle and a planar surface……. 84
4.2.1 Simulation box…… 84
4.2.2 Potential energy of the system…… 85
4.2.3 Simulation parameters…… 88
4.3 EDL overlap in the presence of a single electrolyte…… 92
4.3.1 EDL interaction in symmetric electrolytes……. 92
4.3.2 EDL interaction in asymmetric electrolytes……... 99
4.4 EDL overlap in the presence of mixtures of symmetric and asymmetric electrolytes……... 104
4.4.1 Weak repulsive interactions in mixtures of symmetric and asymmetric electrolytes……... 105
4.4.2 Intermediate repulsive interactions in mixtures of symmetric and asymmetric electrolytes……. 108
4.5 Conclusions……. 112
4.6 Summary……. 113

CHAPTER 5 ELECTROSTATIC INTERACTION FORCES IN SYMMETRIC AND ASYMMETRIC ELECTROLYTES…….. 115

5.1 Introduction……. 115
5.2 Simulations of the electrostatic force between a spherical particle and a planar surface…… 120
5.2.1 Evaluation of the potential energy of the system…….... 120
5.2.2 CMC calculation of the interaction force……... 121
5.2.3 Simulation parameters…… 125
5.2.4 Classical calculation of the interaction force between a spherical particle and a planar surface in a 1:1 electrolyte……... 128
5.3 Interaction force between a spherical particle and a planar surface in a single electrolyte solution…… 132
5.3.1 Electrostatic force at low surface charge densities……. 132
5.3.2 Electrostatic force at intermediate surface charge densities…….. 140
5.4 Interaction between a spherical colloidal particle and a planar surface in mixtures of symmetric and asymmetric electrolytes…….. 145
5.4.1 Low surface charge densities……. 146
5.4.2 Intermediate values of surface charge densities……. 151
5.5 Conclusions……. 156
5.6 Summary……. 159

CHAPTER 6 INTERPARTICLE INTERACTIONS IN NON-INDIFFERENT ELECTROLYTES: SURFACE CHARGE MODIFICATION… 160
6.1 Introduction……. 160
6.2 Procedure for the experimental determination of interparticle forces……... 163
6.2.1 Silica surfaces and standard silicon nitride tips…….. 164
6.2.2 Solutions of indifferent and non-indifferent electrolytes…….. 165
6.2.3 Determination of the surface charge of the silica surfaces and the silicon nitride tips……. 166
6.2.4 AFM force measurements…….. 166
6.2.5 Surface analysis: determination of the presence of non-indifferent electrolyte on the silica surface……. 168
6.3 Interaction between silica and silicon nitride in a 1:1 indifferent electrolyte solution……. 169
6.4 Interaction between silica and silicon nitride in a 2:1 non-indifferent electrolyte solution……. 174
6.5 Conclusions……. 185
6.6 Summary……. 188

CHAPTER 7 CONCLUSIONS……. 189

CHAPTER 8 RECOMMENDATIONS…… 196

APPENDIX…… 199
A.1 Derivation of the classical expression for the calculation of the interaction force between a spherical particle and a planar surface in a 1:1 electrolyte…… 199
A.2 Program for the CMC simulation of the EDL structure of a planar surface in a mixture of electrolytes……... 200

REFERENCES……... 220

VITA…….. 229

LIST OF TABLES

Table 3.1	Summary of simulations performed for EDL structure calculations…….	62
Table 4.1	Summary of the preliminary simulations performed for 1:1 electrolyte at an ionic strength of 0.1 M…….	90
Table 4.2	Summary of the simulations performed with 1:1, 2:1 and 3:1 electrolytes at an ionic strength of 0.05 M…….	91
Table 5.1	Simulations performed for the calculation of the interaction force between a spherical colloidal particle and a discretely charged planar surface……	126
Table 6.1	Summary of the force-imaging experiments……..	172

LIST OF FIGURES

Figure 2.1	Schematic of the EDL around a spherical particle……..	16
Figure 2.2	Schematic of the traditional numerical integration procedure to find the area under a curve……..	29
Figure 2.3	Schematic of an "experimental" numerical calculation of the area under a curve……...	30
Figure 2.4	Schematic of a CMC simulation box……..	32
Figure 2.5	Schematic of the criterion for "move" acceptance in CMC simulations (adapted from Allen and Tildesley, 1990)……...	34
Figure 2.6	Schematic of the operation and feedback control of the AFM...	42
Figure 2.7	Schematic depicting the logic behind the AFM control loop…..	42
Figure 2.8	Schematic representation of the curve of tip deflection vs. separation distance …….	45
Figure 2.9	Force-volume data for a fused silica surface in water obtained by AFM……...	47
Figure 3.1	Schematic of the simulation box used in CMC simulations of EDL structure……..	55
Figure 3.2	Schematic of the long-range corrections of electrostatic forces.	58
Figure 3.3	Concentration profiles obtained via CMC simulations and MGC theory calculations for a planar surface with an equivalent surface charge of –16.02 μC/cm^2 and 1:1 electrolyte at concentrations of (a) 0.1 M and (b) 1.0 M……..	63
Figure 3.4	EDL structure at low surface charge (equivalent to –16.02 μC/cm^2), as shown in concentration profiles for 0.1 M solutions of (a) 1:1, (b) 2:1, and (c) 3:1 electrolytes……...	66
Figure 3.5	EDL structure at low surface charge (surface charge equivalent to –16.02 μC/cm^2) in mixtures of 1:1 and 2:1 electrolytes at an ionic strength of 1.0 M for (a) monovalent and divalent counterions of equal diameter (4.25 Å), and (b) 4.25–Å–diameter monovalent counterions and larger (6–Å–diameter)	

divalent counterions…… 69

Figure 3.6 EDL structure at low surface charge (surface charge equivalent to –16.02 μC/cm^2) in mixtures of 1:1 and 3:1 electrolytes at an ionic strength of 1.0 M for (a) monovalent and trivalent counterions of equal diameter (4.25 Å), and (b) 4.25–Å–diameter monovalent counterions and larger (9–Å–diameter) trivalent counterions…… 70

Figure 3.7 EDL structure at low surface charge (surface charge equivalent to –16.02 μC/cm^2) in mixtures of 1:1, 2:1, and 3:1 electrolytes at an ionic strength of 1.0 M for (a) monovalent, divalent and trivalent counterions of equal diameter (4.25 Å), and (b) 4.25–Å–diameter monovalent counterions, and larger (6–Å–diameter) divalent ions and (9–Å–diameter) trivalent ions……. 72

Figure 3.8 Effect of surface charge on the EDL structure of mixtures of 1:1 and 2:1 electrolytes at an ionic strength of 1.0 M for surface charges equivalent to (a) –16.02 μC/cm^2 and (b) –64.08 μC/cm^2……... 73

Figure 3.9 Effect of surface charge on the EDL structure of mixtures of 1:1 and 3:1 electrolytes at an ionic strength of 1.0 M for surface charges equivalent to (a) –16.02 μC/cm^2 and (b) –64.08 μC/cm^2……... 75

Figure 3.10 Effect of surface charge on the EDL structure of mixtures of 1:1, 2:1, and 3:1 electrolytes at an ionic strength of 1.0 M for surface charges equivalent to (a) –16.02 μC/cm^2 and (b) –64.08 μC/cm^2……... 76

Figure 4.1 Schematic of the simulation box used in the CMC simulation of the interaction between a charged spherical particle and a planar surface…….. 84

Figure 4.2 EDL structure and concentration profiles for the colloidal particle in a 1:1 electrolyte of ionic strength 0.1 M. The surface charge densities for the planar surface and the colloidal particle are –2.04 μC/cm^2 and –5.67 μC/cm^2, respectively, and the separation distance between the particle and the planar surface is 120 Å (4•d_M)……... 93

Figure 4.3 EDL structure and concentration profiles for the colloidal particle during EDL overlap in a 1:1 electrolyte of ionic strength 0.1 M. The surface charge densities for the planar surface and the colloidal particle are –2.04 μC/cm^2 and –5.67

μC/cm^2, respectively, and the separation distance between the colloidal particle and the planar surface is 30 Å (d_M)……. 94

Figure 4.4 EDL structure and concentration profiles for the colloidal particle during EDL overlap in a 1:1 electrolyte of ionic strength 0.1 M. The surface charge densities for the planar surface and the colloidal particle are –2.04 μC/cm^2 and +5.67 μC/cm^2, respectively, and the separation distance between the colloidal particle and the planar surface is 30 Å (d_M)……. 96

Figure 4.5 EDL structure during the interaction of the planar surface and the colloidal particle in a 1:1 electrolyte of ionic strength 0.05 M. The surface charge densities of the planar surface and the colloidal particle are –5.23 μC/cm^2 and –17.0 μC/cm^2, respectively, and the separation distances are: (a) 120 Å ($4d_M$), and (b) 30 Å (d_M)…… 97

Figure 4.6 EDL structure during the interaction of the planar surface and the colloidal particle in a 1:1 electrolyte of ionic strength 0.05 M. The surface charge densities of the planar surface and the colloidal particle are –5.23 μC/cm^2 and –17.0 μC/cm^2, respectively, and the separation distances are: (a) 120 Å ($4d_M$), (b), 60 Å ($2d_M$), (c) 30 Å (d_M), and (d) 16.5 Å (contact, $[d_W+d_M]/2$)……..... 98

Figure 4.7 EDL structure during the interaction of the planar surface and the colloidal particle in a 2:1 electrolyte of ionic strength 0.05 M. The surface charge densities of the planar surface and the colloidal particle are –1.78 μC/cm^2 and –5.67 μC/cm^2, respectively, and the separation distances are (a) 120 Å ($4d_M$), and (b) 30 Å (d_M)……. 100

Figure 4.8 EDL structure during the interaction of the planar surface and the colloidal particle in a 3:1 electrolyte of ionic strength 0.05 M, for surface charge densities of the planar surface and the colloidal particle of –1.78 μC/cm^2 and –5.67 μC/cm^2, respectively, and separation distances of (a) 120 Å ($4d_M$), and (b) 30 Å (d_M). 99

Figure 4.9 EDL structure during the interaction of the planar surface and the colloidal particle in a 2:1 electrolyte of ionic strength 0.05 M. The surface charge densities of the planar surface and the colloidal particle are –5.23 μC/cm^2 and –17.0 μC/cm^2, respectively, and the separation distances are: (a) 120 Å ($4d_M$), and (b) 30 Å (d_M)…… 101

Figure 4.10 EDL structure during the interaction of the planar surface and the colloidal particle in a 3:1 electrolyte of ionic strength 0.05 M. The surface charge densities of the planar surface and the colloidal particle are –5.23 μC/cm^2 and –17.0 μC/cm^2, respectively, and the separation distances are: (a) 120 Å (4d_M), and (b) 30 Å (d_M)…… 103

Figure 4.11 EDL structure during the interaction of the planar surface and the colloidal particle in a mixture of 2:1 and 1:1 electrolytes of ionic strength 0.05 M. The surface charge densities of the planar surface and the colloidal particle are –1.78 μC/cm^2 and –5.67 μC/cm^2, respectively, and the separation distances are: (a) 120 Å (4d_M), and (b) 30 Å (d_M)……. 106

Figure 4.12 EDL structure during the interaction of the planar surface and the colloidal particle in a mixture of 3:1 and 1:1 electrolytes of ionic strength 0.05 M. The surface charge densities of the planar surface and the colloidal particle are –1.78 μC/cm^2 and –5.67 μC/cm^2, respectively, and the separation distances are: (a) 120 Å (4•d_M), and (b) 30 Å (d_M)…… 107

Figure 4.13 EDL structure during the interaction of the planar surface and the colloidal particle in a mixture of 3:1, 2:1 and 1:1 electrolytes of ionic strength 0.05 M. The surface charge densities of the planar surface and the colloidal particle are –1.78 μC/cm^2 and –5.67 μC/cm^2, respectively, and the separation distances are: (a) 120 Å (4d_M), and (b) 30 Å (d_M)… 108

Figure 4.14 EDL structure during the interaction of the planar surface and the colloidal particle in a mixture of 2:1 and 1:1 electrolytes of ionic strength 0.05 M. The surface charge densities of the planar surface and the colloidal particle are –5.23 μC/cm^2 and –17.0 μC/cm^2, respectively, and the separation distances are: (a) 120 Å (4•d_M), and (b) 30 Å (d_M)…… 109

Figure 4.15 EDL structure during the interaction of the planar surface and the colloidal particle in a mixture of 3:1 and 1:1 electrolytes of ionic strength 0.05 M, for surface charge densities of the planar surface and the colloidal particle of –5.23 μC/cm^2 and –17.0 μC/cm^2, respectively, and separation distances of (a) 120 Å (4d_M), and (b) 30 Å (d_M)…….. 110

Figure 4.16 EDL structure during the interaction of the planar surface and the colloidal particle in a mixture of 3:1, 2:1 and 1:1 electrolytes of ionic strength 0.05 M. The surface charge densities of the planar surface and the colloidal particle are –

5.23 μC/cm^2 and –17.0 μC/cm^2, respectively, and the separation distances are: (a) 120 Å (4d_M), and (b) 30 Å (d_M)… 111

Figure 5.1 Schematic of the algorithm used to calculate the pair-wise interaction forces between the colloidal particle and ions or charged groups on the surface……. 123

Figure 5.2 Force experienced by a colloidal particle as a function of distance when interacting with a planar surface obtained by classical DLVO theory calculations and CMC simulations. The surface charge densities of the spherical particle and the planar surface are equivalent to –5.67 μC/cm^2 (ψ_M = –103.9 mV) and –1.78 μC/cm^2 (ψ_W = –32.6 mV), respectively. A 1:1 electrolyte solution of ionic strength equal to 0.05 M is employed……. 133

Figure 5.3 Force experienced by a colloidal particle as a function of distance when interacting with a planar surface. The surface charge densities of the spherical particle and the planar surface are equivalent to –5.67 μC/cm^2 (ψ_M = –103.9 mV) and –1.78 μC/cm^2 (ψ_W = –32.6 mV) respectively. Solutions of ionic strength 0.05 M are employed, containing (a) 1:1 electrolyte, (b) 2:1 electrolyte, and (c) 3:1 electrolyte……... 137

Figure 5.4 Force experienced by a colloidal particle as a function of separation distance when interacting with a planar surface, obtained by classical DLVO theory calculations and CMC simulations. The surface charge densities of the spherical particle and the planar surface are equivalent to –17.0 μC/cm^2 (ψ_M = –311.5 mV) and –5.23 μC/cm^2 (ψ_W = –95.8 mV) respectively. A 1:1 electrolyte solution of ionic strength equal to 0.05 M is employed……. 141

Figure 5.5 Force experienced by a colloidal particle as a function of separation distance when interacting with a planar surface. The surface charge densities of the spherical particle and the planar surface are equivalent to –17.0 μC/cm^2 (ψ_M = –311.5 mV) and –5.23 μC/cm^2 (ψ_W = –95.8 mV) respectively. Solutions of ionic strength 0.05 M are employed, containing (a) 1:1 electrolyte, (b) 2:1 electrolyte, and (c) 3:1 electrolyte…. 144

Figure 5.6 Force experienced by a colloidal particle as a function of distance when interacting with a planar surface. The surface charge densities of the spherical particle and the planar surface are equivalent to –5.67 μC/cm^2 (ψ_M = –103.9 mV) and –1.78 μC/cm^2 (ψ_W = –32.6 mV) respectively. Solutions of ionic

strength 0.05 M containing (a) 1:1 electrolyte, (b) 2:1 electrolyte, and (c) mixture of 2:1 and 1:1 electrolytes……... 146

Figure 5.7 Force experienced by a colloidal particle as a function of distance when interacting with a planar surface. The surface charge densities of the spherical particle and the planar surface are equivalent to –5.67 μC/cm^2 (ψ_M = –103.9 mV) and –1.78 μC/cm^2 (ψ_W = –32.6 mV) respectively. Solutions of ionic strength 0.05 M are employed, containing (a) 1:1 electrolyte, (b) 3:1 electrolyte, and (c) mixture of 3:1 and 1:1 electrolytes... 149

Figure 5.8 Force experienced by a colloidal particle as a function of distance when interacting with a planar surface. The surface charge densities of the spherical particle and the planar surface are equivalent to –5.67 μC/cm^2 (ψ_M = –103.9 mV) and –1.78 μC/cm^2 (ψ_W = –32.6 mV), respectively. Solutions of ionic strength 0.05 M are employed, containing mixtures of (a) 2:1 and 1:1 electrolytes, (b) 3:1 and 1:1 electrolytes, and (c) 3:1, 2:1 and 1:1 electrolytes……... 151

Figure 5.9 Force experienced by a colloidal particle as a function of distance during the interaction with a planar surface. Solutions of ionic strength 0.05 M containing a mixture of 2:1 and 1:1 electrolytes are employed. The surface charge densities of the spherical particle and the planar surface are equivalent to: (a) –5.67 μC/cm^2 (ψ_M = –103.9 mV) and –1.78 μC/cm^2 (ψ_W = –32.6 mV) respectively, and (b) –17.0 μC/cm^2 (ψ_M = –311.5 mV) and –5.23 μC/cm^2 (ψ_W = –95.8 mV) respectively…….. 153

Figure 5.10 Force experienced by a colloidal particle as a function of distance during the interaction with a planar surface. Solutions of ionic strength 0.05 M containing a mixture of 3:1 and 1:1 electrolytes are employed. The surface charge densities of the spherical particle and the planar surface are equivalent to: (a) –5.67 μC/cm^2 (ψ_M = –103.9 mV) and –1.78 μC/cm^2 (ψ_W = –32.6 mV) respectively, and (b) –17.0 μC/cm^2 (ψ_M = –311.5 mV) and –5.23 μC/cm^2 (ψ_W = –95.8 mV) respectively…….. 155

Figure 6.1 (a) Zeta potential of silicon nitride and silica for different pH values, measured by Zee Meter, in NaCl solutions of ionic strength 0.005 M. (b) Interaction force curves between silicon nitride and silica as a function of pH, measured by AFM, in NaCl solutions of ionic strength 0.005 M…… 170

Figure 6.2 Force image and interaction force curves for silica and silicon nitride at pH 5.5 and ionic strength of 0.1 M (NaCl used as 1:1

indifferent electrolyte or background electrolyte)……... 173

Figure 6.3 Force image and interaction force curves for silica and silicon nitride at pH 4.5, ionic strength of 0.1 M (NaCl used as background electrolyte), and total copper ion concentration of 0.0076 M……. 177

Figure 6.4 Force image and interaction force curves for silica and silicon nitride at pH 4.5, ionic strength of 0.1 M (NaCl used as background electrolyte), and total copper ion concentration of 0.0304 M……. 178

Figure 6.5 Force image and interaction force curves for silica and silicon nitride at pH 5.5, ionic strength of 0.1 M (NaCl used as background electrolyte), and total copper ion concentration of 0.0016 M……. 180

Figure 6.6 Force image and interaction force curves for silica and silicon nitride at pH 5.5, ionic strength of 0.1 M (NaCl used as background electrolyte), and total copper ion concentration of 0.0076 M……. 181

Figure 6.7 Force image and interaction force curves for silica and silicon nitride at pH 5.5, ionic strength of 0.5 M (NaCl used as background electrolyte), and total copper ion concentration of 0.0076 M……. 184

LIST OF SYMBOLS OR ABBREVIATIONS

A	Helmhotz free energy
A_H	Hamaker constant
a	area of interaction
a_i	radius of a spherical particle
D	separation distance between two interacting surfaces
d	diameter of a hydrated ion
d_M	diameter of the colloidal particle
dr_{iM}	distance between the center of an ion or of a charged group i and the center of the colloidal particle M
d_w	diameter of a charged group on the charged planar surface
$\bar{e}$	charge of the electron
F	component in the Z direction (perpendicular to the planar surface) of the force experienced by the colloidal particle
$F_{M\text{-}W}$	component in the Z direction of the force exerted on the colloidal particle by the charged planar surface
$F_{M\text{-}EDLW}$	component in the Z direction of the force exerted on the colloidal particle by the EDL associated to the planar surface
$F_{M\text{-}EDLM}$	component in the Z direction of the force exerted on the colloidal particle by the EDL associated to it
F_{TiM}	force exerted by an ion or charged group i on the colloidal particle M
F_{iM}	Z component of the force exerted by an ion or charged group i on the colloidal particle M.
$F(D)$	electrostatic interaction force between two charged surfaces as a function of separation distance
$F(x)$	generic function

$H(p,q)$	Hamiltonian
i	label of ion or charged group
j	label of ion or charged group
$K(p)$	kinetic energy
k	spring constant
k_B	Boltzmann constant
L	height or length of the simulation box
N	number of atoms, molecules or ions
n_i	local number concentration of ion i
n_{i0}	bulk concentration of ion i
n_∞	ionic strength of the bulk solution
P	pressure or force per unit area between two infinite planar charged surfaces
P_z	pressure inside the gap formed between two approaching surfaces
p	conjugate momenta
Q_{ens}	partition function
Q_{NVT}	canonical partition function
Q_M	charge of colloidal particle C
Q_i	charge of ion i
q	generalized coordinates
R	radius of a spherical particle
r	vector
r_{iM}	distance between the centers of ions i and the center of the colloidal particle C

r_{ij}	distance between the centers of ions i and j
T	temperature
$u_{i,jcsh}(z_i,z_j,L)$	interaction energy between ion i and a charged sheet of dimensions L x L associated to ion j
$u_{i,jcsh}(z_i,z_j,\infty)$	interaction energy between ion i and an infinitely charged sheet associated to ion j
$V(D)$	interaction potential between two charged surfaces as a function of separation distance
$V(q)$	potential energy
W	Width of the simulation box
W_{VdW}	interaction energy
x	generic variable, coordinate in the X direction
x_i	value of generic variable or position of ion i in the X direction
y	coordinate in the Y direction
y_i	position of ion i in the Y direction
z	distance from a charged planar surface in the direction perpendicular to it, coordinate in the Z direction
z_i	position of an ion or a charged group i in the Z direction
z_M	position of the colloidal particle M in the Z direction
α	angle formed by dr_{iM} and the plane XZ
β	angle formed by the projection of dr_{iM} on the plane XZ and the coordinate axis Z
Δl	deflection of the atomic force microscope's (AFM) cantilever
ε	dielectric permittivity
ε_0	dielectric permittivity of vacuum
ε_r	relative dielectric permittivity

Φ_i	reduced electric potential at the surface
Φ_M	reduced electric potential at the surface of the colloidal particle
Φ_W	reduced electric potential at the surface of the planar surface
ζ_ι	random number
κ	Debye length
Λ	Broglie wavelength
ν	valence of a generic ion or electrolyte, or potential energy of electrolyte
ν_i	valence of ion i or potential energy of ion i
v_{ij}	pair interaction potential between ions i and j
τ	number of trials
ρ_{elec}	charge density in the electrical double layer (EDL)
$\rho(x)$	arbitrary probability density function
σ_0	surface charge density
σ_{iM}	maximum distance of approach between ion i and colloidal particle C
σ_{ij}	maximum distance of approach between ions i and j
ψ	local electrical potential
ψ_M	electrical potential at the surface of a spherical colloidal particle
ψ_W	electrical potential at the surface of a charged planar surface
ψ_δ	electrical potential at the plane of maximum approach of hydrated counterions to a charged surface
ψ_m	electrical potential in the mid-plane of the separation distance between two interacting surfaces

SUMMARY

The classical theory of colloids and surface science developed more than 70 years ago has been universally applied in modeling and calculations involving solid-liquid interfaces encountered in natural and engineered environments. However, several discrepancies between experimental observations of the behavior of charged solid-liquid interfaces and predictions of the classical theory have been reported in the past decades. The hypothesis that the mean-field, pseudo-one-component approximation adopted within the framework of the classical theory is responsible for the differences observed between theory and practice was tested in this work via the application of modeling and experimental techniques at a molecular level. Silica and silicon nitride were selected as model charged solid surfaces, and mixtures of symmetric and asymmetric indifferent and non-indifferent electrolytes were used as liquid phases. The study of the effects of discreteness of surface charge and charges within the liquid phase was carried out through molecular modeling and experiments.

Canonical Monte Carlo simulations (CMC) of the electrical double layer (EDL) structure of a discretely charged planar silica surface, embedded in solutions of indifferent electrolytes, revealed the presence of a size exclusion effect that is enhanced at larger values of surface charge densities. That effect translated into an unexpected behavior of the interaction forces between a charged planar surface and a spherical particle. CMC simulations of the electrostatic interactions and calculations of the electrostatic force

between a charged spherical colloidal particle and a charged planar surface, which were similarly charged, revealed the presence of two attractive force components: a depletion or volume exclusion effect almost at contact and a long-range attractive force of electrostatic origin due to ion-ion correlation effects. Those two force components are a direct result of the consideration of discreteness of charge in the interaction of solid-liquid interfaces, and they contradict the classical theory predictions of electrostatic repulsive interaction between similarly charged surfaces.

Direct interaction force measurements between a charged planar surface and a colloidal particle, performed by atomic force microscopy (AFM), revealed that, when indifferent and non-indifferent electrolytes are present in solution, surface charge modification occurs in addition to the effects on the EDL behavior reported for indifferent electrolytes. Non-uniformity and even heterogeneity of surface charge were detected due to the action of non-indifferent, asymmetric electrolytes. The phenomena observed in the present work explain much of the differences between the classical theory predictions and the experimental observations reported in the open literature, proving that the mean-field, pseudo-one-component approximation within the framework of the classical theory is at least partly responsible for these differences.

CHAPTER 1

INTRODUCTION

Colloidal particles and solid-liquid interfaces are ubiquitous in natural and engineered aqueous environments. Coagulation, flocculation, sedimentation, dispersion, flotation, emulsification, filtration, membrane separations, deposition, and transport of particles are some of the processes involving colloidal particles and solid-liquid interfaces. Additionally, biological processes such as cellular attachment, membrane fusion, adsorption and transport of nutrients through cellular membranes, and blood clotting involve solid-liquid interfaces and biological colloidal particles.

The behavior of solid-liquid interfaces is governed by the characteristics of the interfaces involved as well as by the nature of their interactions. The interaction between solid-liquid interfaces, i.e., interparticle interactions, can have different origins. Van der Waals or dispersion forces are originated by the instantaneous delocalization of the electrons pertaining to the atoms at the surface that induces dipole and quadrupole moments (Israelachvili, 1998). These forces are always present and, in general, attractive in nature (Elimelech et al., 1995; Hiemenz and Rajagopalan, 1997; Israelachvili, 1998; Hunter, 2001). Solid surfaces acquire charge in aquatic environments due to different charging mechanisms that are usually chemical, like deprotonation of surface groups, as well as

adsorption of metal ions or other molecules (Elimelech et al., 1995; Hiemenz and Rajagopalan, 1997). As an example, most of the components of soils (silicates and metal oxides) contain hydroxyl, OH, surface groups that undergo protonation or deprotonation depending on conditions of pH (Ryan and Elimelech, 1996; Kretzschmar et al., 1999). The surface charge gives rise to the formation of what is known as electrical double layer (EDL), and the overlap of EDLs generates electrostatic interactions (Elimelech et al., 1995; Hiemenz and Rajagopalan, 1997; Nguyen et al., 2000; Hunter, 2001). The electrostatic interactions can be attractive or repulsive depending on the sign of the surface charge of the particles or interfaces involved.

Besides dispersion and electrostatic interactions, which constitute the basic interparticle forces, other types of interactions can be present in different systems depending on the specific characteristics of the solutions and interfaces involved. Structural and entropic forces result from the presence of adsorbed molecules on solid or liquid surfaces (Hu and Dai, 2003; Guzmán and de Pablo, 2003), hydration forces result from the ordering and interaction of the first layer of solvent molecules with solid or liquid surfaces (Waite et al., 2001; Runkana et al., 2005), magnetic forces result from polar magnetic moments associated to solid surfaces in the system (Tsouris et al., 1995; Chin et al., 2001; Chin et al., 2002a), short-range Born repulsion occurs due to the overlap of electron orbitals at very short separation distances (Israelachvili, 1998), and hydrodynamic forces arise from the interaction of particles with the fluid (Elimelech et al., 1995).

Traditionally, Van der Waals and electrostatic or EDL interactions are assessed within the framework of the Derjaguin-Landau-Verwey-Overbeek (DLVO) theory (Elimelech et al., 1995 ; Hiemenz and Rajagopalan, 1997; Hunter, 2001), which is widely used in all the theoretical calculations dealing with processes involving solid-liquid interfaces. The DLVO theory constitutes a mean-field approximation within the framework of a McMillan-Mayer theory in which solutions containing colloidal dispersions or solid-liquid interfaces are represented as pseudo-one-component systems (Derjaguin and Landau, 1941; Verwey and Overbeek, 1948). Therefore, electrolytes and solvent effects are neglected within the calculation of the effective interparticle potential which includes a screened electrostatic potential component and a dispersion (Van der Waals) term. The electrolyte ions present in the solution are considered point charges and the solvent is considered a continuum of constant dielectric permittivity. One of the critical electrolyte effects neglected in the formulation of the DLVO theory is ion-ion correlations, or the interactions between the ionic species present in the electrolyte solution. Additionally, the charged interacting surfaces of solid-liquid interfaces are assumed to be smooth and uniformly charged within the framework of the DLVO theory.

Due to the simplifications involved in its conception and the mathematical complexity of the treatment of the electrostatic component of the interactions, the DLVO theory is applicable to solid-liquid systems with solutions of one electrolyte (usually a symmetric electrolyte) at very low concentrations. The range of solid-liquid surface potential values recommended for the application of the DLVO theory is between -25 mV to 25 mV (Valleu et al., 1991; Hiemenz and Rajagopalan, 1997). The DLVO predictions of

interaction potentials are more accurate between solid-liquid interfaces in geometries with separation distances longer than the Debye length (Yang et al., 2002a, 2002b).

In spite of all its inherent restrictions, the DLVO theory is widely used in the prediction of important parameters governing processes involving colloidal particles and solid-liquid interfaces, e.g., attachment efficiencies, stability ratios, and collision efficiencies. Unfortunately, most of surfaces and electrolyte solutions involved in natural and engineered processes do not comply with the conditions necessary for the application of the DLVO theory. Observations of natural systems and studies on deposition, and on transport of colloidal particles have shown that the DLVO theory fails to accurately describe them. In the case of particle deposition, observed attachment efficiencies are less sensitive to the chemistry of the solution in contradiction to the strong dependence on ionic strength predicted by the DLVO theory (Ryan and Elimelech, 1996; Kretzschmar et al., 1999). For example, experiments on deposition and reentrainment of colloidal particles in porous media with symmetric electrolyte solutions have shown that deposition occurs under unfavorable conditions at larger rates than expected from calculations based on the classical theory (Shellenberger and Logan, 2002; Hahn and O'Melia, 2004). Furthermore, experimentally observed attachment efficiencies are almost independent of particle size, in contradiction to the predictions of the DLVO theory about the functionality of the attachment efficiencies with respect to particle diameter (Elimelech and O'Melia, 1990).

Aggregation and coagulation experiments with colloidal particles of different nature in symmetric electrolyte solutions have shown a gradual increase of instability with EDL thickness reduction (i.e., increase of electrolyte concentrations), whereas a sharp increase is predicted by the DLVO Theory (Behrens et al., 2000). Furthermore, instability of dispersions of similarly charged nanoparticles has been observed even at very low ionic strengths and very low surface charges (i.e., the ranges of applicability of DLVO theory) in contradiction to DLVO theory calculations that predict stability of the dispersions at these conditions (Kallay and Žalac, 2002). Additionally, a limiting stability ratio (i.e., a limit in aggregation) has been experimentally observed for particles of different sizes even if the particles are fully destabilized (Grolimund et al., 2001). The DLVO theory fails to describe the observations discussed here. In addition, the DLVO theory is employed in the calculation of collision efficiency (i.e., the ratio of the number of particle collisions resulting in the formation of an aggregate to the total number of collisions), which constitutes a key parameter in the evaluation of aggregation kinetics. An experimental limit for collision efficiencies and restriction of further aggregation has been experimentally detected, which cannot be captured by the DLVO theory, especially as the polydispersity (i.e., diversity in particle size) increases in the system (Hiemenz and Rajagopalan, 1997; Taboada-Serrano et al., 2005c).

The discrepancies between DLVO theory and experimental observations, discussed here, were detected in systems containing symmetric electrolyte solutions. When asymmetric electrolytes, specifically 2:1 electrolytes, were used in similar experiments, the differences between experimental observations and theoretical predictions accentuated.

Deposition experiments reported attachment efficiencies smaller than the ones predicted by the DLVO theory under favorable conditions, while attachment efficiencies were found to be orders of magnitude larger than theoretical predictions under unfavorable conditions (Elimelech and O'Melia, 1990; Grolimund et al., 2001). Additionally, such phenomena as the contraction of lyotropic liquid lamellar phases, and the condensation of colloidal biopolymers have been observed in solutions containing 2:1 electrolytes, when fully stable conditions were predicted by DLVO calculations (Angelescu and Linse, 2003; Lobaskin and Quamhieh, 2003).

Several explanations have been proposed to account for the differences between the predictions of the classical theory and experimental observations. The existence of secondary minima in the DLVO interaction potential due to comparable magnitudes of the attractive Van der Waals term and the repulsive electrostatic term has been proposed as an explanation for the gradual increase in deposition and reentrainment rates of colloidal particles in porous media; an observation that contradicts the sharp changes predicted by the DLVO theory. It has been proven by simulations that the DLVO interparticle potentials may present shallow secondary minima resulting in reversible deposition and reentrainment of colloidal particles (Hahn and O'Melia, 2004). Furthermore, some of the assumptions of the DLVO theory have been examined. The validity of the assumption within the DLVO theory that surfaces are smooth and uniformly charged has been studied both theoretically and experimentally. Surface roughness and its implications on interparticle interactions have been addressed in an attempt to explain the difference between theory and experiments on the dependence of

deposition efficiencies and stability ratios on chemical conditions and on particle size (Suresh and Walz, 1996; Shellenberger and Logan, 2002; Snowswell et al., 2005). It has been concluded that surface roughness favors aggregation and deposition. Some work on the non-uniformity of surface charge has proven that charged particles tend to rotate or align with applied electric fields in rotational electrophoresis experiments (Feick et al., 2004). This observation implies that non-uniformity in charge distribution might result in favorable interactions depending on the relative orientation of the colloidal particles or charged surfaces with respect to each other even if the overall conditions are unfavorable.

The electrostatic component of the interparticle interactions results from the overlap of the associated EDLs to the interacting surfaces. The structure of the EDLs determines the nature and strength of the resulting electrostatic interaction. The Poisson Boltzmann (PB) equation, which is used in the DLVO theory to describe the structure of the EDL, has been improved to extent its application to larger surface potentials (Nguyen et al, 2000) or to the presence of asymmetric electrolytes (Chan, 2002). However, the intrinsic mean-field nature of the PB equation and the DLVO theory limits the applicability of those approaches.

Theoretical and modeling studies have been oriented to investigate the effect of ion size and ion-ion correlations in the structure of the EDL in order to overcome the mean-field approximation of the PB equation and the DLVO theory. One of the first studies includes the introduction of a maximum distance of approach of ions to the charged surface equal to the radius of the bare or hydrated counterions (i.e. ions bearing charge opposite to the

one of the surface) as a boundary condition for the PB equation. This approach is called the modified Gouy-Chapman theory (GC) (Elimelech et al., 1995; Hiemenz and Rajagopalan, 1997; Hunter, 2001). Additional contributions to the GC theory include the consideration of counterion size within a mean spherical approximation (Blum, 1977) and consideration of counterion and coion sizes (Valleau and Torrie, 1982). Statistical mechanics approaches, such as the hypernetted-chain (HNC) theory to systems of different geometries (Jönsson et al., 1980; Vlachy et al., 1989), or the generalized Van der Waals theory (Boyle et al., 1987), have been employed as substitutes to the PB equation in an attempt to include ion-ion correlations. The suitability of alternate expressions for the interparticle interactions, e.g. the Yukawa potential, has also been assessed (Lai and Wu, 2002), as well as the direct inclusion of polar interaction between the ionic species into the interparticle potentials (Tavares et al., 2004). Due to the complexity of the mathematical expressions associated with the strictly theoretical approaches to the assessment of the EDL structure and its associated electrostatic interactions, molecular modeling approaches have been pursued (Valleau and Torrie, 1982; Boda and Chan, 1998; Messina, 2002; Yang et al., 2002; Boda et al, 2004). The advantage of molecular modeling approaches is that it allows the consideration of ion size and ion-ion correlation effects simultaneously. As a result of all this work, some phenomena inherent to the behavior of charged surfaces have been explained, for example the dependence of the point of zero charge of surfaces on the concentration of the electrolyte they are immersed in. Additionally, interesting facts on the behavior of the ions near charged surfaces have been theoretically predicted.

The extrapolation of modeling results on the EDL structure to predict interparticle interactions has been attempted in very few cases. And in those cases, many simplifications to the original approach employed to model the EDL were used (Guldbrand et al., 1984; Valleau et al., 1991; D'Amico and Löwen, 1997; Linse and Lobaskin, 2000; Meyer et al., 2001; Lobaskin and Quamhieh, 2003; Angelescu and Linse, 2003). Most of the cited work focused on the observation of the phase separation of charged colloids as a means to conjecture on the interparticle interactions in play.

The present work is an attempt to analyze the consequences of adopting a mean-field, pseudo-one-component approximation in the calculation of electrostatic interactions within the classical theory, and to relate these simplifications to the discrepancies between classical theoretical predictions and the experimentally observed phenomena reported in the literature. Specifically, the ionic species responsible for the development of surface charge and the formation of EDL will be studied as separate entities with unique associated charge and size. This consideration will allow the direct inclusion of the effects of ion-size, ion-ion correlations, and discrete, non-uniform or heterogeneous distribution of surface charge in the interactions between solid-liquid interfaces. For that purpose, the electrostatic interaction between charged solid-liquid interfaces will be quantified via the application of molecular simulation techniques and molecular experimental measurements. The ultimate goal is to quantify the contribution of the discrete nature of the electrolyte solutions and the surface charge to the behavior of solid-liquid interfaces in natural and engineered environments.

The discussion and presentation of the findings of this work are organized in chapters, as described below. Chapter 2 presents a brief description of interparticle interactions focusing on the origin, nature and classical modeling of electrostatic interactions. In this part of the work, the modeling and experimental techniques used for this study will be introduced and described, and a brief explanation on the suitability of the techniques will be offered. Chapter 3 presents simulation work on the EDL structure when ions and charged groups are treated as discrete species with associated charge and size. The effects of charge and size asymmetry are extensively discussed in the case of indifferent electrolytes, i.e. electrolytes formed by ions that do not adsorb onto charged surfaces. Chapter 4 contains a description of the work performed in terms of developing a simulation protocol suitable for the calculation of the electrostatic interactions between a charged spherical particle and a planar surface embedded in solutions of indifferent electrolytes. Some interesting results on the effects of overlapping of the associated EDLs will be analyzed in this chapter as well. Chapter 5 presents the results on EDL force calculations between a charged spherical particle and a charged planar surface obtained via molecular modeling. The effects of ion size and charge asymmetry are discussed. Chapter 6 presents the effects of the discreteness of ions and charged species on the EDL interactions between a spherical particle and a charged planar surface via direct force measurements. In this case, non-indifferent electrolytes were used in order to account for the possibility of adsorption of ions onto the charged surface. The thesis will be completed with two chapters: one of them dealing with the discussion of the overall findings and conclusions, and the other one dealing with recommendations for future work on the subject.

CHAPTER 2

INTERPARTICLE INTERACTIONS: MODELING AND MEASUREMENT

2.1 Introduction

The behavior of solid-liquid interfaces and solid particles in several natural and engineered processes reflects the interplay of the interactions between them. A brief description on the origins and characteristics of the two basic interactions, dispersive and electrostatic, is addressed in this chapter.

The hypothesis of the present work is that the mean-field, pseudo-one-component approximation within the framework of the classical theory can be related to the discrepancies between experimental observations of the behavior of engineered and natural processes and the classical theory. To test the hypothesis, modeling and experimental techniques will be employed for the study of the interactions between charged surfaces, and, specifically, the effects of discreteness of charge on the surface and the electrical double layer (EDL), ion-size, and ion-ion correlations will be addressed in this work. A brief description of the modeling and experimental techniques

used is presented in this chapter, along with a justification for the selection of those methods of study.

2.2 Interparticle interactions

The two basic components of interparticle interactions considered in the modeling of solid-liquid interfaces and colloidal particles are the Van der Waals dispersive interactions and the electrostatic or EDL interactions. Traditionally, the interplay of both types of interactions is analyzed within the framework of the Derjaguin-Landau-Verwey-Overbeek (DLVO) theory, a theory on the stability of colloids derived in the 1940s (Derjaguin and Landau, 1941; Verwey and Overbeek, 1948). The application of the principles of this theory enables, at least qualitatively, the study and interpretation of a large amount of experimental data regarding aggregation processes of droplets and solid particles; phase separations; deposition and transport of immiscible phases and solid particles; membrane separations; electrochemical processes; and processes involving biological membranes and macromolecules.

In the DLVO theory, the total interaction between two solid surfaces in aquatic media is calculated as the addition of two independent terms: a dispersive interaction potential (i.e., Van der Waals interaction potential) and an electrostatic interaction potential (i.e., EDL interactions). Both components are derived independently as they have completely different origins.

2.2.1 Van der Waals or dispersion forces

Van der Waals forces or dispersion forces are a consequence of the existence of matter, i.e., they are associated to all atoms independently of their electronic structure or charged state. They are usually long-range attractive forces that do not follow a simple power law (Israelichvili, 1998), and they are quantum mechanical in origin. For example, a helium atom has a time-average dipole moment of zero; however, at any instant there exists a finite dipole moment arising from the instantaneous localization of the electrons at different positions around the atom nucleus. The finite dipole moment of one helium atom polarizes any other helium atom nearby, inducing a dipole moment in it. The interaction between the two dipoles gives rise to an instantaneous attractive force between the two atoms. The time average of the generated force, the Van der Waals force, is finite (Israelachvili, 1998).

In the case of interacting surfaces, the quantification of the Van der Waals forces rests on the assumptions that the dispersive forces between the atoms on the interacting surfaces are non-retarded and additive. Therefore, the interaction energy between two surfaces can be calculated as the sum of the interaction energies of all atoms on the first surface with all the atoms on the second surface. The sum or integration procedure leads to the following expression for the Van der Waals interaction energy between a spherical particle and a planar surface (Israelachvili, 1998):

$$W_{VdW} = -\frac{A_H R}{6D} \tag{2.1}$$

where W_{VdW} is the interaction energy, A is the Hamaker constant, R is the radius of the spherical particle, and D is the separation distance between the spherical particle and the planar surface. The Van der Waals interaction force is simply equal to the negative value of the first derivative of the interaction energy with respect to the separation distance D evaluated at a finite separation distance.

Since Van der Waals forces are always present, they are detected and measured, experimentally, along with the electrostatic forces. However, Van der Waals forces depend basically on the geometric characteristics of the system, on the polarizability of the surfaces and the media, and on the separation distance as shown by equation 2.1. It can be assumed that for a fixed separation distance the contribution of the Van der Waals force component to the total interaction force is unaffected by electrolyte-concentration changes in a specific system. Therefore, variations in the total interaction force measured experimentally will basically reflect changes in the electrostatic component of the total interaction force.

2.2.2 Electrostatic or EDL forces

Electrostatic forces arise from the Coulombic interaction between two charged atoms, molecules or ions, i.e., the electric interaction between two charges embedded in a medium (Israelachvili, 1998). The origin of the charge is a direct consequence of the depletion or surplus of electrons in the charged species.

Solid surfaces, solid-liquid interfaces, and colloidal particles develop surface charge in aqueous media due to different charging mechanisms. Some of those mechanisms include the ionization or dissociation of surface groups and the adsorption of ions or charged molecules onto the surfaces (Kallay and □alac, 2000). Basically, most charged surfaces have charged atoms or molecules on the surface or at the solid-liquid interface that are responsible for the surface charge. In the case of silica, the material selected as a model surface for this work, the presence of sylanol groups (OH groups) allows the development of positive or negative charge via protonation or deprotonation reactions (Craven, 2000):

$$\begin{aligned} \triangleright Si-OH &\leftrightarrow \triangleright Si-O^- + H^+ \\ \triangleright Si-OH + H^+ &\leftrightarrow \triangleright Si-OH_2^+ \end{aligned} \tag{2.2}$$

In the specific case of silica, the surface charge can be controlled via the regulation of the conditions of pH in the aqueous medium.

The presence of surface charge results in the formation of a region or atmosphere around the solid-liquid interface or the colloidal particle where the local concentration of counterions (i.e., ions with an opposite charge to the surface charge) is higher than the concentration in the bulk solution. There is an accumulation of counterions and a depletion of coions (i.e., ions with similar charge to the surface charge) within a short distance near the surface that is known as the electrical double layer (EDL). Figure 2.1 shows a schematic of that phenomenon:

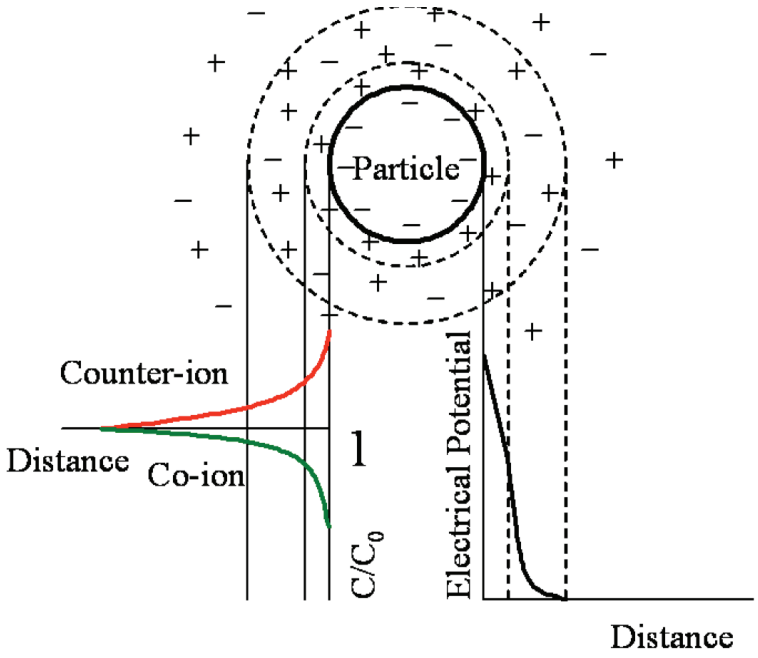

Figure 2.1 Schematic of the EDL around a spherical particle.

Some counterions may dehydrate and become transiently bound to the surface (i.e., adsorbed onto the surface) within a region called Stern layer or inner Helmhotz plane. Those ions modify the surface charge at the solid-liquid interface. Other counterions and coions stay within the EDL in constant thermal motion. Electrolytes composed by ions that do not adsorb on the surface are called indifferent electrolytes. The first part of the present work focuses on the electrostatic interactions resulting from the presence of indifferent electrolytes, while the last part deals with non-indifferent electrolytes, ions that are capable of adsorbing onto the silica surface.

The electrostatic interaction between two charged particles is the direct result of the overlap of their associated EDLs and has two components. One component of the interaction is electrostatic and results from the Coulombic interactions between the

counterions and coions that form the EDLs associated to both surfaces. The second component is entropic or osmotic and arises from the high local concentration of ionic species in the space between the interacting surfaces. This term is usually the dominant one (Israelachvili, 1998). Although the second component is not electrostatic in nature, its existence depends on the presence of surface charge and the consequent formation of the EDL. In conclusion, there are two factors that determine the nature of the electrostatic interactions between two charged surfaces: the strength and sign of the surface charge, and the concentration and nature of the electrolyte solution forming the EDL.

2.3 Classical theory on electrical double layer and electrostatic interactions

The electrostatic interactions between charged solid-liquid interfaces and colloidal particles arise from the overlap of their associated EDLs. Therefore, the interactions are strongly dependent on the structure of the EDL. Modeling electrostatic EDL interactions between charged surfaces implies modeling their EDL structures.

2.3.1 The Gouy-Chapman theory: solving the Poisson-Boltzmann equation

The structure of the EDL is described in terms of the distribution of electrical potential and electrolyte species near a charged surface. Those distributions are obtained from the combination of two equations: the Boltzmann distribution and the Poisson equation

within the framework of the Gouy-Chapman (GC) double layer model. The GC theory, which is based on a mean-field, pseudo-one-component approximation, rests on the following assumptions for the solution of the Poisson equation and the Boltzmann distribution:

- the charged surface possesses an impenetrable interface,
- the surface charge and potential are uniformly smeared out over the surface,
- the ions forming the EDL are point charges, and
- the solvent constitutes an infinite medium with properties independent from the distance to the surface.

The Boltzmann distribution results from the imposition of the thermodynamic equilibrium requirement that the chemical potential must be uniform throughout the system. It is mathematically expressed as (Hiemenz and Rajagopalan, 1997; Hunter, 2001):

$$\frac{n_i}{n_{i0}} = \exp\left(-\nu_i \bar{e}\psi \Big/ k_B T \right) \tag{2.3}$$

where n_i and n_{i0} are the local number concentration and bulk number concentration of ion i, respectively; ν_i is the valence of ion i; □ is the charge of the electron, ψ is the local electrical potential; k_B is the Boltzmann constant; and T is the temperature. Basically, the probability of finding an ion at a certain distance from the surface depends on the amount of electric work (term in the nominator of the exponential) required to keep it in that

position while overcoming the thermal energy. The electric work comes from the charged surface.

The charge density in the EDL (ρ_{elec}) can be obtained from the sum of the number of charges of each charged species in the system, given by the Boltzmann distribution, as follows:

$$\rho_{elec} = \sum_i \nu_i \bar{e} n_{i0} \exp\left(- \nu_i \bar{e}\psi \Big/ k_B T \right) \tag{2.4}$$

The Poisson equation establishes the relationship between charge density and electric potential at any point:

$$\nabla^2 \psi = - \frac{\rho_{elec}}{\varepsilon} \tag{2.5}$$

where ε is the electric permittivity of the medium.

The combination of the Boltzmann distribution and the Poisson equation for the EDL of an infinite charged planar surface embedded in a symmetric ν:ν electrolyte solution results in the following differential Poisson-Boltzmann (PB) equation:

$$\frac{d^2\psi}{dz^2} = \frac{2 n_0 \bar{e} \nu}{\varepsilon} \sinh\left(\frac{\nu \bar{e}\psi}{k_B T} \right) \tag{2.6}$$

Two boundary conditions are required to solve this equation. Traditionally, the GC theory considers the potential at the surface ($z = 0$) as one of the boundary conditions, since the ions conforming the EDL are point charges and, thus, can be found at the solid-liquid interface as well. In the present work, the concept of a "closest distance of approach for the ions" is employed, i.e., what has been called the modified GC theory. The closest distance of approach corresponds to the radius of a fully hydrated counterion, in the case of indifferent electrolytes. Basically, it is considered that the counterions are not point-charges, at least in the first layer of fluid adjacent to the surface. The boundary conditions employed are:

$$\begin{cases} \psi\left(z = d/2\right) = \psi_\delta \\ \left.\dfrac{d\psi}{dz}\right|_{z=\infty} = 0 \end{cases} \tag{2.7}$$

where d is the diameter of the hydrated counterion.

The analytical solution of the PB equation with those two boundary conditions is:

$$\tanh\left(\frac{\nu \bar{e}\psi}{4k_B T}\right) = \tanh\left(\frac{\nu \bar{e}\psi_\delta}{4k_B T}\right)\exp\left[\kappa\left(z - d/2\right)\right] \tag{2.8}$$

where κ corresponds to the Debye length defined by:

$$\kappa = \left[\frac{2n_0 \nu^2 e^{-2}}{\varepsilon k_B T} \right]^{1/2} \tag{2.9}$$

Although equation 2.8 is an analytical expression for the electric potential as a function of distance from the charged surface, the term ψ_δ has to be determined from a charge balance at the solid-liquid interface as follows:

$$\sigma_0 = \varepsilon \left. \frac{d\psi}{dz} \right|_{z=0} = \varepsilon \left. \frac{d\psi}{dz} \right|_{z=d/2} \tag{2.10}$$

where σ_0 corresponds to the surface charge density. Equation 2.10 implies that the potential drop between the solid-liquid interface and the point $z = d/2$ (closest distance of approach to the surface) is assumed to be linear. The gap between the solid-liquid interface and the first layer of counterions is treated as an electric capacitor.

The concentration profiles of the counterion and the coion can be found by replacing the values of electrical potential with distance in the Boltzmann distribution for each ion (equation 2.3).

2.3.2 Modeling EDL interactions

As stated previously, the EDL interaction force between two charged surfaces has two components: an electrostatic interaction between the species in the associated EDLs and

an osmotic pressure resulting from the accumulation of ions next to the charged surfaces. The force is calculated from the change in pressure that results from bringing two charged surfaces together from an infinite separation (Israelachvili, 1998). In the case of two infinite planar surfaces embedded in a symmetric electrolyte, the expression for the change in pressure is (Israelachvili, 1998):

$$P_z = -\int_{D/2}^{\infty} \left[\nu \bar{e} n_0 \left(\frac{d\psi}{dz} \right) \Big|_z dz + k_B T dn \right] \tag{2.11}$$

where P_z is the pressure inside the gap formed between the two approaching surfaces and D is the distance between the surfaces. Usually, the force is evaluated in the mid-plane of the gap.

Combining equation 2.11 with equation 2.3 (the Boltzmann distribution), the following general expression for the pressure or force per unit area, P, between two infinite planar charged surfaces measured at the mid-plane can be obtained (Elimelech et al., 1995):

$$P = n_0 k_B T \left[2\cosh\left(\frac{\nu \bar{e} \psi_m}{k_B T} \right) - \left(\frac{d\psi}{dz} \right)^2 \Big|_{z=D/2} - 2 \right] \tag{2.12}$$

where ψ_m is the value of the electrical potential at the mid-plane ($z=D/2$), and D is the separation distance between the charged surfaces.

It should be noted that the mathematical expression for the EDL force between two charged surfaces depends strongly on the model of the EDL adopted and the mathematical functionality of the solution for the PB equation. Furthermore, the calculation of EDL forces is restricted to the range of applicability of the EDL model.

2.4 Molecular modeling of electrolytes and electrostatic interactions

The use of molecular modeling allows the solution of problems in statistical mechanics for which exact analytical solutions are very hard to obtain. The application of molecular modeling and its solutions, obtained via computer simulation, include the description of a wide range of physical phenomena, from the molecular scale to the galactic scale (Allen and Tildesley, 1990; Pang, 1997). Furthermore, molecular modeling can provide detailed information on the microstructure of the systems being studied, and, through a careful averaging procedure, the values of their thermodynamic properties. The accuracy of the modeling results ultimately depends on the averaging procedure used to obtain thermodynamic properties, and on how close the description of the system is to its real physics.

2.4.1 Modeling systems at a microscopic scale

The microscopic state of a system is specified in terms of the positions and momenta of its constituents, i.e., atoms, molecules, ions or particles. The property of the system that

contains the information of all the momenta and the positions of all its constituents is called the Hamiltonian and is expressed as:

$$H(q,p) = K(p) + V(q) \tag{2.13}$$

where *H(p,q)* is the Hamiltonian of the system, *K(p)* constitutes the kinetic energy of the system, *V(q)* corresponds to the potential energy of the system, and *p* and *q* correspond to the conjugate momenta and the generalized coordinates of all the constituents of the system, respectively. The kinetic energy of the system is basically a sum of all the different components of the momentum of all its constituents. The term of the potential energy contains information regarding intermolecular interactions calculated from the forces and torques acting on all the constituents of the system. Strictly speaking, the potential energy of a system is the sum of several terms. The first term is the energy associated with the interaction of each constituent of the system with any existent external fields. The second term is a sum of all the two-body interactions among constituents of the systems. The third term includes the sum of all the three-body interactions among constituents of the system, and so on. Usually multi-body interactions are not as significant as two-body and three-body interactions in terms of their numerical contribution to the potential energy even for dense systems like liquids, therefore, they are not considered in molecular modeling (Allen and Tildesley, 1990; Pang, 1997). Furthermore, only very few simulations include three-body interactions because the calculation of the triple sums involved is very demanding in terms of computational resources. A traditional approach is to replace the sum of two-body and

three body interactions by an effective pair interaction potential that depends not only on the distance between the interacting bodies, but may also include parameters such as density or temperature to account for three-body effects (Allen and Tildesley, 1990; Pang, 1997, Grotendorst et al., 2002).

There are several effective pair-potential models for atomic systems, for example the Lennard-Jones potential, the hard-sphere potential, the square-well potential, and the soft-sphere potential. In the case of molecules, one may combine different kinds of effective interaction potentials with terms that correct for the existence of different interactions depending on the orientations of molecules with respect to each other. That approach is especially useful when dealing with asymmetric molecules, or molecules with different kinds of functional groups. Finally, in the case of ions, one may also combine any of the expressions for effective interaction potentials for atoms but one must supplement the resulting effective interaction potential equation with a term accounting for the Coulomb charge-charge interaction. This will be discussed with further detail later in the chapter.

Once a model for the pair-wise interactions and the interactions with external fields are defined, the Hamiltonian of the system is established and can be employed in simulations to obtain the thermodynamic properties of the system.

2.4.2 Calculating thermodynamic properties: averaging procedures and ensembles

As discussed earlier, the collection of momenta and positions of the constituents of a system (i.e., the Hamiltonian) defines the system's micromechanical state. The collection of momenta and positions of a system in a specific unique state can be thought of as a point in a multidimensional space: the phase space, which will have a total number of dimensions equal to six times the number of constituents (e.g. atoms, molecules, ions, particles). Any thermodynamic property, A, will have an instantaneous value associated to a specific point in phase space, Γ. Therefore, the thermodynamic property, A, will ultimately be a function of Γ, $A(\Gamma)$.

Systems evolve in time (i.e., the positions and momenta of the atoms change), then Γ evolves in time and thermodynamic properties evolve in time. One way to calculate the average of any thermodynamic property will be to take a time average of $A(\Gamma)$ over a long time interval. This procedure involves the solution of Newton's equations of motion for the system with an associated Hamiltonian. The specific simulation method based on this approach is known as molecular dynamics (MD) and can be used not only to obtain thermodynamic properties of a system, but also transport properties. However, as the systems become larger, the computational cost of this approach increases exponentially.

When one is dealing with systems in thermodynamic equilibrium, one can visualize the macroscopic state of the system as a collection of microstates, or a collection of points in

phase space distributed according to a probability density. Such collection of points in phase space is called ensemble. Therefore, one can replace the time-averaging procedure for the calculation of thermodynamic properties of systems in equilibrium by an ensemble-averaging procedure. The only condition for the ensemble-averaging procedure to be successful is that the calculation has to be performed throughout all the probable points in phase space, i.e., the system visits each point in phase space or the system is "ergodic". In lay terms, ensemble-averaging is like taking snap-shots during a party and using those snap-shots to deduce the macroscopic characteristics of the event.

The probability density distribution function of an ensemble is usually replaced by a weight function with a normalizing factor known as the partition function or sum over states composing the ensemble: Q_{ens}. The partition function, $Q_{ens,}$ is a function of the macroscopic properties defining the ensemble and it can be unequivocally connected with a thermodynamic potential or classical thermodynamic property that will have a minimum value at thermodynamic equilibrium. There are four basic types of ensembles, depending on which thermodynamic properties are kept constant during their definition: (1) the microcanonical ensemble (constant number of atoms or molecules, constant volume and constant energy), (2) the canonical ensemble (constant number of atoms, constant volume and constant temperature), (3) the isothermal-isobaric ensemble (constant number of atoms or molecules, constant pressure and constant temperature), and (4) the grand canonical ensemble (constant chemical potential, constant volume and constant temperature).

The canonical ensemble, chosen for the present work, is defined by the following partition function, Q_{NVT}, which is connected to the Helmhotz energy, A, of the system (Greiner et al., 2000):

$$\frac{A}{k_B T} = -\ln Q_{NVT} = -\ln\left\{\frac{1}{N!\Lambda^{3N}}\int dq \exp\left[-V(q)/k_B T\right]\right\} \tag{2.14}$$

where T is the temperature, k_B is the Boltzmann constant, N is the number of atoms or molecules, Λ is the Broglie wavelength and $V(q)$ is the potential energy of the system. So, basically, by calculating the value of the partition function of a given system, one can obtain the Helmhotz energy that is connected to all other thermodynamic properties via Maxwell relations. Unfortunately, it is not possible to calculate Q_{NVT}. However, finding a way to generate a set of states in phase space, sampled from the complete set of states of any ensemble, in agreement with the ensemble's probability density is the idea behind the Monte Carlo molecular simulation technique (Allen and Tildesley, 1990).

2.4.3 Monte Carlo methods and molecular modeling

Monte Carlo methods, which obtained this name due to the extensive use of random numbers, are used in different kinds of calculations dealing with discrete applications (Allen and Tildesley, 1990). In the case of molecular simulations where discrete states have to be generated as samples from an ensemble, they become especially useful.

2.4.3.1 Rationale behind Monte Carlo methods

Numerical integration is one of the most common applications of Monte Carlo methods. Therefore, the calculation of the area under a curve will be used as an example to illustrate how Monte Carlo methods work. Figure 2.2 shows the schematic of a traditional numerical integration procedure:

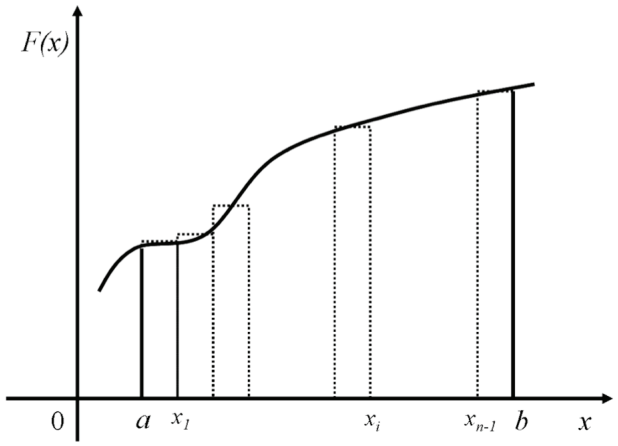

Figure 2.2 Schematic of the traditional numerical integration procedure to find the area under a curve.

The traditional numerical approach is to divide the area under the curve in smaller areas. In the case of the simplest approach, the divisions would be rectangles. The area is then calculated as the sum of the areas of all the rectangular sections:

$$Area \cong \sum_{i} \left(x_i - x_{i-1}\right) \cdot F\left(x_i\right) \tag{2.15}$$

A different approach is presented in Figure 2.3:

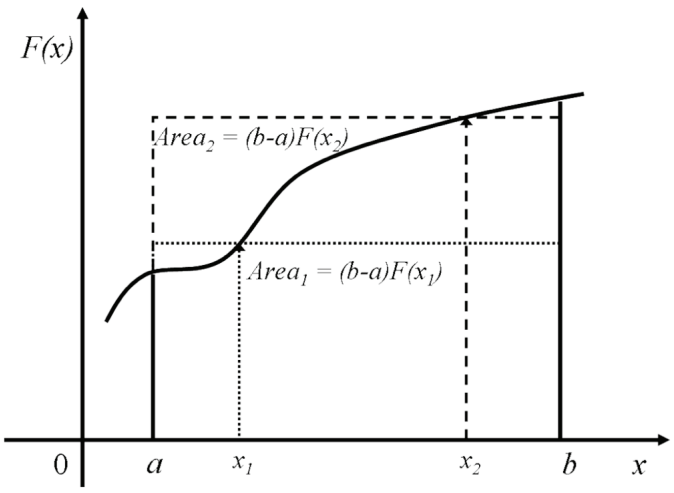

Figure 2.3 Schematic of an "experimental" numerical calculation of the area under a curve.

If the area under the curve, and thus *F(x)* for different values of *x*, were to be determined experimentally, one could choose values of *x* in the interval *[a,b]*, obtain *F(x)* for the values of *x* chosen, and calculate the area simply as an average of the products of *(b-a)* by the *F(x)* values experimentally obtained:

$$Area \cong \frac{1}{\tau}\sum_{i}\left[(b-a)F(x_i)\right] \tag{2.16}$$

where τ corresponds to the number of experiments performed (i.e., number of values x_i) to calculate the area. The accuracy of the calculation will increase as the number of experiments increases. Monte Carlo methods work with a similar rationale to this latter approach. The area under the curve would be defined as (Allen and Tildesley, 1990):

$$Area = \int_a^b dx F(x) = \int_a^b dx \left[\frac{F(x)}{\rho(x)}\right]\rho(x) \cong \left\langle \frac{F(\xi_i)}{\rho(\xi_i)} \right\rangle_\tau \tag{2.17}$$

where τ corresponds to the number of trials, ξ_i corresponds to the random numbers generated for each trial in the interval *[a,b]*, and $\rho(x)$ is an arbitrary probability density function. The use of a finite number of random numbers, τ, in the interval *[a,b]* rests on the assumption that a good sampling of the interval will be made and that a high level of accuracy will be obtained with a relatively small number of trial calculations. In the present example, one could define a uniform probability function of the following functionality:

$$\rho(x) = \frac{1}{(b-a)} \qquad x \in [a,b] \tag{2.18}$$

And, finally, the area would be calculated from the following expression:

$$Area \cong \frac{(b-a)}{\tau} \sum_{i=1}^{\tau} F(\xi_i) \tag{2.19}$$

As can be deduced from the example, Monte Carlo methods can be applied to any discrete problem where a probability density function can be defined. The definition of ensemble is given by a probability function in terms of the thermodynamic properties of a system. Therefore, Monte Carlo methods can be successfully applied to thermodynamic equilibrium calculations based on ensemble-averaging.

2.4.3.2 Canonical Monte Carlo (CMC) simulations

Any molecular Monte Carlo simulation starts with the choice of a type of ensemble and the definition of a simulation box. In the case of the present work, the Canonical ensemble was chosen, i.e., constant fixed volume, constant fixed temperature, and constant fixed number of molecules. When dealing with ions, one must ensure that electroneutrality prevails inside the simulation box at all times. The simplest way to achieve this is to keep the number of ions in the system constant.

A simulation box is an enclosed space of fixed or variable size, depending on the choice of ensemble that contains the atoms, molecules or particles to be studied. Figure 2.4 shows a schematic of a simulation box:

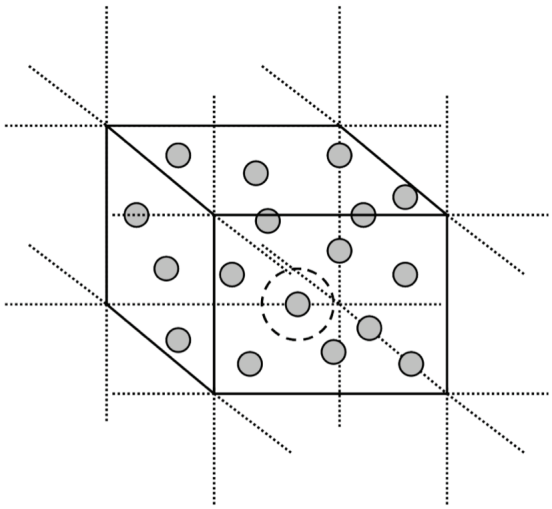

Figure 2.4 Schematic of a CMC simulation box.

In order to initiate the simulation, a random configuration of the atoms, molecules or ions composing the system must be generated and the energy of the configuration calculated.

Since we are dealing with different configurations of the system, the variations in the total energy of the system when a new configuration or state is achieved will respond to variations in the potential energy. Therefore, the potential energy term is the only one calculated during Monte Carlo simulations.

Once an initial configuration is generated, an atom, molecule or ion is randomly chosen and displaced a distance δr_{max} in a random direction to generate a new configuration. The change in energy associated with the transition from the old to the new configuration is calculated. The attempted "move" is accepted according to the following criteria:

- if the move results in a lower energy state, the move is always accepted.
- if the move results in a higher energy state, it is accepted with an associated probability that corresponds to the Canonical probability distribution function.

In practice, for every move that results in a higher energy state a random number is generated. If the random number has a lesser or equal value than the Canonical probability for the variation of energy between the two states, the movement is accepted with the Canonical probability associated with it. If, on the other hand, the random number generated has a higher value than the Canonical probability associated with the change in energy resulting from the migration of one state to the other, then the "move" is rejected. This criterion is depicted as a schematic in Figure 2.5:

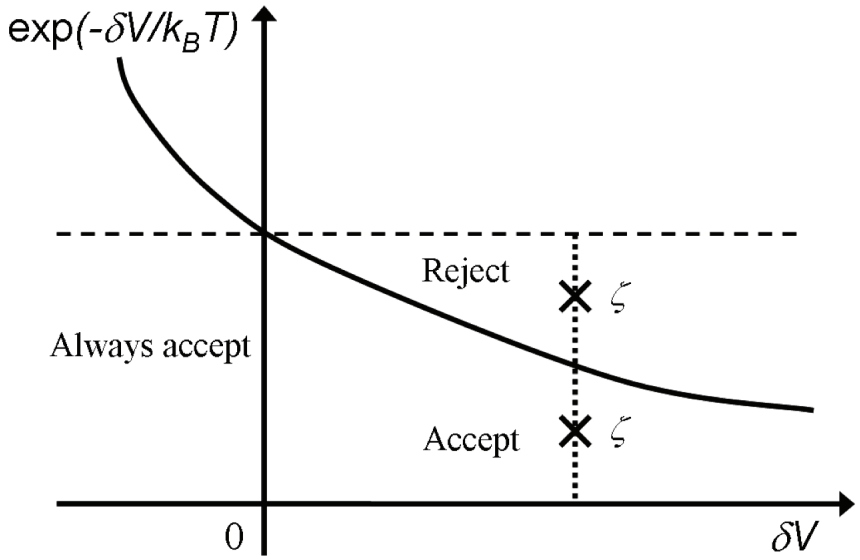

Figure 2.5 Schematic of the criterion for "move" acceptance in CMC simulations (adapted from Allen and Tildesley, 1990).

It is common practice in molecular modeling to have the atoms, molecules, or ions to be chosen and moved sequentially (Allen and Tildesley, 1990). This procedure is comparably less computationally costly than choosing the species randomly and still has the advantage of constituting an ergodic Markov chain, i.e., every state can eventually be reached from another state.

Since the simulation box is usually small and constitutes only a very small portion of a system, periodic boundary conditions are applied to mimic the presence of bulk fluid or solid. Periodic boundary conditions in all directions imply that the simulation box is replicated in all directions, and each atom, molecule or ion within the simulation box has an "image" ion in all the adjacent boxes of fluid. When an atom, molecule or ion moves outside the simulation box, one of its image ions enters the simulation box from the opposite direction.

2.4.4 Canonical Monte Carlo simulations of electrolyte solutions

Most of the molecular-modeling work on electrolyte solutions follows the primitive model, i.e., the solvent is regarded as a continuum with an associated electric permittivity. Therefore, the only discrete entities in the simulation box are the ions.

The potential energy of the system results from the sum of two components or contributions for all the ions present in the system: an effective interaction potential term and a potential energy term associated to the different position of each ion inside the simulation box.

The ions are modeled as charged hard spheres, thus two kinds of effective pair-interaction potentials are combined: hard sphere interactions and Coulombic interactions. The effective pair interaction potential is defined as follows:

$$v_{ij} = \begin{cases} +\infty & r_{ij} < \sigma_{ij} \\ \dfrac{Q_i Q_j}{4\pi\varepsilon_0\varepsilon_r r_{ij}} & r_{ij} \geq \sigma_{ij} \end{cases} \tag{2.20}$$

where v_{ij} is the pair interaction potential of ions i and j, r_{ij} is the distance between the centers of ions i and j, σ_{ij} is the maximum distance of approach between the ions i and j (i.e., the square root of the sum of the radius of each ion squared), Q_i and Q_j are the charges of ions i and j, respectively, and ε_0 and ε_r correspond to the permittivity of vacuum and relative permittivity of the solvent. In order to calculate the distance

between the centers of the ions *i* and *j*, the minimum image convention is employed, i.e., the separation distance is calculated between ion *i* and the closest representative of ion *j*, either the ion itself or its closest image in the adjacent replicas of the simulation box.

The potential energy term associated to the position of each ion in the simulation box arises from the periodic boundary conditions imposed, because Coulombic forces or Coulombic interaction potentials are long-ranged. The range of the Coulombic interactions might exceed the length of the simulation box. One of the most common techniques used to calculate the potential energy term associated with long-range corrections is the Ewald summation. The method is basically an averaging procedure of the force associated with the interaction of each ion in the system with the replicas of the simulation box outside the central cell or box. Although the method is very reliable when dealing with electrolyte bulk solutions, a periodicity is introduced into the Hamiltonian that might distort the charge distributions in the system when periodic boundary conditions are not applied in all directions (Torrie and Valleau, 1980).

2.4.5 Monte Carlo modeling of the electrical double layer and the interactions between charged surfaces

Modeling of the EDL implies introducing at least one impenetrable wall in the simulation box containing the electrolyte solution. Therefore, periodic boundary conditions do not prevail in at least one direction. Some adjustments to the protocol developed for the simulation of electrolyte solutions have to be made especially when dealing with long-

range corrections. One approach is to account for the interaction of all the ions in the central simulation box with the ions in the adjacent replicas of it where periodic boundary conditions prevail.

Most of the methods encountered in literature model the image ions outside the central simulation box as charged sheets with an equivalent charge to that of all the image ions in all the directions where periodic boundary conditions prevail. Basically, the effective interaction potential can be calculated as the sum of the effective interaction between the ions in the central simulation box and the uniformly charged planar sheets outside the central simulation box. Several authors use equispaced planar sheets with associated charges determined by an "average charge distribution" calculated from the positions of the ions in the central simulation box during previous steps of the simulation (Torrie and Valleau, 1980; Van Megen and Snook, 1980; Torrie et al., 1982). Other authors use a screened Coulomb potential for charge averaging purposes (Hayment and Vlachy, 1988). However, any of these approaches might result in loss of the random character of the CMC simulations therefore, resulting in a loss of ergodicity, i.e., some configurations might be favored over other configurations.

A recently developed approach to deal with long-range corrections in the directions where periodic boundary conditions are applied constitutes the modeling of the image ions outside the simulation box as independent infinitely charged sheets (Boda and Chan, 1998; Boda et al. 2004). The difference with the previous approaches is that each ion in the central simulation box has an associated infinitely charged sheet that accounts for all

its image ions outside the simulation box. That infinitely charged sheet moves along with the ion inside the simulation box. Therefore, there is neither a "charge-averaging" procedure required nor the utilization of configuration data obtained in previous simulation steps. This method complies with the requirement of Monte Carlo simulations to be random in nature, and it will be fully introduced in the following chapter because it is adopted in this work.

Another aspect that has to be taken into account is the polarization of the charged surface when dealing with impenetrable uniformly charged surfaces of different dielectric constant than that of the medium due to the discontinuity in the dielectric constant at the interface (Torrie et al., 1982). This effect can be taken into account and modeled by a set of fictitious "image" charges associated with the ions close to the surface behind the impenetrable charged surface. For each ion in a position (x_i,y_i,z_i) inside the central simulation box, there will be an associated image charge at a position $(x_i,y_i,-z_i)$ that will possess a fraction of the charge of the original ion. Therefore, each ion will now interact not only with all the other ions in the central simulation box, the charged surface and the infinitely charged sheets outside the simulation box; but also with the image charges behind the impenetrable wall. This correction is especially important when the EDL simulation is performed with uniformly charged surfaces with high values of surface charge density (Torrie et al., 1982).

The basics and protocols employed in all the molecular simulation work dealing with the EDL structure and formation, found in literature, follow the basic characteristics

described in this section. Most simulations of the EDL have been performed for planar surfaces with 1:1 electrolytes in order to compare the simulation results with the PB equation predictions (Torrie and Valleau, 1980; Van Megen and Snook, 1980; Torrie et al., 1982; Boda and Chan, 1998). Some work has also been attempted with asymmetric electrolytes, specifically 2:1 electrolytes, but without considering differences in ion sizes (Vlachy et al., 1989) or with ion radii that do not correspond to fully hydrated ions (Boda et al., 2004). In all those cases, uniformly planar charged surfaces were employed and the presence of mixtures of electrolytes was not examined.

In the case of the evaluation of EDL interactions and forces between charged surfaces, very few molecular simulations have been attempted. One of the first attempts dealt with the interaction of similarly charged surfaces with uniform charge distribution (Guldbrand et al., 1984; Delville, 1994). In that case, the interaction between the two planar approaching surfaces was calculated but applying the concept of pressure developed within the classical theory (equation 2.11), i.e., as the contribution of an osmotic term and an electrostatic term:

$$P = k_B T \sum_i n_i(0) - \left(\frac{\partial A}{\partial z}\right)\frac{1}{a} \tag{2.21}$$

where A corresponds to the Helmhotz energy of the system, and a corresponds to the area of interaction. However, the use of the Helmhotz energy of the system implies adding interactions that might not be part of EDL overlapping.

Some researchers have attempted to model charged particles and surfaces as macroions, i.e., large hard spheres with high valences. Then, the interactions between the charged particles were calculated as the Coulombic interaction between the macroions (D'Amico and Löwen, 1997), or they were inferred from the behavior of the dispersion of macroions and their corresponding counterions (Lobaskin and Linse, 1999; Linse and Lobaskin, 2000; Meyer et al., 2001; Lobaskin and Quamieh, 2003). The application of molecular modeling for the direct calculation of the net force between interacting charged surfaces and their associated EDLs has not been attempted yet.

2.5 Experimental determination of the interactions between charged surfaces: the atomic force microscope

In parallel to the theoretical effort, relative success has been achieved in the experimental study of interactions between surfaces and particles. The different methods of experimental determination of interparticle interactions can be classified as indirect or direct. Examples of indirect methods are contact angle measurements, measurements of interparticle spacing of colloidal suspensions by light scattering, and osmotic pressure measurements (Israelachvili, 1998). The direct methods are based on positioning two bodies, surfaces or particles, close to each other and directly measuring the force between them via the application of some known physics law. Although this principle is straightforward, the challenge of direct force measurements resides in the detection of the weak forces at very small separation distances (Israelachvili, 1998). In the last 20 years, different instruments have been developed that are capable of measuring interparticle

forces; two of the most widely spread ones are the surface force apparatus (SFA) and the atomic force microscope (AFM).

Invented by Binnig, Quate and Gerber (Binnig et al., 1986), the AFM was initially developed as an imaging tool. However, the operating principle of the AFM allows its application for direct measurements of the interaction force between its normal stylus tip or a colloidal probe and a planar surface (Butt, 1991; Zauscher and Klingenberg, 2000).

2.5.1 Operating principle of AFM

In an AFM, a sharp tip, usually a single silicon nitride crystal, attached to a cantilever scans in a plane presumed to be parallel to the surface of interest (Butt, 1991). The surface exerts a force on the cantilever, i.e., an interaction force prevails between the two surfaces. The magnitude and the direction of the force during the scanning process are inferred from the measured deflection of the cantilever, which has a known spring constant. The deflection is measured using an optical sensor. A laser beam is focused on to the backside of the cantilever, and the beam is reflected to a multisegmented photodetector that can resolve the relative position of the laser beam as a function of the output voltage of each respective photodetector segment. First, the deflection of the cantilever tip is recorded. Then, the signal is used by a feedback control loop to restore the user-specified force on the cantilever tip by adjusting the altitude of the surface of interest. The altitude of the surface is changed by applying a voltage to a piezoelectric actuator. The voltage applied is recorded and use to infer the displacement of the sample

with the known piezoelectric constant of the actuator. Figure 2.6 shows a simplified schematic of the AFM:

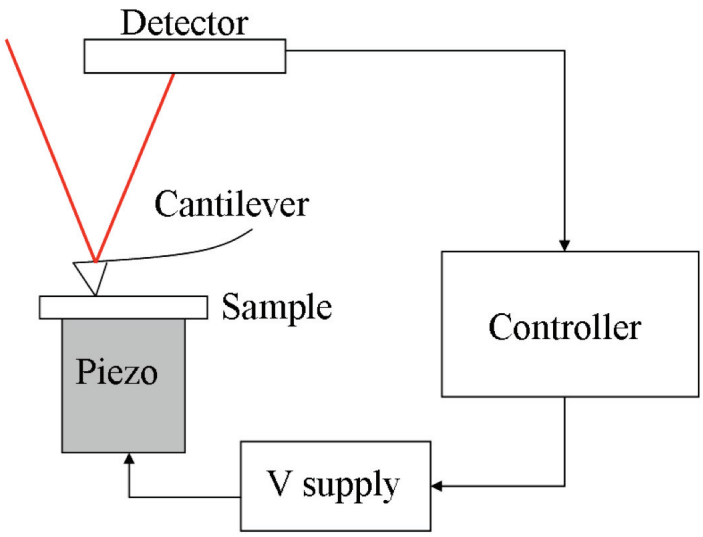

Figure 2.6 Schematic of the operation and feedback control of the AFM.

The logic of the AFM control loop can be explained through a simple analogy depicted in Figure 2.7:

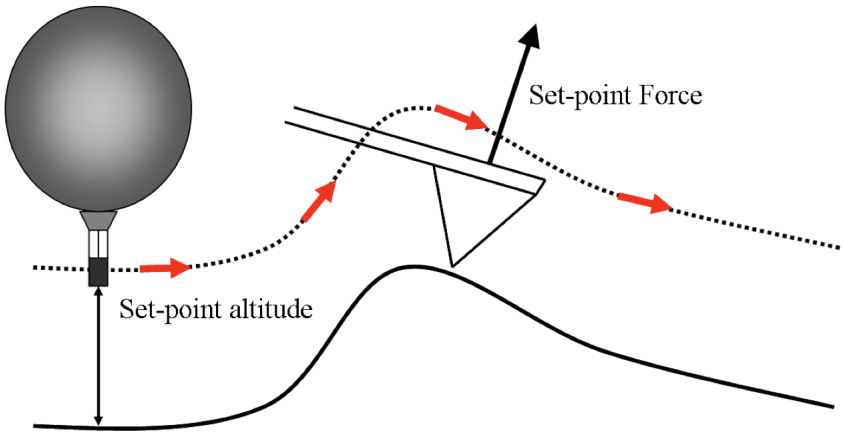

Figure 2.7 Schematic depicting the logic behind the AFM control loop.

A navigator is trying to reproduce the topography of certain terrain from a hot air balloon. The navigator represents the AFM photodetector and controller, while the balloon represents the cantilever tip. In order to achieve this objective, the navigator flies the balloon at a fixed height (i.e. set point altitude) from the surface. In the case of AFM, the set-point value is the force sensed by the cantilever or the cantilever's deflection, which are a function of the separation distance between the sample surface and the cantilever's tip. The navigator uses radar to measure the distance between the balloon and the surface. The radar is equivalent to the laser beam in an AFM. As the navigator flies along the surface, he/she encounters mountains and valleys. As the balloon approaches a mountain, it gets closer to the surface. Then, the navigator allows hot air into the balloon to maintain the set-point altitude. When the balloon approaches valleys, the navigator releases hot air from the balloon in order to keep the altitude of the balloon with respect to the surface constant. When the AFM tip encounters protuberances on the surface scanned, it senses a strong attractive force. The piezoelectric actuator moves the surface away from the cantilever tip to restore the value of the set-point deflection. On the other hand, when the AFM tip encounters valleys on the surface of interest, it senses a weak force or even zero force, and the surface is moved towards the tip by the photoelectric element. Then, the hot air is equivalent to the voltage applied to the piezoelectric element used in the AFM to displace the surface closer to or away from the surface. The record of the amount of hot air allowed into the balloon or released from the balloon during the scanning of the surface can be related to the distance traveled by the balloon upwards or downwards while scanning the surface. And, processing of that data, will allow the reproduction of the topography of the surface scanned by the balloon. In the

case of AFM, the upward/downward movements of the sample and the deflection experienced by the cantilever are recorded by the controller of the AFM. The processing of that data allows the reconstruction of the topographic characteristics of the surface scanned.

It is very important to keep in mind that the surface features reflected in the image are closely related to the dependence on the separation distance of the interaction forces acting between the cantilever tip and the surface being scanned. "Well behaved forces" like Van der Waals forces result in accurate images. However, in most cases, forces other than Van der Waals may act between the cantilever tip and the sample. In the case of aquatic media, electrostatic forces play an important role if the surfaces scanned are capable of developing surface charge (Butt, 1991; Veeramasuneni et al., 1996; Hillier et al., 1996; Hüttl et al., 1997). In other cases, even hydration forces have to be taken into consideration (Zauscher and Klingenberg, 2000). The quality of the images and the relevance of the information obtained require knowledge of the forces acting on the cantilever tip and a careful calibration procedure of the deflection with separation distance in order to avoid image artifacts.

2.5.2 The AFM force curve

The calibration of the deflection of the cantilever as a function of the separation distance between the surface of interest and the cantilever's tip is performed via the recording of

deflection data when the tip of the cantilever is brought vertically towards the surface. Figure 2.8 shows a schematic of the information obtained through this procedure:

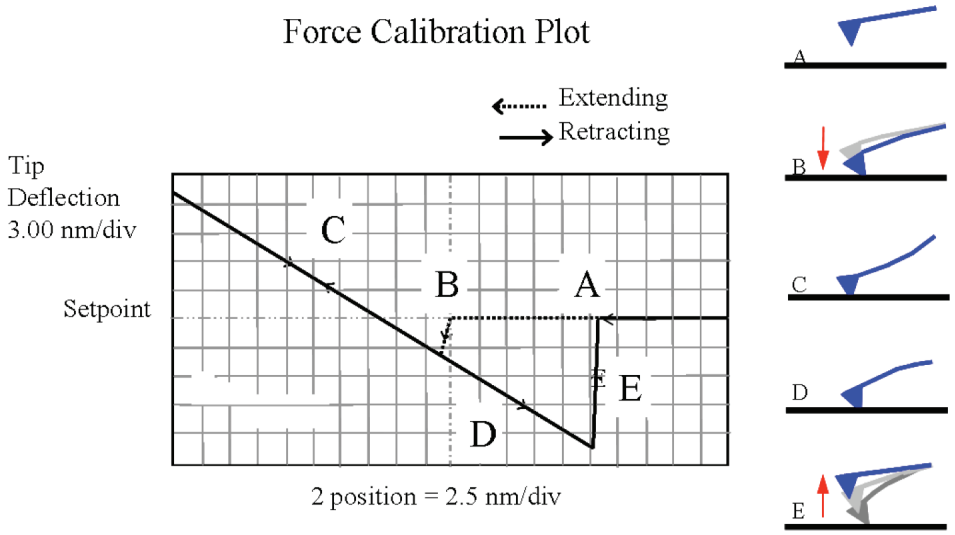

Figure 2.8 Schematic representation of the curve of tip deflection vs. separation distance.

Two sets of data are recorded during the vertical approach of the cantilever to the surface: extending and retracting data. The behavior of the deflection of the cantilever with the separation distance between the tip and the surface being scanned is used to determine a set-point value that will allow accurate imaging. Furthermore, the deflection information can be used to directly provide information about interaction forces with separation distance.

Extending data are usually employed to determine the interaction force between the tip and the surface in the case of Van der Waals and electrostatic contributions (Butt, 1991, 1992; Veerasuneni et al., 1996; Hillier et al., 1996; Rotsch and Radmacher, 1997; Hartley et al., 1998; Heinz and Hoh, 1999; Gavoille and Takadoum, 2002). On the other hand, retracting data are usually utilized in the determination of adhesive forces (Kramer et al.,

1998; Camesano and Logan, 2000; Teran Arce et al., 2003). The interaction force (F) between the tip and the cantilever can be found via the application of Hooke's Law:

$$F = k\Delta l \tag{2.22}$$

where k is the spring constant of the cantilever and Δl corresponds to the measured deflection of the tip. The spring constant depends on the geometric characteristics of the cantilever and can be calculated from its dimensions and its Young's modulus (Veeramasuneni et al., 1996). The spring constant can also be experimentally obtained from the comparison of the natural frequency of vibration of the cantilever plus the tip and the cantilever without tip (Cleveland et al., 1993).

The force calibration curves provide information on the variation of interaction force with distance for a specific region of contact between the tip and the surface being scanned. Depending on the topography of the surface and the distribution of the surface charge, the interaction force may have different values at different points on the surface.

2.5.3 Force-volume AFM

In force-volume (FV) imaging, the deflection of the cantilever as a function of separation distance is sampled at regular intervals across the surface. Therefore, a two-dimensional array (X-Y) of data of deflection vs separation distance is obtained. Figure 2.9 depicts the type of data obtained:

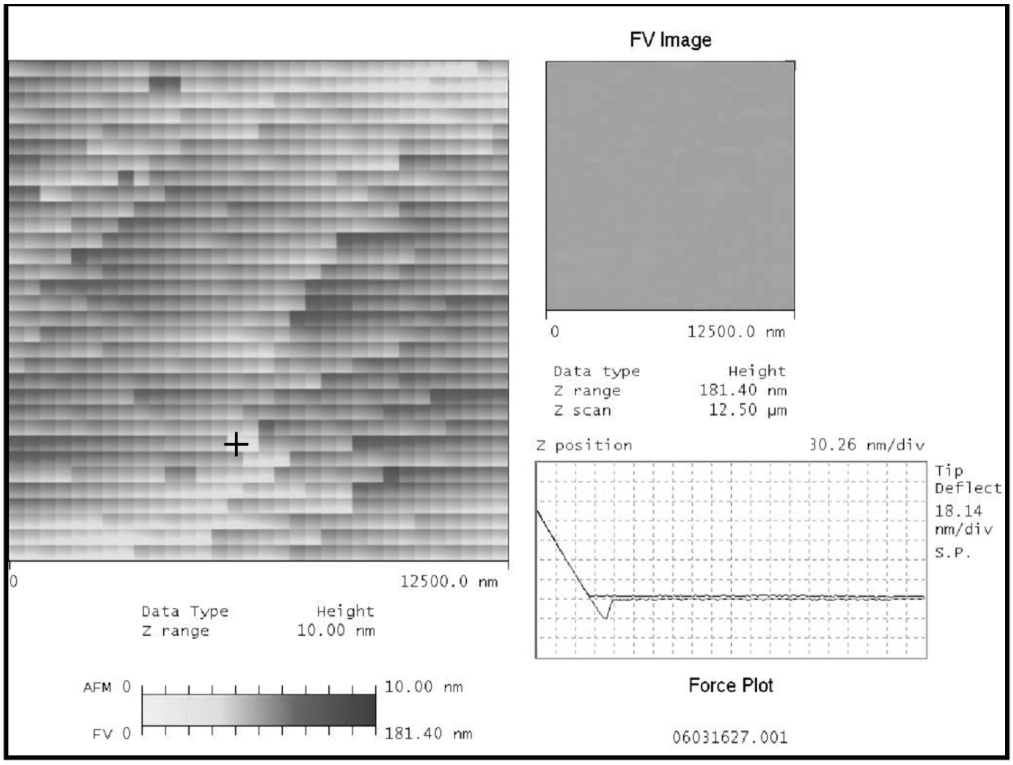

Figure 2.9 Force-volume data for a fused silica surface in water obtained by AFM.

Three different kinds of information are obtained during force-volume imaging. The largest mosaic image on the left of Figure 2.9 corresponds to a force-based height image, i.e., a topography construction based on the interaction forces or deflection. That image can be read with the scale on the left lower corner of the screen. The different shades in color are matched with different values of "topographic height" (AFM scale) and "deflection height" (FV scale). It should be noted that the image is not as sharp as a conventional AFM image, because the acquisition of data during FV imaging is not performed every 1024 x 1024 pixels as it is done during conventional AFM imaging. There is a limit in terms of memory on the acquisition of data during FV imaging given by the following expression:

$$(Force\ per\ line\ scanned)^2 * \#\ of\ samples\ per\ force\ curve * 4 \leq 1Mb \qquad (2.23)$$

The second set of data corresponds to stratified layers at various separation distances above the sample surface (FV Image, on the higher right corner of Figure 2.9). Basically, one can select a finite distance from the surface and obtain information on the value of the interaction force at that particular separation. Different shades of color imply different values of deflection.

Finally, each element on the scanned surface (each small square force-based height image) has a complete force curve associated with it, i.e., deflection of the cantilever vs separation distance during extension and retraction. Therefore, one can obtain information of the local value of interaction forces at different positions X-Y on the scanned surface. Figure 2.9 depicts in the lower right corner the force curve associated with the square element where the cursor is positioned on the force-based height image.

2.6 Conclusions

The application of AFM for the direct measurement of interaction forces between charged surfaces or solid/liquid interfaces is very useful in terms of direct test of the hypothesis of this work. Electrolytes of different size and charge can be use in order to probe the effect that the presence of this charged species has on EDL interactions. Furthermore, the application of FV imaging allows the study of local differences of interaction forces resulting from the discrete nature of charge, both on the surface and the

EDL. The discrete nature of charge and its effects on EDL structure and EDL interactions can be fully predicted by Monte Carlo simulations, since ions and charged groups present in the system are accounted as individual entities. Simulations can provide insight on the structural behavior of EDLs resulting in interactions of different types. Finally, although the DLVO theory has shortcomings, it is known to give an accurate description on the EDL structure and the resulting EDL interactions for 1:1 electrolytes at low ionic strength and low values of surface charge. These conditions will be used as a means to test the reliability of the Monte Carlo simulations as they were used to test the accuracy of AFM force measurements in the past (Butt, 1991; Veeramasumeni et al., 1996; Heinz and Hoh, 1999; Zauscher and Klingenberg, 2000; Camesano and Logan, 2000).

CHAPTER 3

ELECTRICAL DOUBLE LAYER STRUCTURE WITH ASYMMETRIC INDIFFERENT ELECTROLYTES

3.1 Introduction

The Gouy-Chapman (GC) theory, referred to here as classical theory, describes the EDL structure through the solution of the Poisson-Boltzmann (PB) equation for the distribution of potential and ion species near a charged surface. It also allows the calculation of the thickness and capacitance of the EDL, as well as the electrostatic forces resulting from interacting EDLs. Because of the complexity of the phenomenon and the resulting mathematical expressions, the classical theory has several limitations. It is applicable to solutions of one electrolyte (usually a symmetric electrolyte), the ions present in the EDL are considered to be point charges, the surfaces are assumed to be uniformly charged, and the interaction or correlations between the ions forming the EDL are not considered (Hiemenz and Rajagopalan, 1997). Unfortunately, ions are not point charges, and natural aquatic environments and industrial solutions usually contain complex mixtures of ions of different size and charge. Also, in aqueous environments, particles and solid surfaces develop charge via chemical charging mechanisms such as protonation and deprotonation of surface groups, as well as adsorption of metal ions or

other charged molecules. In the case of inorganic particles, for example, charge might arise from selective ion adsorption to different crystal planes (Feick et al., 2004). Many natural colloidal particles, including protein complexes, have different chemical groups on their surfaces (Hartley et al., 1998; Kallay and Žalac, 2000; Keslareck et al., 2002). Therefore, surface charge is discrete in nature. Furthermore, surface charge may even be nonuniform (i.e., different regions on the surface bearing charge of the same sign but of different magnitude) and in some cases heterogeneous (i.e., different regions on the surface bearing charge of different magnitude and sign) (Taboada-Serrano et al., 2005a).

In order to overcome the simplifications of the classical theory, different modifications to this theory, statistical-mechanics-based models, and molecular simulations have been introduced during the last decades. One of the first approaches was the utilization of mean spherical approximations for the modeling of the EDL (Blum, 1977). As an additional feature of the modified GC (MGC) theory, Valleau and Torrie included the consideration of unequal ion sizes when deriving a distance of closest approach to the charged surface and were able to explain the dependence of the point of zero charge on the concentration of electrolyte, i.e., ionic strength. However, their analysis of the limitations of the MGC revealed that the theory overestimates the potential (i.e., the local concentration of ions) even at low surface charges and low surface potentials (Valleau and Torrie, 1982). Grand Canonical Monte Carlo (GCMC) simulations were introduced in order to perform calculations of activity coefficients for electrolyte solutions and were subsequently employed in EDL calculations (Torrie and Valleau, 1982; Valleau and Cohen, 1980; Valleau et al., 1980; Bester and Vlachy, 1992).

Torrie and Valleau, among others, performed the first molecular simulations of the EDL structure for symmetric electrolytes near uniformly charged surfaces within the framework of the primitive model. They showed that for 1:1 electrolytes at low concentrations and low surface charges, qualitative agreement existed between the MGC theory predictions and results from molecular simulations. However, at higher surface charges, they detected a layered structure of the counterions close to the surface (Torrie and Valleau, 1980; VanMengen and Snook, 1980). The initial approach for the molecular modeling of EDL was perfected by the combination of GCMC and Canonical Monte Carlo (CMC) simulation techniques, introduction of different methods to account for long-range electrostatic force corrections, surface polarization, and inclusion of molecular solvent in the case of highly concentrated systems (Torrie et al., 1982; Torrie et al., 1989; Boda et. al, 1998) Applications of all the important developments in terms of molecular modeling, other theories including the hypernetted-chain (HNC) theory, and even improvements to the GC theory targeted the modeling of the EDL structure in lamellar liquid crystals (Jönsson et al., 1980), the modeling of the EDL near polyelectrolytes (Murthy et al., 1985; Vlachy et al., 1989; Lobaskin and Linse, 1999), and the formation of EDL in micropores and nanopores (Jamnik and Vlachy, 1993; Hribar et al., 2000; Carrera et al., 2001; Yang et al., 2002a, 2002b; Huang and Hebert, 2004).

The work cited in the preceding paragraph deals with symmetric electrolytes of equal size (e.g., 4.25 Å for hydrated ions in most cases). However, real systems usually contain ions of different size and charge. Torrie et al. (1989) analyzed the structure of the EDL

in the presence of ions of different sizes (diameters equal to 2.35, 3.02, and 4.25 Å) and concluded that the smallest ions interact strongly with the surface for intermediate values of surface potential. Recent work by Boda and coworkers (1998, 2004) has coupled the study of the effect of ion size (diameters equal to 2, 3, and 4.25 Å) with charge asymmetry, specifically 1:1 and 2:1 electrolytes. Parallel to molecular modeling efforts, ion size effects have also been studied through the application of the HNC theory and its variations, as well as different upgrades of the GC theory and the density functional theory (DFT) (Torrie et al., 1989; Boda et al., 1998; Bohinc et al., 2001; Martín-Molina et al., 2002; Boda et al., 2004; Valiskó et al., 2004).

Another characteristic of real systems is that surface charge is usually the result of the presence of charged groups on the surface; therefore, considering the surface charge as uniform might not be an accurate representation of those systems. Messina (2002) used molecular dynamics (MD) in order to model the behavior of a spherical colloid with discrete surface charge and only counterions at ground state and finite temperature. The conclusion of Messina's work was that coupling exists between the charged groups on the surface and the counterions in the first layer of fluid adjacent to the surface (Messina, 2002).

In this part of the work, we pursued the extension of the application of molecular simulations to predict the structure of the EDL for surfaces with discrete surface charge (charge resulting from the presence of charged groups on the surface) in the presence of mixtures of symmetric and asymmetric indifferent electrolytes. The effects of the

discretization of surface charge, symmetry and asymmetry of charge, and ion size are specific focuses of this work. The intent is to examine the formation of EDL in systems that resemble real charged interfaces in natural and engineered aquatic environments.

3.2 CMC simulations of the EDL structure

GCMC simulations are the natural choice for EDL calculations since the introduction and deletion of neutral pairs of charged species allow the easy development of bulk conditions away from the charged wall. However, when dealing with mixtures of electrolytes of different charges, adding and/or removing neutral groups of charged species from the simulation box would be extremely challenging. Therefore, CMC simulations were used in this work.

3.2.1 Simulation box

Figure 3.1 depicts a schematic of the system. The system consisted of a simulation box of equal length (L, in the X direction) and height (L, in the Y direction), but greater width (W, in the Z direction). Periodic boundary conditions were employed in the X and Y directions (Allen and Tildesley, 1990), whereas the Z direction was enclosed between two impenetrable walls: one of them, uncharged, and the other, containing charged groups. The minimum image convention was employed in the X and Y directions (Allen and Tildesley, 1990), i.e., whenever an ion was moved outside of the simulation box an

image ion was introduced into the simulation box at the opposite end in the planes X-Z and Y-Z.

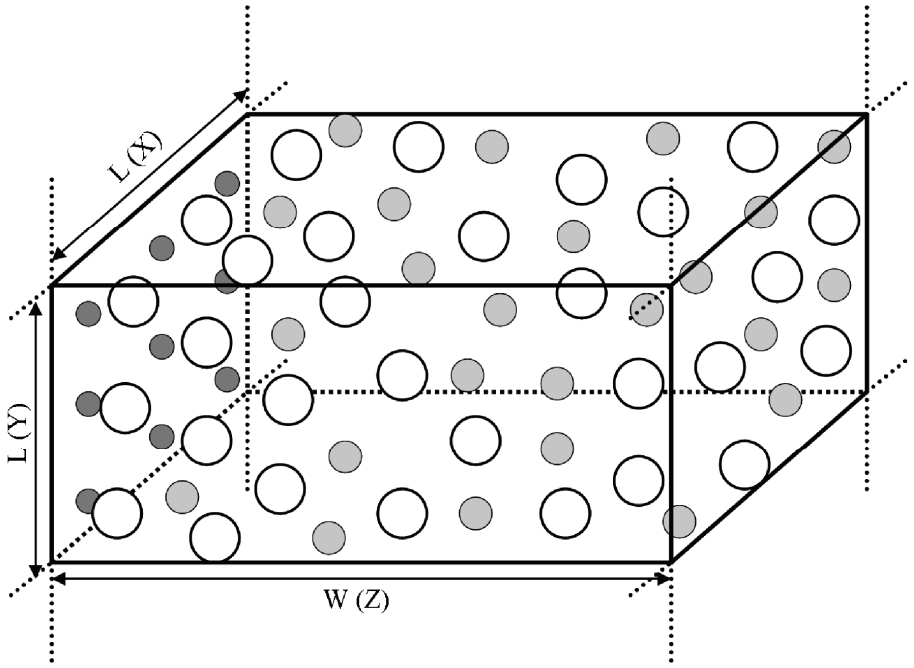

Figure 3.1 Schematic of the simulation box used in CMC simulations of EDL structure.

In the schematic, the big white spheres represent the counterions, the medium-size light gray spheres represent the coions, and the small dark gray spheres represent the surface ions responsible for the surface charge.

3.2.2 Potential energy of the EDL

The potential energy of the EDL, v, was calculated as the sum of individual potential energies associated with the position of each ionic species in the simulation box and the sum of the pair-wise interactions of all the ionic species present in the simulation box including the ions on the charged wall.

$$v = \sum_i v_i + \sum_{i>j} \sum_j v_{ij} \tag{3.1}$$

where v_i is the potential energy of ion i and v_{ij} is the energy of interaction between ions i and j. The potential energy v_i depends on the position of each ion inside the simulation box and it is given by the interaction of the particular ion with the electric field generated by all the ions outside the simulation box, i.e., conditions generated by the imposition of periodic boundary conditions. The interaction energy v_{ij} is given by the pair-wise interactions of all the ions and charged wall groups inside the boundaries of the simulation box.

3.2.2.1 Interaction potential between ionic species

The charged groups and ions were modeled as charged hard spheres, and their interactions were accounted for within the framework of the primitive model as described in the publications by Valleau and coworkers (Valleau and Cohen, 1980; Valleau et al., 1980; Torrie and Valleau, 1980; Torrie et al., 1982). The interaction potentials between the ions were calculated via the application of Coulomb's Law with the following functionality (Israelachvili, 1998):

$$v_{ij} = \begin{cases} +\infty & r_{ij} < \sigma_{ij} \\ \dfrac{Q_i Q_j}{4\pi\varepsilon_0 \varepsilon r_{ij}} & r_{ij} \geq \sigma_{ij} \end{cases} \tag{3.2}$$

where v_{ij} is the pair interaction potential of ions i and j, r_{ij} is the distance between the centers of ions i and j, σ_{ij} is the maximum distance of approach between the ions i and j (i.e., the square root of the sum of each ion's radius squared), Q_i and Q_j are the charges of ions i and j, respectively, and ε_0 and ε correspond to the permittivity of vacuum and relative permittivity of the solvent. The solvent was considered as a continuum with an associated permittivity. Unlike the cited works, the present work addresses a discrete charge on the surface. Therefore, individual interactions between charged groups on the charged surface and ions in the simulation box were accounted for.

3.2.2.2 Long-range corrections of Coulombic interactions

The long-range corrections needed due to the probability of greater range of the electrostatic interactions with respect to the dimensions of the simulation box were performed following the method employed by Boda and coworkers (Boda et al., 1998). Additionally, the imposition of periodic boundary conditions in the X and Y directions requires the Coulombic forces of the "outside" ions to be accounted for. Therefore, each ion and charged group on the surface had an associated charged sheet of infinite dimensions outside the simulation box, parallel to the impenetrable walls. Figure 3.2 depicts a schematic of the long-range corrections.

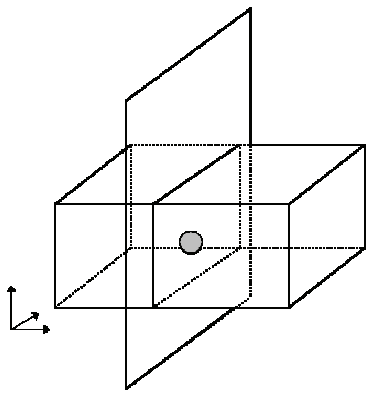

Figure 3.2 Schematic of the long-range corrections of electrostatic forces.

Each ion in the simulation box has a potential energy due to the presence of infinite charged sheets associated with all the charged species present in the system given by the following expression:

$$v_i = u_{i,jcsh}\left(z_i, z_j, \infty\right) - u_{i,jcsh}\left(z_i, z_j, L\right) \tag{3.3}$$

where $u_{i,jcsh}(z_i,z_j,\infty)$ and $u_{i,jcsh}(z_i,z_j,L)$ are the interaction energy between ion *i* and an infinitely charged sheet associated to ion *j*, and the interaction energy between ion *i* and a charged sheet of dimensions L x L associated to ion *j*, respectively. z_i and z_j correspond to the distances of ions *i* and *j* from the charged wall (i.e., the wall at z = 0). The expression for $u_{i,jcsh}(z_i,z_j,L)$, for example, is given by the following expression:

$$u_{i,jcsh}\left(z_i, z_j, L\right) = \frac{Q_i Q_j}{L^2} \int_{-L/2}^{L/2} \int_{-L/2}^{L/2} \frac{dxdy}{r} \tag{3.4}$$

where r is the vector that points from the unit area $dx \bullet dy$ of the sheet to ion i.

The chosen approach for the long-range corrections seemed to be more appropriate for the simulation of EDL in the sense that it does not employ distribution functions for the ions obtained during previous steps, like the methods proposed by other researchers (Valleau and Cohen, 1980; Valleau et al., 1980; Torrie and Valleau, 1980; Torrie et al., 1982). Therefore, it guarantees the random character of the CMC simulations. For a more detailed description of the mathematical treatment of long-range corrections and the ions near charged surfaces, the original references cited in this work should be consulted.

3.2.3 Simulation Parameters

As described earlier, one of the impenetrable walls was discretely charged by the presence of negatively charged groups on the surface (with a diameter of 3 Å) at a varying density of 1, 2, 3, and 4 ions per square nanometer (equivalent to surface charge values from –16.02 to –64.08 $\mu C/cm^2$). These values are typical for silica at different conditions of pH (Craven, 2000) and they are larger than those encountered in most simulations. The indifferent electrolytes were of three types: 1:1, 2:1, and 3:1. The coions were hydrated and monovalent, with a diameter of 4.25 Å, whereas the counterions had different hydrated diameters depending on their charge. Monovalent counterions had a diameter of 4.25 Å, divalent counterions had a diameter of 6 Å, and trivalent counterions had a diameter of 9 Å. The sizes of the ions were selected in order

to specifically target the effect of the size and charge of the ions on the structure of the electrical double layer.

Several trial simulations were performed in order to define the simulation parameters. The goal was to produce results that were independent of the system size and to allow bulk fluid conditions to be developed inside the simulation box, away from the charged wall. The simulation parameters investigated were number of ions in the system, ratio of width to length (W/L), and acceptance ratio (number of accepted moves divided by the total number of moves attempted). These parameters play a very important role in the reliability and reproducibility of the simulation results. The number of ions used is limited by two factors: a minimum number of ions have to be included in any simulation for the results to be independent of the system size. Additionally, increase in the number of ions in the simulation box results in exponential increase of the computation time. The selection of ions in each case responded to both restrictions. All the simulations were performed with 500 to 1000 ions and charged groups present in the system.

The ratio of the dimension W (width of the simulation box in the Z direction) to L (length of the simulation box in the X direction) was kept above 15 in all cases. The length of the simulation box, L, was 30 Å. As the ionic strength (i.e., concentration of ionic species in the system) diminishes, the ratio W/L had to be increased. In the case of simulations at an ionic strength of 0.1, M for example, a W/L ratio of 45 was employed. The W/L parameter is important because it enables the development of bulk conditions in the center of the simulation box away from both the charged surface and the uncharged

impenetrable wall. The zone of bulk condition has to be thick enough to minimize the effect of the presence of an impenetrable wall at the other end of the simulation box (i.e., at z = W).

It is common practice in Monte Carlo simulations to work with an acceptance ratio of less than 0.30. One of the reasons is that a smaller acceptance ratio implies the performance of a small number of large moves of ions. This allows a better sampling of the phase space and, therefore, computationally it is more cost effective (Allen and Tildesley, 1990).

Finally, an equilibration period greater than 80% of the total run time was used in order for results to be considered for averaging purposes. This parameter was determined after several trial simulations where the development of the value of the potential energy for the whole system was monitored in terms of computation time.

The simulations were performed by a code developed in Fortran 90/95 under a UNIX environment run on high performance computers (IBM and SGI Origins 3000). An example of one of those codes can be found in the Appendix of the present work along with some algorithms employed during the simulations. Table 3.1 presents a summary of the simulations performed in this work that were selected for discussion.

Table 3.1 Summary of simulations performed for EDL structure calculations.

Electrolyte Surface Charge	1:1	2:1	3:1	1:1+2:1	1:1+3:1	1:1+2:1+3:1
–16.02 μC/cm^2 1 site/nm^2	C	C C,S	C C,S	C C,S	C C,S	C C,S
–64.08 μC/cm^2 4 sites/nm^2	C	C C,S	C C,S	C C,S	C C,S	C C,S

C = only the charge of the ions was taken into account. C,S = both charge and size of the counterions were taken into consideration.

Some simulations were performed at the intermediate surface charge values of –32.04 μC/cm^2 (2 sites/nm^2) and –48.06 μC/cm^2 (3 sites/nm^2), and some other simulations were performed for 2:2 electrolytes. However, those results are not discussed in the present chapter.

All the results discussed in this chapter are presented in terms of dimensionless concentration profiles (C/C_0, ratio of the local concentration of a particular ion to the concentration of that ion in bulk conditions) with respect to distance z (in angstroms) from the surface.

3.3 EDL structure in the presence of a single electrolyte

First, CMC simulation results for a 1:1 electrolyte were compared with predictions from the classical theory on concentration profiles with distance from the surface (z) at different bulk concentrations or ionic strengths. Since no direct experimental data for the

structure of the EDL in terms of concentration profiles have been obtained so far, the comparisons pursued validating the simulation protocol proposed in this work as well as testing its reliability. The conditions used for comparison comply with the range of applicability of the Poisson-Boltzmann equation for the description of the EDL. Then, the structure of the EDL double layer was obtained in the cases of pure 2:2 symmetric electrolytes, and pure 2:1 and 3:1 asymmetric electrolytes.

3.3.1 EDL structure in the presence of a 1:1 electrolyte: CMC simulations versus MGC theory predictions.

As discussed in Chapter 2, the MGC theory includes the definition of a closest distance of approach of ions to the surface, in this case the hydrated ionic radius (2.125 Å). Therefore, the domain of the solution of the PB equation is [2.125 Å, ∞[, and it is given by the following analytical expression:

$$\tanh\left(\frac{\nu\bar{e}\psi}{4k_BT}\right) = \tanh\left(\frac{\nu\bar{e}\psi_\delta}{4k_BT}\right)\exp\left[-\kappa\left(z-\frac{d}{2}\right)\right] \tag{3.5}$$

where ψ and ψ_δ are the potentials at any distance z away from the surface and at the distance of maximum approach of the hydrated counterion, respectively; q is the absolute value of the valence of the counterion or coion; κ is the Debye length introduced in Chapter 2; and d is the hydrated diameter of the counterion. This equation was solved numerically via the application of the Newton-Raphson method, and the potential profiles

obtained were employed in the calculation of the concentration profiles of the counterions and the coions via the application of the Boltzmann distribution:

$$\frac{n}{n_0} = \exp\left[-\frac{\nu \bar{e} \psi}{4 k_B T} \right] \tag{3.6}$$

Although comparisons between molecular simulation results and classical theory are usually performed in terms of a corrected distance (i.e., the distance divided by the radius of the hydrated counterion) from the surface in order to account for the fact that the classical theory considers ions to be point charges (Valleau and Cohen, 1980; Valleau et al., 1980; Torrie and Valleau, 1980; Torrie et al., 1982; Boda et al., 1998), the comparisons of simulation results with calculations based on the MGC theory are shown as concentration profiles with actual distance in this work.

Figure 3.3 presents the results for the concentration profiles of counterions and coions at 0.1 and 1.0 M and a discrete surface charge equivalent to –16.02 μC/cm^2. There is qualitative agreement between MGC theory predictions and CMC simulation results. The local concentrations of counterions at the closest distance to the surface have almost the same values for both electrolyte solutions. Discrepancies exist at further distances because the MGC predicts an abrupt decay in concentration towards the bulk concentration value (i.e., a thinner EDL thickness), while the CMC simulations predict a greater EDL thickness. These discrepancies are a consequence of ions being considered point charges within the MGC theory formulation. In the case of the lower concentration (0.1 M), depicted in Figure 3.3(a), the EDL extends for 100 Å, while an EDL thickness of

approximately 50 Å is predicted by the MGC. The EDL extends for 50 Å in the case of the higher concentration (1 M), depicted in Figure 3.3(b), but an EDL thickness of only 20 Å is predicted by the MGC. It is interesting to note that concentrations of coions reach bulk conditions faster than counterions in both cases for the CMC simulations. This is a direct result of the correlations between ionic species that are not taken into account in the MGC model. High local concentrations of counterions result in a larger presence of coions than expected.

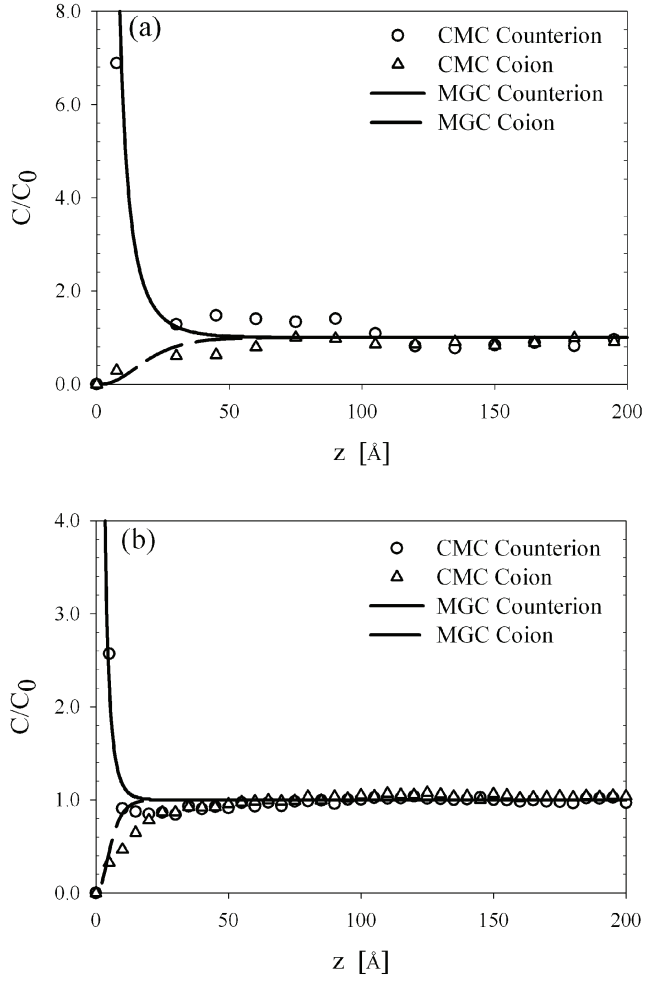

Figure 3.3 Concentration profiles obtained via CMC simulations and MGC theory calculations for a planar surface with an equivalent surface charge of –16.02 μC/cm^2 and 1:1 electrolyte at concentrations of (a) 0.1 M and (b) 1.0 M. *(Taboada-Serrano et al., 2005b)*

Finally, the fact that the surface is discretely charged leaves some open space for coions to get closer to the surface, where the effects of the surface charged groups are not as strong.

3.3.2 EDL structure in the presence of asymmetric electrolytes

Figure 3.4 presents the structure of the EDL for solutions containing 1:1, 2:1, or 3:1 electrolytes of concentration 0.1 M.

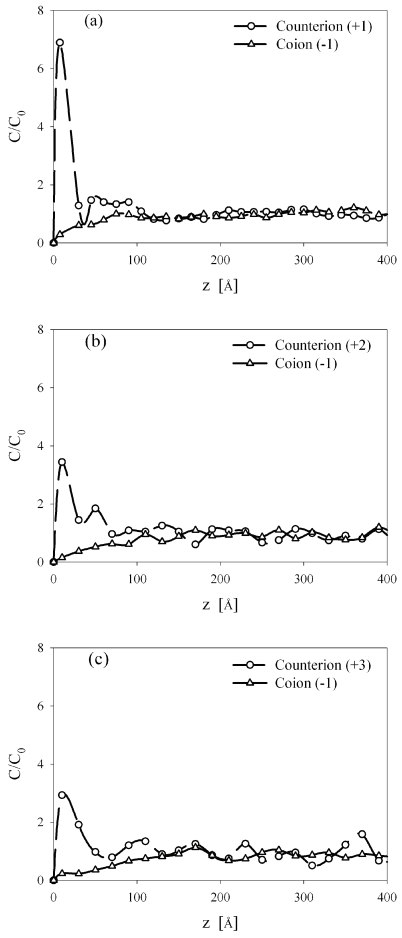

Figure 3.4 EDL structure at low surface charge (equivalent to –16.02 μC/cm^2), as shown in concentration profiles for 0.1 M solutions of (a) 1:1, (b) 2:1, and (c) 3:1 electrolytes. *(Taboada-Serrano et al., 2005b)*

The monovalent counterions and coions had a diameter of 4.25 Å, the divalent counterions had a diameter of 6 Å, and the trivalent counterions had a diameter of 9 Å. The extension of the EDL layer in each of the cases is a function of the size of the counterion. Simulations of counterions with different charge but the same diameter (results not shown) did not show differences in the thickness of the double layer.

Since divalent counterions have a larger capacity to screen the surface charge, the local concentration of divalent counterions next to the charged surface, as seen in Figure 3.4(b), is almost half of the value of the local concentration of monovalent counterions next to the surface, as seen in Figure 3.4(a). The value of the local concentration next to the surface is almost the same as the one obtained for simulations with a 2:2 electrolyte (results not shown). However, the local concentration of trivalent counterions next to the surface, as shown in Figure 3.4(c), does not correspond to a third of the value for monovalent counterions, as seen in Figure 3.4(a), as one would expect. Repeated simulations with different intervals for sampling to construct distribution functions and concentration profiles gave the same result. The simulations with 3:1 electrolyte seem to result in an oscillatory behavior. Although overall bulk conditions are achieved within the simulation box, there are regions where depletion of trivalent ions or accumulation of trivalent ions occurs. This effect might result from the ion–ion correlations and the size difference between counterions and coions. Trivalent counterions repel one another very strongly and are excluded from larger volume portions. Because of their smaller size, monovalent coions, however, are able to fill in empty spaces. Local accumulation of

coions in a fluid layer might result in local accumulation of counterions in the subsequent fluid layer followed by depletion of counterions further away.

3.4 EDL structure in mixtures of symmetric and asymmetric electrolytes

Simulations were performed with mixtures of different composition in an attempt to model real electrolyte solutions. The mixtures were 1:1 and 2:1 electrolytes; 1:1 and 3:1 electrolytes; and 1:1, 2:1 and 3:1 electrolytes. Besides analyzing the specific effect of size of the ions composing the electrolytes under study, we focused on the effect of the surface charge strength on the structure of the electrical double layer.

3.4.1 Mixtures of symmetric and asymmetric electrolytes: charge versus size

Figure 3.5 presents the concentration profiles for the EDL formed by a mixture of a 1:1 and a 2:1 electrolyte at an ionic strength of 1 M. When the difference in size between monovalent and divalent ions is not taken into account [i.e., in Figure 3.5(a)] the divalent ions have the same capacity as the monovalent ions to get close to the surface. A higher local concentration of divalent ions is detected close to the surface because it is energetically more favorable for the higher–valence ions to screen the surface charge. However, if the difference in size of the ions is taken into consideration [i.e., in Figure 3.5(b)], size is an important factor. Divalent ions are larger in this case (they have a diameter of 6 Å compared to 4.25 Å for the monovalent ions), and their larger size

prevents them from getting as close to the surface as their monovalent peers. In this case, the local concentration of monovalent ions is almost as high as the one of divalent ions, and it decays rapidly at higher separations from the charged surface. In regions further away from the surface, most of the screening of surface charge is done by divalent ions. Note that the EDL is approximately 15 to 20 Å in this case. The EDL thickness for the 1:1 electrolyte at the same ionic strength (1 M) was calculated to be approximately 50 Å.

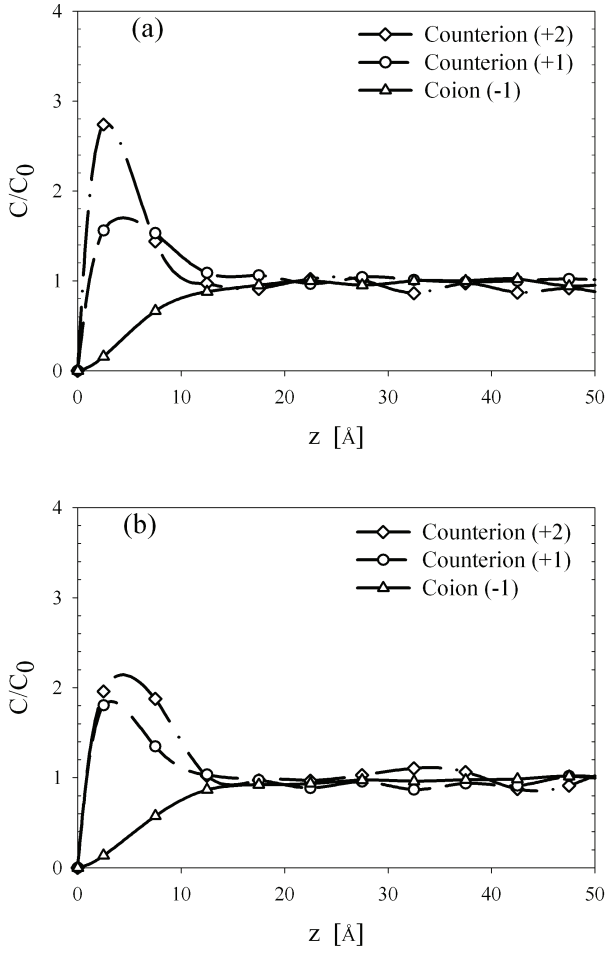

Figure 3.5 EDL structure at low surface charge (surface charge equivalent to –16.02 μC/cm^2) in mixtures of 1:1 and 2:1 electrolytes at an ionic strength of 1.0 M for (a) monovalent and divalent counterions of equal diameter (4.25 Å), and (b) 4.25–Å–diameter monovalent counterions and larger (6–Å–diameter) divalent counterions. *(Taboada-Serrano et al., 2005b)*

Figure 3.6 presents the same behavior for the structure of the EDL formed by a mixture of a 1:1 and a 3:1 electrolyte at an ionic strength of 1 M. When the size of the trivalent ions is not taken into consideration, as depicted in Figure 3.6(a), the trivalent counterions get very close to the surface and screen most of the surface charge. The concentration of monovalent counterions close to the surface is almost equal to the bulk concentration.

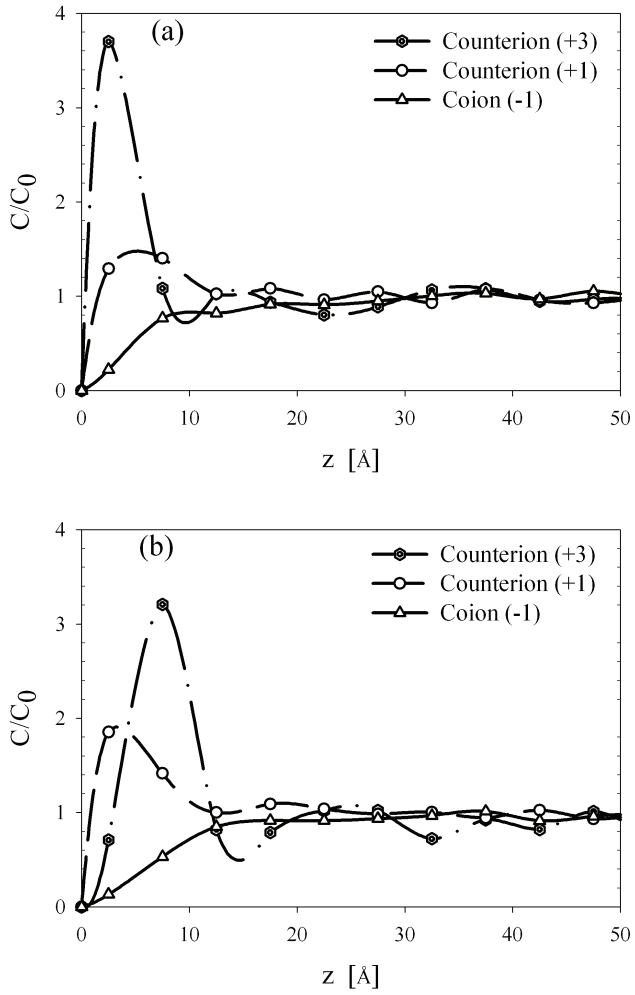

Figure 3.6 EDL structure at low surface charge (surface charge equivalent to –16.02 μC/cm^2) in mixtures of 1:1 and 3:1 electrolytes at an ionic strength of 1.0 M for (a) monovalent and trivalent counterions of equal diameter (4.25 Å), and (b) 4.25–Å–diameter monovalent counterions and larger (9–Å–diameter) trivalent counterions. *(Taboada-Serrano et al, 2005b)*

The capacity of trivalent ions to screen the charge is comparatively larger than that of divalent ions, depicted in Figure 3.6(a), as one would expect. Basically, only the first layer of fluid next to the surface presents a peak local concentration of trivalent ions. However, the trivalent counterions are twice as large in diameter as the monovalent counterions. When one takes the size of the ions into account, as depicted in Figure 3.6(b), the monovalent counterions are able to get closer to the surface. One can see a first layer of fluid next to the charged surface dominated by the presence of monovalent counterions, while the local concentration of trivalent counterions peaks in the second layer of fluid. The thickness of the EDL in the case of 1:1 and 3:1 electrolyte mixtures is approximately 15 Å, smaller than that for mixtures of 1:1 and 2:1 electrolytes as one would expect.

Figure 3.7 presents the EDL structure in the case of mixtures of 1:1, 2:1, and 3:1 electrolytes at an ionic strength of 1 M. Figure 3.7(a) presents the case in which ions have the same diameter (i.e., the same capacity to get close to the surface). As expected, trivalent counterions screen most of the surface charge, while the local concentration of monovalent counterions is barely higher than the bulk concentration. In Figure 3.7(b), when the size of the ions is taken into consideration, an "ordering" of ions according to their size can be observed. Monovalent counterions can get closer to the surface than their trivalent peers. The difference in radius between monovalent and divalent counterions is not very large (less than 1 Å). Therefore, both species achieve peak concentrations in the first layer of fluid next to the surface. This behavior is very similar to that observed in Figure 3.5(b) for mixtures of 1:1 and 2:1 electrolytes. The

concentration of trivalent counterions peaks in the second layer of fluid next to the surface, and its value is comparatively smaller than that in Figure 3.7(a). This finding would be expected because some screening of the surface charge has already been performed by smaller ions in the system.

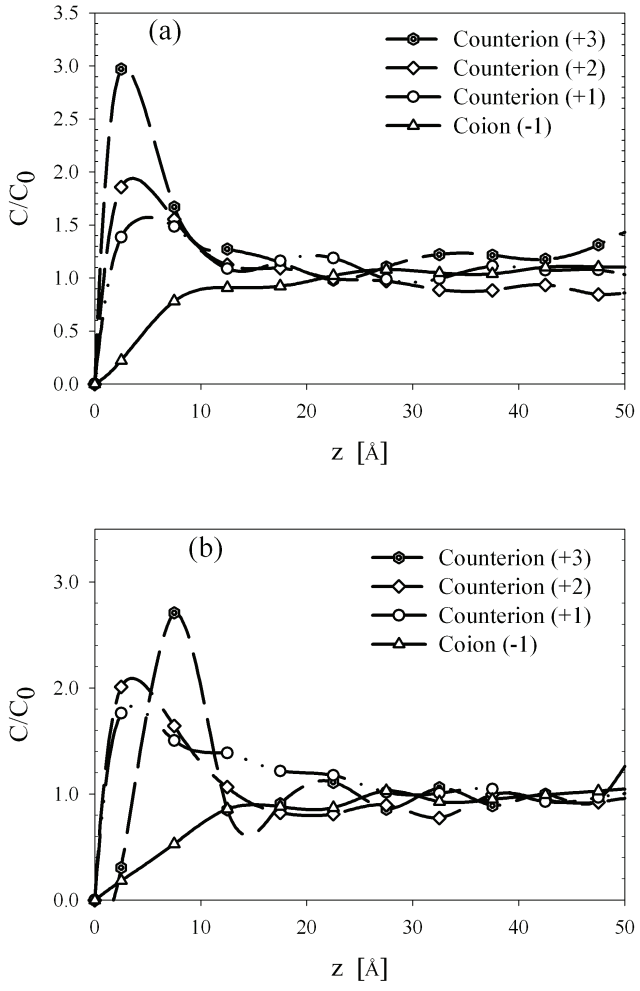

Figure 3.7 EDL structure at low surface charge (surface charge equivalent to –16.02 μC/cm^2) in mixtures of 1:1, 2:1, and 3:1 electrolytes at an ionic strength of 1.0 M for (a) monovalent, divalent and trivalent counterions of equal diameter (4.25 Å), and (b) 4.25–Å–diameter monovalent counterions, and larger (6–Å–diameter) divalent ions and (9–Å–diameter) trivalent ions. *(Taboada-Serrano et al., 2005b)*

The size of the ions plays a determining role on the species screening the surface charge and the structure of the EDL in terms of local concentrations of ionic species. Size and charge of counterions have an opposing effect: although charge favors higher–valence ions in terms of screening of charge, ions bearing higher charge are usually larger, and their size prevents them from getting close to the charged surface.

3.4.2 Surface charge and EDL structure in mixtures of symmetric and asymmetric electrolytes

The results presented in this section depict the effect of surface charge on the structure of the EDL formed by mixtures of symmetric and asymmetric electrolytes when the different size of monovalent, divalent, and trivalent ions is considered.

Figures 3.8(a) and 3.8(b) present the EDL structure in terms of concentration profiles for mixtures of 1:1 and 2:1 electrolytes at an ionic strength of 1 M and surface charges equivalent to –16.02 and –64.08 $\mu C/cm^2$, respectively. While there is a comparable high local concentration for monovalent and divalent counterions next to the surface in the case of the lower surface charge, as depicted in Figure 3.8(a), the higher surface charge in Figure 3.8(b) results in a very high local concentration of monovalent counterions in the first layer of fluid next to the surface. The monovalent counterions that are smaller in size are able to get closer to the surface and perform most of the screening of surface charge, as shown in Figure 3.8(b).

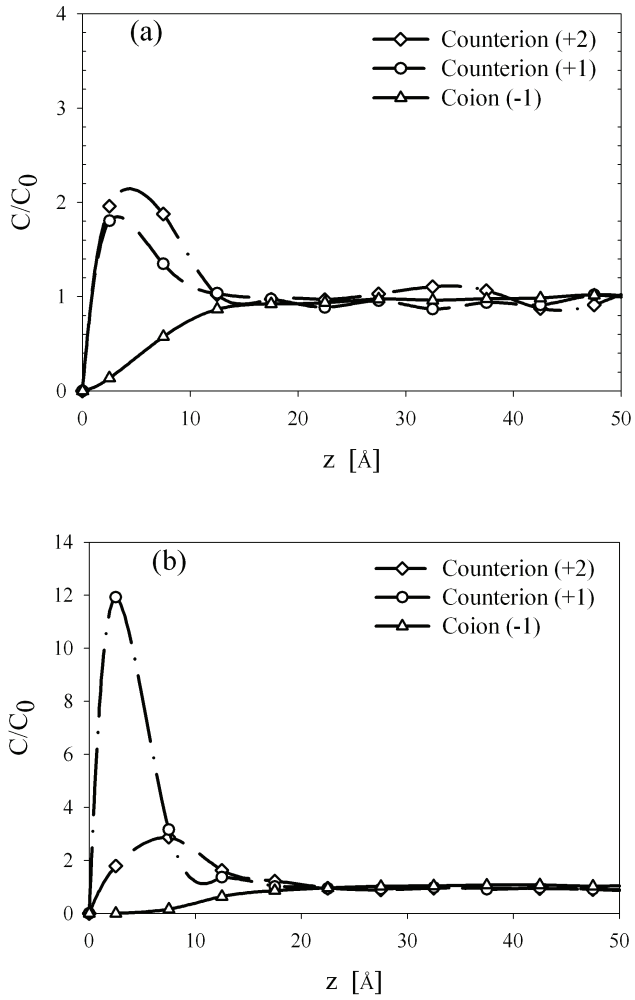

Figure 3.8 Effect of surface charge on the EDL structure of mixtures of 1:1 and 2:1 electrolytes at an ionic strength of 1.0 M for surface charges equivalent to (a) –16.02 μC/cm^2 and (b) –64.08 μC/cm^2. *(Taboada-Serrano et al., 2005b)*

Figures 3.9(a) and 3.9(b) depict the same kind of behavior for mixtures of 1:1 and 3:1 electrolytes at an ionic strength of 1 M and surface charge values of –16.02 and –64.08 μC/cm^2, respectively. The size difference between monovalent counterions (with a diameter of 4.25 Å) and trivalent counterions (with a diameter of 9 Å) increases the effect of size on the distribution of ionic species in the EDL. Figure 3.9(a) shows a first peak of local concentration of monovalent ions in the first layer of fluid next to the surface,

followed by a peak in concentration of trivalent counterions in the second layer of fluid next to the surface. In this case, the local concentration of trivalent counterions is still larger than that of monovalent counterions. However, for the case of higher surface charge, a very large concentration peak occurs for the monovalent counterions on the first layer of fluid next to the surface, as depicted in Figure 3.9(b). The concentration of trivalent counterons is barely higher than that at bulk conditions.

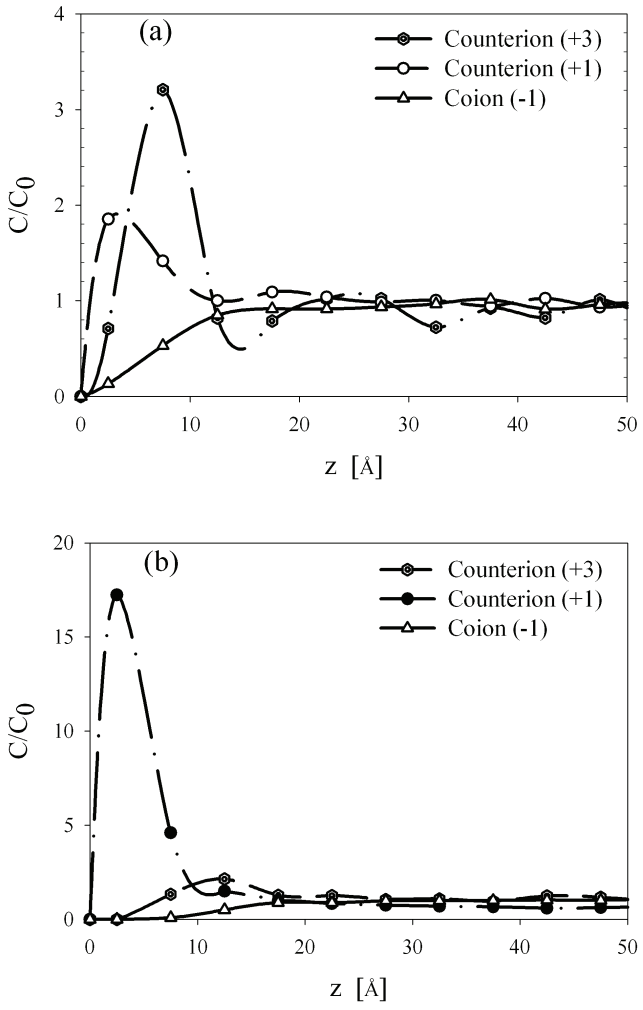

Figure 3.9 Effect of surface charge on the EDL structure of mixtures of 1:1 and 3:1 electrolytes at an ionic strength of 1.0 M for surface charges equivalent to (a) –16.02 μC/cm^2 and (b) –64.08 μC/cm^2. *(Taboada-Serrano et al., 2005b)*

The same behavior can be observed in the case of mixtures of 1:1, 2:1, and 3:1 electrolytes at low and high surface charge and an ionic strength of 1 M (Figure 3.10). The higher surface charge enhances the "ordering" in peak concentrations detected at low surface charge. Monovalent counterions get closer to the surface and perform almost all the screening of surface charge in the first couple of layers of fluid next to the surface.

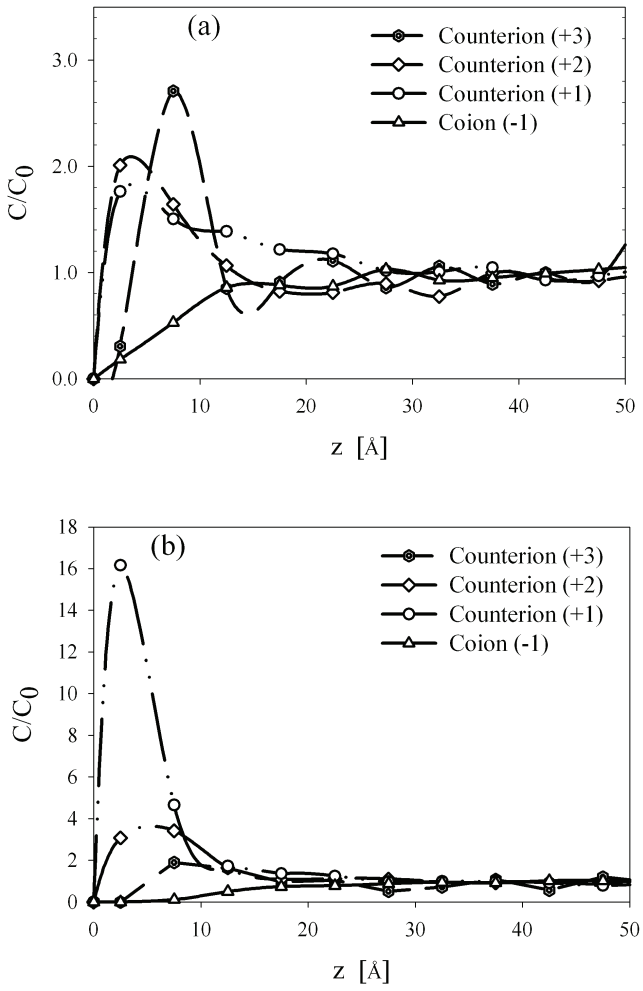

Figure 3.10 Effect of surface charge on the EDL structure of mixtures of 1:1, 2:1, and 3:1 electrolytes at an ionic strength of 1.0 M for surface charges equivalent to (a) –16.02 μC/cm^2 and (b) –64.08 μC/cm^2. *(Taboada-Serrano et al., 2005b)*

3.5 Conclusions

The consideration of discrete charge on the planar surface resulted in ions being able to get closer to the surface in the regions where no charged group was to be found. That also allowed coions to get closer to the surface. The distribution of ions in the X and Y directions did not show any coupling between negatively charged surface groups and positively charged counterions. This fact might result from the high temperature (298 K) in the present simulation system in contrast to the MD simulations by Messina, which were performed at ground state and temperatures close to ground state (Messina, 2002).

The size of the ionic species forming the EDL plays a determining role in its structure. The extent of the EDL, or EDL thickness, is determined not only by the concentration of ions or ionic strength in the system but also by the size of the ions and their associated charge. The prediction of the classical theory that the EDL thickness is proportional to the ionic strength is qualitatively correct. However, the size of the ions changes the functionality of that proportion. Furthermore, when mixtures of electrolytes of different sizes and charges are involved, the thickness of the EDL seems to be reduced by the availability of more than one charged species to screen the surface charge even if the ionic strength is the same as that of solutions involving only one electrolyte.

The size of the ionic species present in the system also plays an important role in the species involved in the screening of the surface charge, specifically in the nature of the ions and their concentrations in the first layers of fluid adjacent to the surface. Although

it is energetically favorable for surface charge to be screened by higher-valence ions, their larger size prevents them from getting close to the surface. Therefore, lower-valence ions with smaller sizes are able to screen most of the surface charge in the first layer of fluid adjacent to the charged surface. A size exclusion effect is observed that is contrary to the energetic effect. In the case of mixtures, ordering of counterions occurs next to the surface in terms of size. Monovalent and divalent ions can be found in the first layer of fluid next to the surface, while trivalent counterions can be found in the second layer of fluid next to the surface. In the case of low surface charge, the screening of surface charge is performed within a length that includes several layers of fluid adjacent to the surface with concentrations of different ionic species peaking at different distances from the charged surface according to their sizes. On the contrary, at very high surface charges, most of the screening of the surface charge is done within the first or second layer of fluid adjacent to the surface. Therefore, a marked difference in the peak concentration of monovalent ions is noted with respect to their divalent and trivalent peers. In that case, the EDL is composed mostly of monovalent ions. The size exclusion effect is enhanced as the magnitude of surface charge increases. It is interesting to note that as the surface charge increases, the EDL might as well be described in terms of monovalent ions present in the system, even if other ionic species are present.

The effects of ion size and surface charge on the structure and distribution of ionic species near charged surfaces have further implications. Interactions between charged surfaces are in part determined by the overlap of their associated EDLs. The thickness of the EDL determines the range of those interactions, and the local concentrations of ionic

species play an important role in the osmotic component of the interactions (Israelachvili, 1998; Belloni, 2000). The higher the valence of the ion, the smaller number concentration of ions required to screen the surface charge. However, the size exclusion effect noted earlier implies that smaller ions in larger numbers do preferentially participate in the EDL structure, therefore affecting the forces associated with them via the osmotic term.

The present work deals only with indifferent electrolytes (i.e., electrolytes that remain fully hydrated and do not adsorb onto charged surfaces). However, depending on the surface charge, divalent and trivalent ions dehydrate next to charged surfaces and undergo adsorption (Hiemenz and Rajagopalan, 1997; Kallay and Žalac, 2000). Because they are much smaller than fully hydrated ions, the dehydrated ions get in contact with the surface inside what is called the inner Helmhotz plane (the region immediately adjacent to the surface). This phenomenon changes the nature of the surface charge, the electrical double layer, and, therefore, the nature of the interparticle interactions.

When electrosorption occurs, it may be more energetically favorable for higher-valence ions of larger sizes to dehydrate and screen the surface charge than for smaller hydrated ions to screen the surface charge at longer separation distances. However, at large surface charges, where ion exclusion effects are stronger, dehydration and subsequent adsorption of higher–valence ions may be hindered.

3.6 Summary

In this part of the work, CMC simulations were performed to study the EDL structure of discretely charged planar surfaces in the presence of symmetric and asymmetric indifferent electrolytes.

Asymmetry in charge involves asymmetry in size. The size of the ionic species present in the EDL plays an important role not only in the extension or thickness of the EDL but also in local concentrations of ions in the EDL. Although the phenomenon is energetically less favorable, preferential screening of surface charge by smaller ions has been detected (i.e., the size exclusion effect) and it is enhanced at higher values of surface charge. In such conditions, the EDL is almost completely formed by monovalent ions, even if other ionic species are present. The size exclusion effect may be a reason that adsorption occurs, since that process, including dehydration of higher–valence ions and their placement adjacent to the surface, might result in lower energies compared with those encountered during the screening of charge by ions of low valence.

The implications of the presence of symmetric and asymmetric electrolytes in the EDLs of interacting charged particles will be analyzed in subsequent chapters in the case of both, indifferent and non-indifferent electrolytes.

CHAPTER 4

ELECTRICAL DOUBLE LAYER INTERACTIONS: A SPHERICAL PARTICLE AND A PLANAR SURFACE

4.1 Introduction

The electrostatic interactions between charged surfaces and interfaces result from the overlap of their associated electrical double layers. The classical theory, or Derjaguin-Landau-Verwey-Overbeek (DLVO) theory, models the electrostatic interparticle interactions via the solution of the Poisson-Boltzmann (PB) equation for the distribution of charge in the region between the interacting surfaces and, through the Boltzmann distribution, the distribution of ionic species (Derjaguin and Landau, 1941; Verwey and Overbeek, 1948; Elimelech et al., 1995; Hiemenz and Rajagopalan, 1997; Israelachvili, 1998; Hunter, 2001;). Since ions are considered point charges during the derivation of the PB equation, there is no restriction in the accumulation of ions in the region of interaction, which results in an increasingly higher osmotic force term of repulsive nature as the surfaces get closer (Israelachvili, 1998). Therefore, the classical theory predicts electrostatic repulsion between two similarly charged surfaces regardless of the nature of the ionic species present in the system.

Although the modified Gouy-Chapman theory (MGC) considers a maximum distance for the approach of counterions to charged surfaces, thus introducing a correction with respect to the size of the counterions, this concept has not been introduced when dealing with interacting surfaces. Most of the work within the framework of the classical theory has focused on developing simpler and more accurate mathematical procedures to solve the PB equation in the space between interacting charged surfaces (Ohshima, 1994; Haughey and Earnshaw, 1995; Stankovich and Carnie, 1996; Ohshima, 1997; Jönsson and Ståhlberg, 1999) or in considering different possibilities in terms of surface charge density (Grant and Saville, 1995). The effects of the mean-field character of the PB equation, i.e., the consideration of ions as point charges, on the EDL interactions between charged surfaces has not been examined. However, there has been an attempt to introduce the ion-ion correlation effects to the PB equation within the mean-field approximation through a semi-empirical effective interaction potential that replaces the Coulombic interaction potential originally used in the derivation of the PB equation (Forsman, 2004).

The work discussed in Chapter 3 leads to the conclusion that the size of the ions forming the EDL determines its structure, not only in terms of the EDL thickness, but also in terms of the composition of the layers of fluid comprising the double layer. At high surface charge densities, ion exclusion effects were detected, i.e., smaller ions with associated lower valences did preferentially screen the surface charge over larger ions with higher valences. The effects of the size of the ions should be noticeable in the case of interacting double layers where there are also spatial constraints. The space between

the interacting surfaces available for counterions and coions gets increasingly smaller as the surfaces approach each other.

EDL overlap occurs not only during the interaction of solid-liquid interfaces and charged surfaces, buy also inside the pores of materials that develop surface charge or materials comprising electrodes. In fact, the occurrence of EDL overlap inside porous structures is the main reason for the discrepancies between experimentally measured porous electric capacitances and those predicted via the application of the PB equation inside nanopores and micropores (Ying et al., 2001). Therefore, most of the molecular simulation work dealing with EDL overlap has focused on the occurrence of EDL overlap inside porous structures (Jamnik and Vlachy, 1993; Hribar et al., 2000; Yang et al., 2002a, 2002b). One of the main conclusions of this simulation effort is that the exclusion of ions from inside the pores occurs as the surface charge density or the solid-liquid interface potential increases and as the diameter of the pores gets smaller. The same phenomenon should be observed between interacting surfaces. All the work cited here dealt with 1:1 electrolytes of ion diameters between 1 and 4.25 Å, so the specific effects of ion size and charge have not been addressed so far.

In this part of the work, the EDL structure of two interacting surfaces in symmetric and asymmetric electrolytes is examined via CMC simulations. A spherical particle and a planar surface were selected for the study, not only because these geometries are fairly common in most processes involving colloidal particles, but also because the interactions can be experimentally obtained via direct measurements of the interaction force, as

discussed in Chapter 2. The objective of the study is to identify the effect of size and charge of the ions within the electrolyte solution on EDL interactions.

4.2 CMC simulations of the interaction of a spherical particle and a planar surface

The same scheme used in Chapter 3 for the CMC simulation of the EDL structure of discretely charged planar surfaces was adopted in this part of the work.

4.2.1 Simulation box

The simulation box described in Chapter 3 was modified via the introduction of a spherical charged particle in the system, as depicted in figure 4.1.

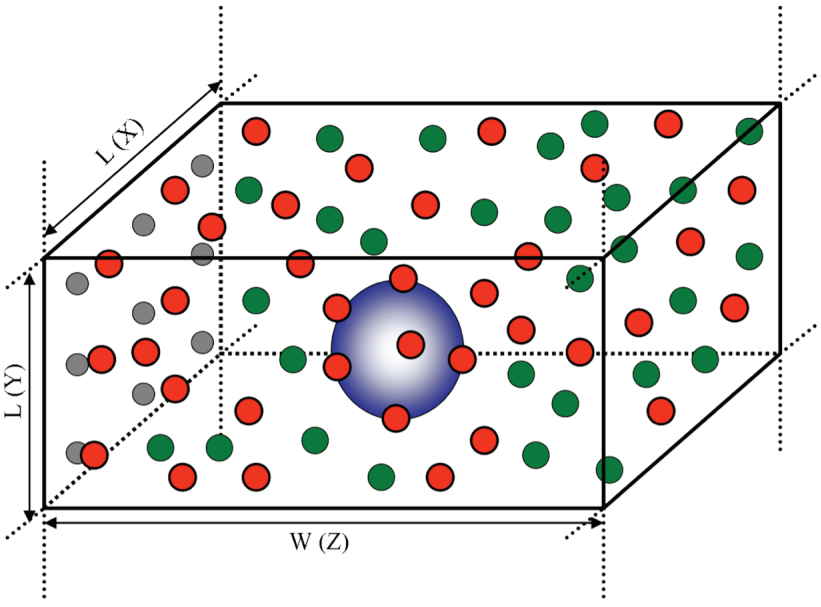

Figure 4.1 Schematic of the simulation box used in the CMC simulation of the interaction between a charged spherical particle and a planar surface.

In the schematic, the big gray shaded sphere represents the spherical colloidal particle, the white spheres represent counterions, the gray spheres represent coions, and the dark gray spheres represent the charged groups on the planar surface. As in the previous case, periodic boundary conditions and the minimum image convention were applied in the X and Y directions (Allen and Tildesley, 1990), while the Z direction was enclosed between two hard, impenetrable walls. The dimensions of the simulation box were modified, specifically the ratio of width (W, in the Z direction) to length (L, in the X direction) and height (L, in the Y direction), in order to achieve bulk conditions in all directions surrounding the spherical particle. The wall is assumed to be of infinite dimensions, so only the presence of the EDL associated to the planar surface was detected in the X and Y directions away from the colloidal particle.

4.2.2 Potential energy of the system

The potential energy of the system was calculated as the sum of individual potential energies associated with the position of each ionic species and colloidal particle in the simulation box and the sum of the pair-wise interactions of all the ionic species present in the simulation box including the ions on the charged wall and the colloidal particle, according to equation 3.1.

4.2.2.1 Interaction potential between charged colloidal particle and the ionic species and charged groups

The ions and charged groups on the surface were modeled as charged hard spheres, and their pair-wise interactions were calculated via the application of Coulomb's Law as described in Chapter 3 (equation 3.2).

The colloidal particle was modeled as a charged hard sphere, or macroion, with the charge concentrated at the center of the particle (Crocker and Grier, 1996; Stevens et al., 1996; D'Amico and Löwen, 1997; Lobaskin and Linse, 1998; Wu et al., 1999; Terao and Nakayama, 2001; Angelescu and Linse, 2003). Therefore, the interactions of the colloidal particle with all charged species and groups are given by Coulomb's Law:

$$v_{iM} = \begin{cases} +\infty & r_{iM} < \sigma_{iM} \\ \dfrac{Q_i Q_M}{4\pi\varepsilon_0 \varepsilon\, r_{iM}} & r_{iM} \geq \sigma_{iM} \end{cases} \tag{4.1}$$

where v_{iM} is the pair interaction potential of ions i and the colloidal particle M, r_{iM} is the distance between the centers of ions i and the colloidal particle M, σ_{iM} is the maximum distance of approach between the ions i and the colloidal particle M (i.e., the square root of the sum of the respective radii squared), Q_i and Q_M are the charges of ions i and the colloidal particle M, respectively, and ε_0 and ε correspond to the permittivity of vacuum and relative permittivity of the solvent.

4.2.2.2 Long-range corrections of Coulombic interactions

The long-range corrections required due to the possibility of the range of the Coulombic interactions exceeding the dimensions of the simulation box and due to the prevalence of periodic boundary condition, was performed in the way described in Chapter 3, i.e. each ion and charged group in the system had an infinitely charged sheet associated with it outside the central simulation box (see Figure 3.2 in Chapter 3).

Although the interactions of the colloidal particle with all the infinitely charged sheets associated with all the ions and charged groups inside the central simulation box were accounted for in the calculation of the total potential energy of the system, the colloidal particle itself did not possess an associated charged sheet. The image boxes surrounding the simulation box contained only electrolyte solution; therefore, there were no replicas or images of the colloidal particle in the surrounding image boxes. However, since all the ions inside the central simulation box possessed associated charged sheets, one would expect that the configuration of the charged sheets reflected the presence of the EDL associated to the colloidal particle in the central simulation box.

The values for the width, height and length of the simulation box were selected in order to ensure the prevalence of bulk conditions inside the central simulation box in the X, Y, and Z directions away from the colloidal particle. Furthermore, bulk conditions were achieved over distances much larger than the diameter of the colloidal particle in an attempt to minimize the influence of the presence of images of the particle EDL in the

image boxes. In the calculation of the total potential energy of the system, the term containing the sum of the pair-wise interactions between the colloidal particle, ions and charged groups inside the central simulation box makes a much larger contribution to the potential energy than the term containing the interactions with the charged sheets associated to ions and charged groups outside the simulation box. Furthermore, if most of the ions within the central simulation box are either part of the bulk solution or the EDL of the infinite discretely charged planar surface, then the contribution of the interactions with the sheets associated to the ions forming the particle EDL is negligible. Therefore, the effect of the image repetition of the particle EDL on the total energy calculation was expected to be minimal.

4.2.3 Simulation parameters

In the simulations, one of the walls contained negatively charged groups of diameter of 3 Å. Three values of surface charge density were considered for the planar surface: –1.78 $\mu C/cm^2$, –2.04 $\mu C/cm^2$ and –5.23 $\mu C/cm^2$. The selection of these values, which are much smaller than the ones used in the study of the EDL structure, responds to the necessity to achieve bulk conditions in the system in all directions after the introduction of the colloidal particle. As in the previous study, 1:1, 2:1, and 3:1 electrolytes were used. The coions were hydrated and monovalent with a diameter of 4.25 Å, whereas the counterions had different hydrated diameters depending on their charge. Monovalent counterions had a diameter of 4.25 Å, divalent counterions had a diameter of 6 Å, and trivalent counterions had a diameter of 9 Å. Finally, the colloidal particle had a diameter of 30 Å

(i.e., the size typical of a nanoparticle), and the following absolute values of surface charge density: 5.67 $\mu C/cm^2$, 10.2 $\mu C/cm^2$ and 17.0 $\mu C/cm^2$.

Three main parameters affect the simulation results: the number of ions present in the system, the ratio of width to length (W/L), and the acceptance ratio. The number of ions in the simulations is affected by three factors in this case: a minimum number of ions is required for the results to be independent of the system size, an increment of number ions results in exponential increments in computational time, and, finally, a small number of ions might prevent the development of bulk conditions in all directions surrounding the colloidal particle. All the simulations were performed with 1000 to 2000 ions and charged groups in the system. One should note that these numbers are twice the number of ions reported in Chapter 3, although the surface charge densities employed here have much smaller values.

Several trial simulations were performed to investigate W/L ratios that would result in the development of bulk conditions surrounding the colloidal particle. The low values of surface charge of the planar surface and the particle resulted in good results at W/L ratios as low as 1.6; and the length of the simulation box was fixed at 300 Å. This value is much lower than the minimum value of 15 used in the study of the EDL structure of the planar surface, but the surface charge densities involved are at least one order of magnitude smaller as well.

Acceptance ratios of less than 30% were used, and averaging procedures were performed after 80% of the total run time was completed. These parameters agree with the ones reported in Chapter 3.

The simulations were performed by a code developed in this work in Fortran 90/95 under a UNIX environment that was run on high performance computers (SGI Origins 3000). Table 4.1 and Table 4.2 present a summary of the simulations performed in this work, some of which were selected for discussion later in this Chapter.

Table 4.1 Summary of the preliminary simulations performed for 1:1 electrolyte at an ionic strength of 0.1 M

Planar surface charge density [$\mu C/cm^2$]	Colloidal particle charge density [$\mu C/cm^2$]	Separation distance, D [Å]
–2.04	–5.7	$4d_M$ $2d_M$ d_M $(d_w+d_M)/2$
–2.04	–10.2	$4d_M$ $2d_M$ d_M $(d_w+d_M)/2$
–2.04	5.7	$4d_M$ $2d_M$ d_M $(d_w+d_M)/2$
–2.04	–10.2	$4d_M$ $2d_M$ d_M $(d_w+d_M)/2$

d_M corresponds to the diameter of the colloidal particle (30 Å), while d_w corresponds to the diameter of the charged groups on the planar surface (3 Å).

Basically, the distance between the planar surface and the center of the colloidal particle was fixed during each simulation. The ions were randomly placed inside the central

simulation box and trial moves were performed until thermodynamic equilibrium was established.

Table 4.2 Summary of the simulations performed with 1:1, 2:1, and 3:1 electrolytes at an ionic strength of 0.05 M

Electrolyte	Planar surface charge density [$\mu C/cm^2$]	Colloidal particle charge density [$\mu C/cm^2$]	Separation distance, D [Å]
1:1	–1.78	–5.67	$5d_M$ $4d_M$ $3.5d_M$ $3d_M$ $2.5d_M$ $2d_M$ $1.5d_M$ d_M $0.8d_M$ $0.75d_M$ $0.6d_M$ $(d_w+d_M)/2$
	–5.23	–17.0	$5d_M$ $4d_M$ $3.5d_M$ $3d_M$ $2.5d_M$ $2d_M$ $1.5d_M$ d_M $0.8d_M$ $0.75d_M$ $0.6d_M$ $(d_w+d_M)/2$
2:1	Id	Id	Id
3:1	Id	Id	Id
2:1 + 1:1	Id	Id	Id
3:1 + 1:1	Id	Id	Id
3:1 + 2:1 + 1:1	Id	Id	Id

Id implies identical conditions as the ones described in the preceding cell of the table.

The simulations summarized in Table 4.2 were simultaneously employed in the calculation of the electrostatic interaction force between the planar surface and the colloidal particle that will be presented and discussed in Chapter 5.

4.3 EDL overlap in the presence of a single electrolyte

Simulations with pure 1:1 electrolyte were employed in order to optimize the simulation parameters as well as to ensure that bulk conditions were obtained in all directions surrounding the colloidal particle.

4.3.1 EDL interaction in symmetric electrolytes

Three cases will be presented for discussion: weak repulsive interactions, weak attractive interactions, and intermediate repulsive interactions.

4.3.1.1 Weak repulsive interactions

Figure 4.2 presents the results for weak repulsive interactions between the particle and the planar surface when EDL overlap does not occur. Both surfaces develop their associated EDLs independently, and bulk conditions prevail in the space between both surfaces.

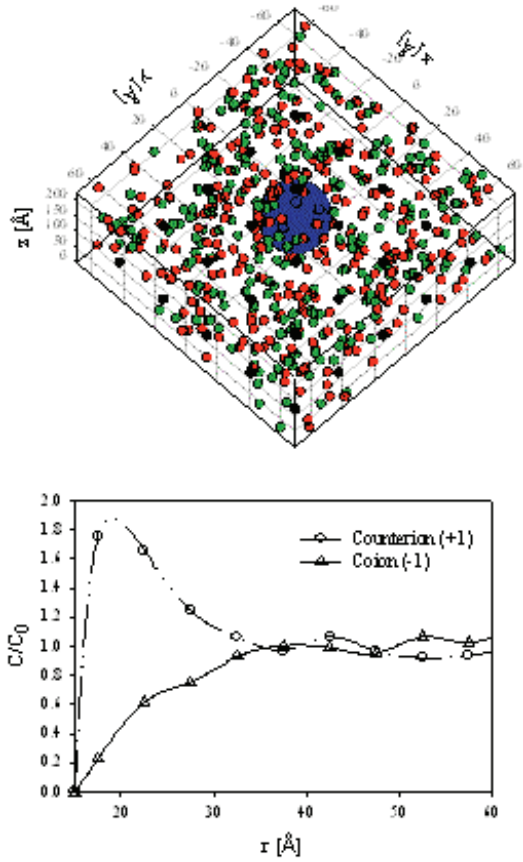

Figure 4.2 EDL structure and concentration profiles for the colloidal particle in a 1:1 electrolyte of ionic strength 0.1 M. The surface charge densities for the planar surface and the colloidal particle are –2.04 μC/cm^2 and –5.67 μC/cm^2, respectively, and the separation distance between the particle and the planar surface is 120 Å ($4d_M$).

The eye of the observer in Figure 4.2 is located behind the charged surface, i.e., the colloidal particle is observed from underneath. The red, green and black spheres correspond to counterions, coions, and charged groups on the surface, respectively. The large blue sphere corresponds to the colloidal particle. As it can be seen from the instantaneous configuration of the system depicted in Figure 4.2, both counterions and coions can be found in the space between the colloidal particle and the planar surface. Additionally, the EDL of the colloidal particle is fully developed in all radial directions, and bulk conditions are achieved.

Figure 4.3 presents the case of EDL overlap during weak repulsive interactions between the charged colloidal particle and the planar surface.

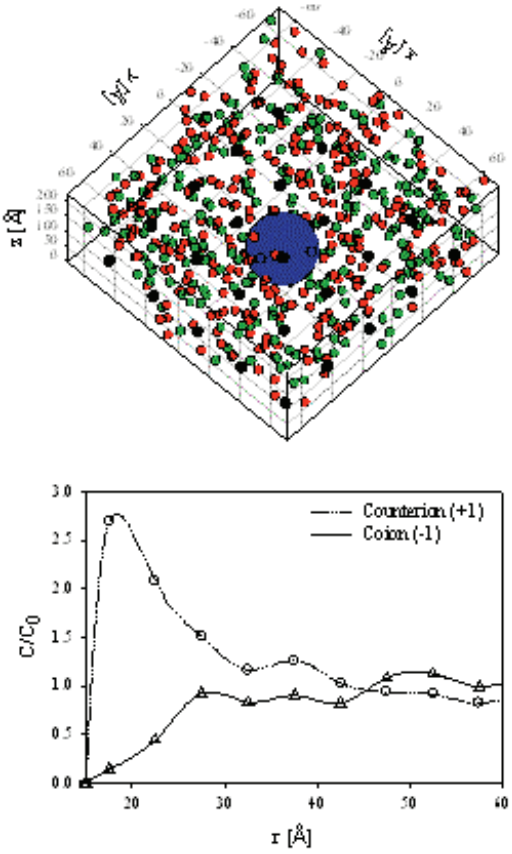

Figure 4.3 EDL structure and concentration profiles for the colloidal particle during EDL overlap in a 1:1 electrolyte of ionic strength 0.1 M. The surface charge densities for the planar surface and the colloidal particle are –2.04 μC/cm^2 and –5.67 μC/cm^2, respectively, and the separation distance between the colloidal particle and the planar surface is 30 Å (d_M).

In Figure 4.3, the eye of the observer is also located underneath the charged wall. One can notice that all the ions are displaced from the region between the colloidal particle and the planar surface, although the surfaces are not yet in contact. The concentration profiles in the radial direction show higher local values than the ones presented in Figure 4.2. There is an accumulation of counterions behind the colloidal particle that results

from the displacement of the ions from the interaction region. The local concentration in the first layer of fluid behind the colloidal particle is $2.7C_0$ during EDL overlap, compared to only $1.8C_0$ in the case of no EDL overlap. C_0 is the concentration in the bulk solution. The occurrence of this phenomenon is not contemplated by the classical theory because ions are regarded as point charges, and therefore, they are not displaced from the interaction region between surfaces until the surfaces are in contact. The displacement of ions and local accumulation of them behind the colloidal particle may have some implications in the interaction force. Additionally, the displacement of counterions and coions from the interaction region may introduce another component to the interaction force between the particle and the planar surface. This additional component is usually recognized as a depletion force and arises from the entropic variations due to the different availability of volume in the system for different species (Oettel, 2004).

4.3.1.2 Weak attractive interactions

During weak attractive interactions, independently developed EDLs for the planar surface and the colloidal particle can be observed for distances larger than 60 Å (2•dm), as in the case of weak repulsive interactions. Figure 4.4 presents the results for weak attractive interactions during EDL overlap.

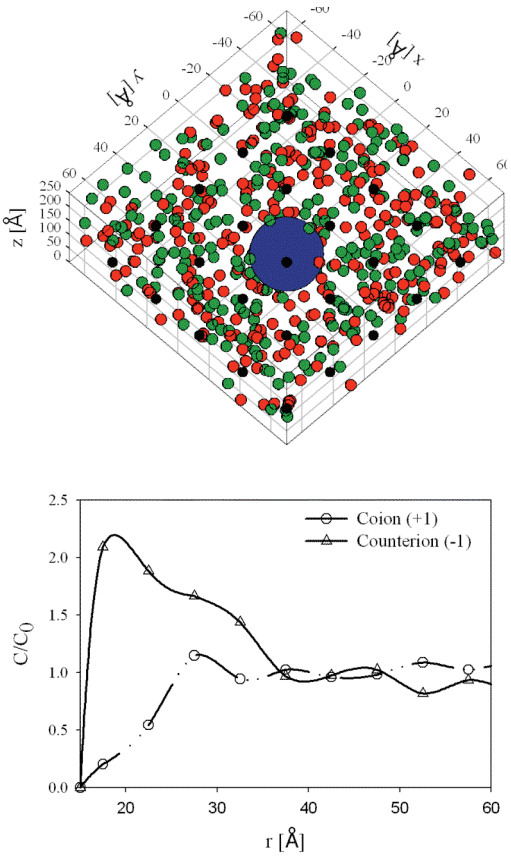

Figure 4.4 EDL structure and concentration profiles for the colloidal particle during EDL overlap in a 1:1 electrolyte of ionic strength 0.1 M. The surface charge densities for the planar surface and the colloidal particle are –2.04 μC/cm^2 and +5.67 μC/cm^2, respectively, and the separation distance between the colloidal particle and the planar surface is 30 Å (d_M).

During EDL overlap, even at weak attractive interactions, ions are displaced from the region between the colloidal particle and the planar surface. Still, an accumulation of both species occurs behind the colloidal particle. Not only a high local concentration of counterions (negatively charged monovalent ions) can be detected behind the colloidal particle, but also a slight high local concentration of coions as well (positively charged monovalent ions). This result was unexpected, and, although the nature of the interaction force is expected to be attractive, the magnitude of the forces will be slightly affected due to the mentioned effect.

4.3.1.3 Intermediate repulsive interactions

Figure 4.5 presents instantaneous configurations for the interaction between the spherical particle and the planar surface in a 1:1 electrolyte solution of ionic strength of 0.05 M.

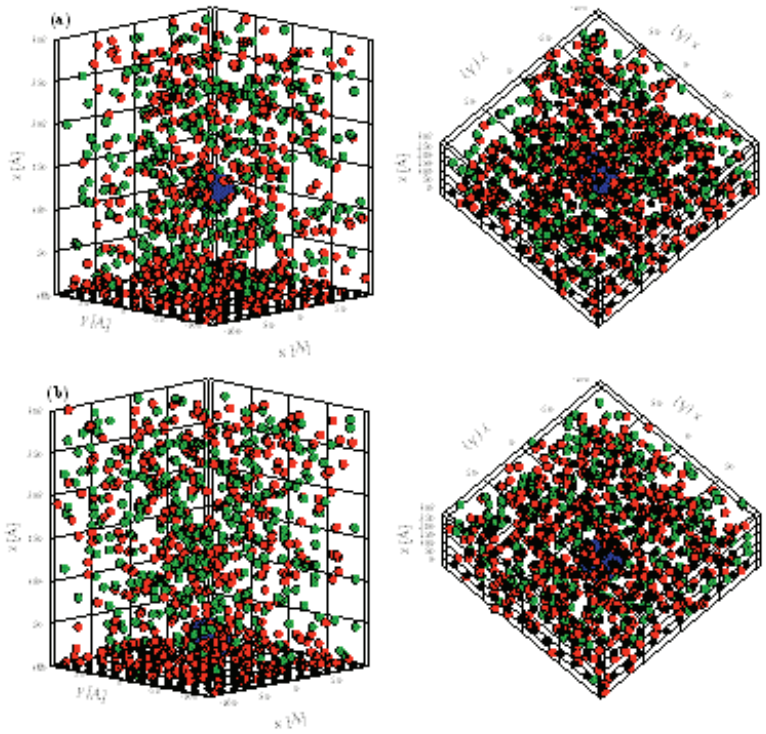

Figure 4.5 EDL structure during the interaction of the planar surface and the colloidal particle in a 1:1 electrolyte of ionic strength 0.05 M. The surface charge densities of the planar surface and the colloidal particle are –5.23 μC/cm^2 and –17.0 μC/cm^2, respectively, and the separation distances are: (a) 120 Å ($4d_M$), and (b) 30 Å (d_M).

Figure 4.5(a) shows that the particle and the planar surface develop independent EDLs and that bulk conditions are achieved in the region comprised between the interacting surfaces. As the surfaces get closer to each other, coions are displaced from the space between interacting surfaces, as seen in Figure 4.5(b). One should note that at higher values of surface charge, the counterions are not displaced from the region between the

interacting surfaces before contact as it was observed at lower surface potentials in Figures 4.3 and 4.4. In this case, the depletion term of the interaction force may be displaced towards lower separation distances between interacting surfaces.

Figures 4.2, 4.3, 4.4 and 4.5 present instantaneous configurations and EDL structures when there is no EDL overlap and when the surfaces are very close to contact. Figure 4.6 on the other hand, presents instantaneous configurations as the surfaces move closer together.

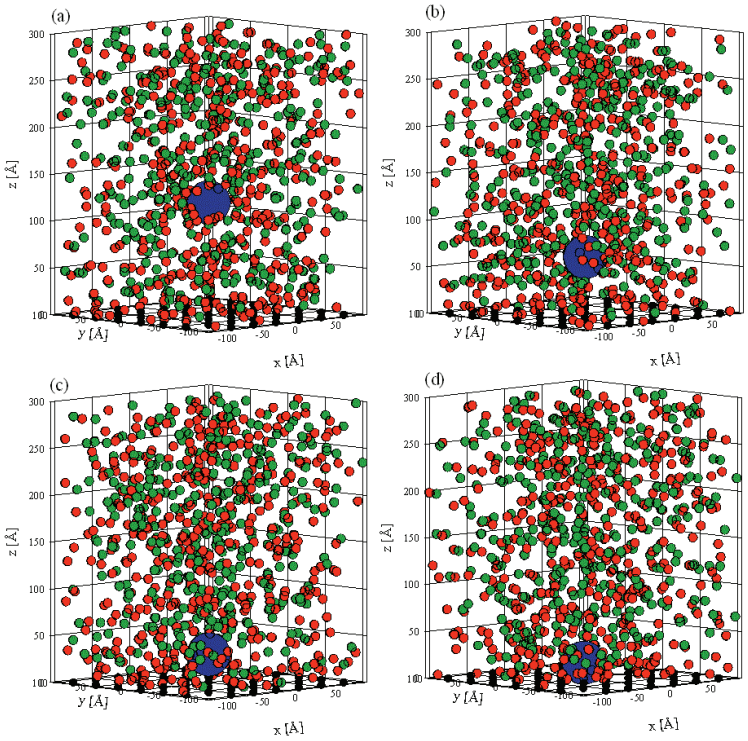

Figure 4.6 EDL structure during the interaction of the planar surface and the colloidal particle in a 1:1 electrolyte of ionic strength 0.05 M. The surface charge densities of the planar surface and the colloidal particle are –5.23 μC/cm^2 and –17.0 μC/cm^2, respectively, and the separation distances are: (a) 120 Å ($4d_M$), (b), 60 Å ($2d_M$), (c) 30 Å (d_M), and (d) 16.5 Å (contact, $[d_W+d_M]/2$).

As the surfaces get closer together, the length of the zone of bulk conditions between the two interacting surfaces decreases. Layers of fluid get squeezed out of the region of

interaction. At sufficiently small separation distances, there seems to be a slight ordering of counterions and coions in that region, i.e. an ordering of layers of fluid containing consecutive local high concentrations of counterions and coions. And, finally, the ions are displaced from the region between the two interacting surfaces. The ordering of ions and counterions, as EDL overlap takes place, might have some effect on the electrostatic force, since at least neutralization of charge between consecutive layers of fluid might occur.

4.3.2 EDL interaction in asymmetric electrolytes

In the previous segment, the results for 1:1 electrolytes comprised of ions of the same charge and size were presented and discussed. In this section, results of the interaction between the spherical particle and the planar surface will be presented for 2:1 and 3:1 electrolytes, where not only asymmetry in charge was considered but also asymmetry in size. As discussed in Chapter 3, the asymmetry in size affects the extension of the EDL away from charged surfaces, while asymmetry in charge determines the value of the local concentrations of counterions and coions close to the charged surfaces.

4.3.2.1 Weak repulsive interactions

Figure 4.7 presents a snapshot of the EDL structures during repulsive interactions between the spherical colloidal particle and the planar surface in a 2:1 electrolyte solution. The pink spheres correspond to the divalent counterions, while the green and

black spheres correspond to the coions and charged groups on the surface, respectively. In this case, both counterions and coions are displaced from the region between the two interacting surfaces even before the surfaces reach contact. This behavior was reported for 1:1 electrolytes as well.

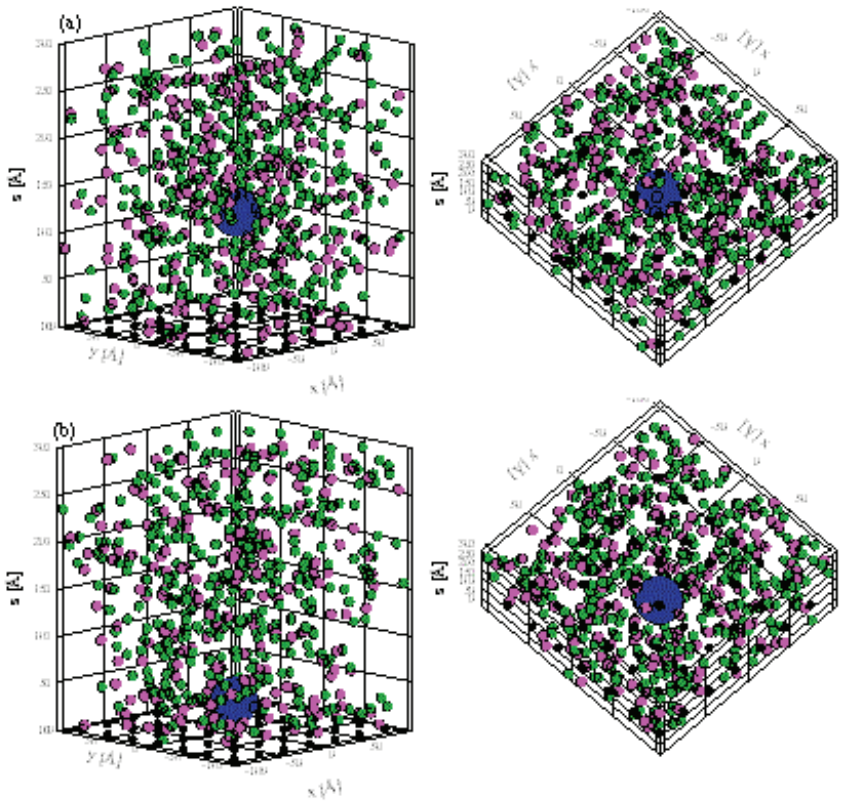

Figure 4.7 EDL structure during the interaction of the planar surface and the colloidal particle in a 2:1 electrolyte of ionic strength 0.05 M. The surface charge densities of the planar surface and the colloidal particle are –1.78 μC/cm^2 and –5.67 μC/cm^2, respectively, and the separation distances are: (a) 120 Å ($4d_M$), and (b) 30 Å (d_M).

The difference in diameter between the monovalent counterions and the divalent counterions utilized in this work is only 1.75 Å, therefore, significant difference between both cases is not expected. However, the analysis of the results for a separation distance of 60 Å ($2d_M$) shows that some exclusion of ions from the interaction region occurs for the 2:1 electrolyte case, while the 1:1 electrolyte still presents independent EDLs (results

not shown). Furthermore, the degree of ordering of layers of fluid with successive high and low values of local concentration of counterions is larger in the case of 2:1 electrolytes than in the case for 1:1 electrolytes (results not shown). The extent of ordering is enhanced by larger values of counterion valence, but its occurrence is limited to fewer layers of fluid at closer separation distances.

Figure 4.8 presents snapshots of the structure of the EDL during the interaction of the spherical colloidal particle and the planar surface in a 3:1 electrolyte solution. The slightly larger dark red spheres represent the trivalent counterion, in this case.

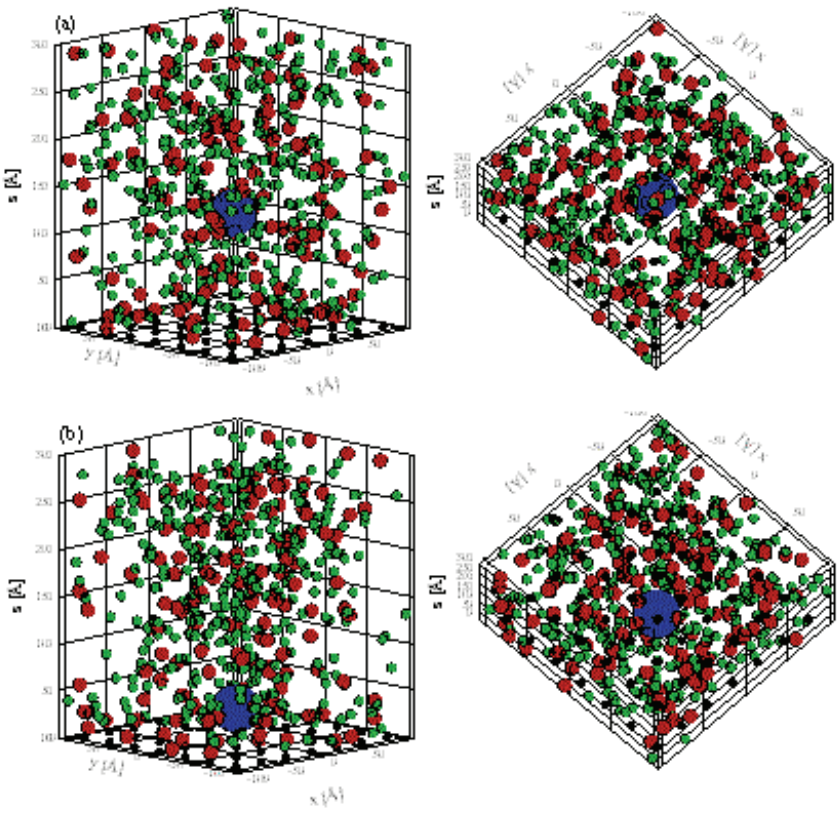

Figure 4.8 EDL structure during the interaction of the planar surface and the colloidal particle in a 3:1 electrolyte of ionic strength 0.05 M. The surface charge densities of the planar surface and the colloidal particle are –1.78 μC/cm^2 and –5.67 μC/cm^2, respectively, and the separation distances are: (a) 120 Å ($4d_M$), and (b) 30 Å (d_M).

In this case, the counterions and coions are excluded from the interaction region before contact, like in the cases of 1:1 and 2:1 electrolytes. Exclusion of ions from the region between the interacting surfaces was detected as early as at separation distances of 60 Å possibly due to their larger size. Electrostatic effects and ordering effects are expected to scale with counterion valence in the same manner described for the 2:1 electrolyte case.

4.3.2.2 Intermediate repulsive interactions

Figure 4.9 presents the interaction between the surfaces in a 2:1 electrolyte.

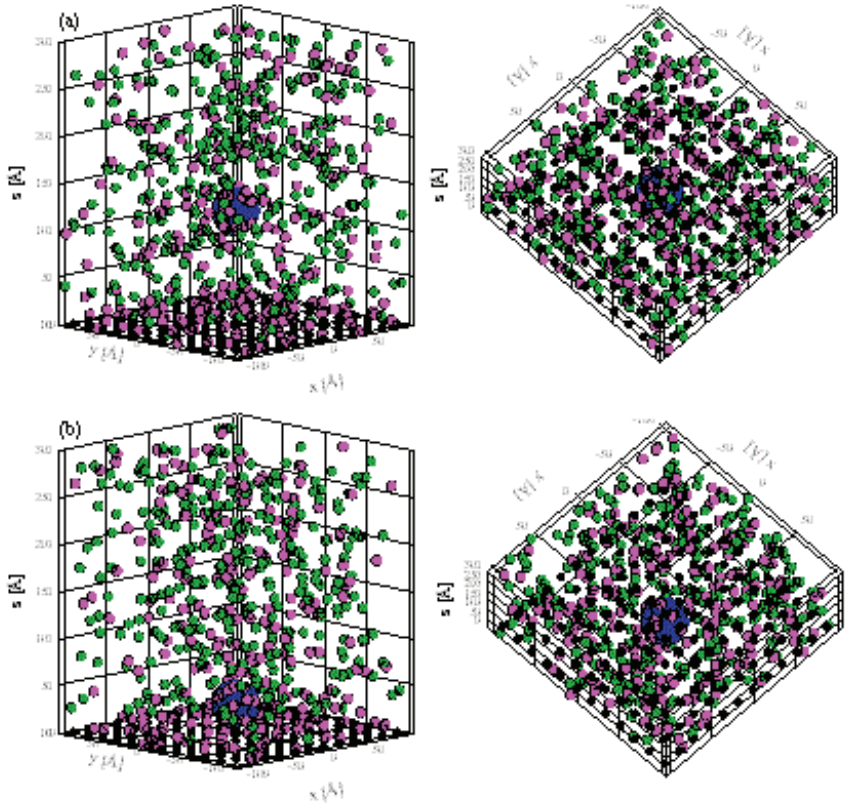

Figure 4.9 EDL structure during the interaction of the planar surface and the colloidal particle in a 2:1 electrolyte of ionic strength 0.05 M. The surface charge densities of the planar surface and the colloidal particle are –5.23 μC/cm^2 and –17.0 μC/cm^2, respectively, and the separation distances are: (a) 120 Å ($4d_M$), and (b) 30 Å (d_M).

The higher electric potential results in ions being excluded from the region between the interacting surfaces at a lesser extent than in the case of low electrostatic potential. However, the extent of exclusion of counterions from the interaction region seems to scale with counterion valence as it can be observed by comparing Figures 4.5 and 4.9 that depict the EDL structure during the interaction of the surfaces at the same conditions of ionic strength and surface charge density values. In the same manner, the ordering effect is noticeable only within short separation distances as the surfaces approach.

Figure 4.10 presents similar results for the case of 3:1 electrolyte.

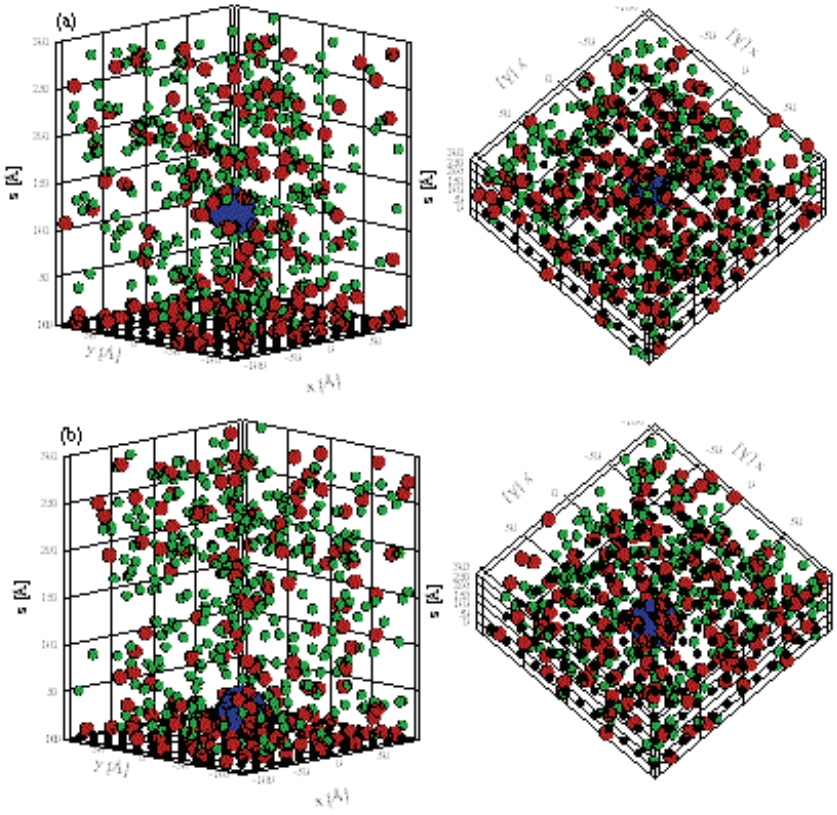

Figure 4.10 EDL structure during the interaction of the planar surface and the colloidal particle in a 3:1 electrolyte of ionic strength 0.05 M. The surface charge densities of the planar surface and the colloidal particle are –5.23 μC/cm^2 and –17.0 μC/cm^2, respectively, and the separation distances are: (a) 120 Å ($4d_M$), and (b) 30 Å (d_M).

In this case, the exclusion of counterions from the region between the colloidal particle and the charged surface occurs at a lesser extent than for lower electrostatic coupling (see Figure 4.8). As in the case of 2:1 electrolytes, the extent of ion exclusion in the region of interaction scales with the ion valence, and the ordering effect extends only to a few layers of fluid or short separation distances.

The extent of exclusion of counterions from the region of interaction between the colloidal particle and the planar surface, and the separation distance of its onset should be reflected in the presence of an excluded volume contribution the total interaction surface. The ordering effect, i.e. the successive occurrence of layers of fluid with high and low local concentrations of counterions, should have an effect on the force at longer separation distances than the depletion effect. These two aspects will be examined in Chapter 5.

4.4 EDL overlap in the presence of mixtures of symmetric and asymmetric electrolytes

Following the design of simulations used in Chapter 3, the outcome of three mixtures will be discussed in this part of the work: 2:1 and 1:1 electrolytes, 3:1 and 1:1 electrolytes, and 3:1, 2:1, and 1:1 electrolytes. The behavior of the interactions in the three mixtures was examined at weak and intermediate values of surface charge.

4.4.1 Weak repulsive interactions in mixtures of symmetric and asymmetric electrolytes

Figure 4.11 presents the results for the interaction of the planar surface and the colloidal particle in a mixture of 2:1 and 1:1 electrolytes. At large separation distances, depicted on Figure 4.11(a), independent EDLs develop for both charged surfaces. Divalent and monovalent ions form the EDLs irrespectively of their size, due to the small values of surface charge involved. As in the case for single electrolytes, the ions are excluded from the region between the charged surfaces even before the surfaces get into contact, as can be seen on Figure 4.11(b). At low surface charges, there does not seem to be any preferential exclusion of ions with respect of its size. In Chapter 3 it was shown that larger ions are excluded from surfaces as surface charge density increases, and that smaller ions preferentially get closer to the surface.

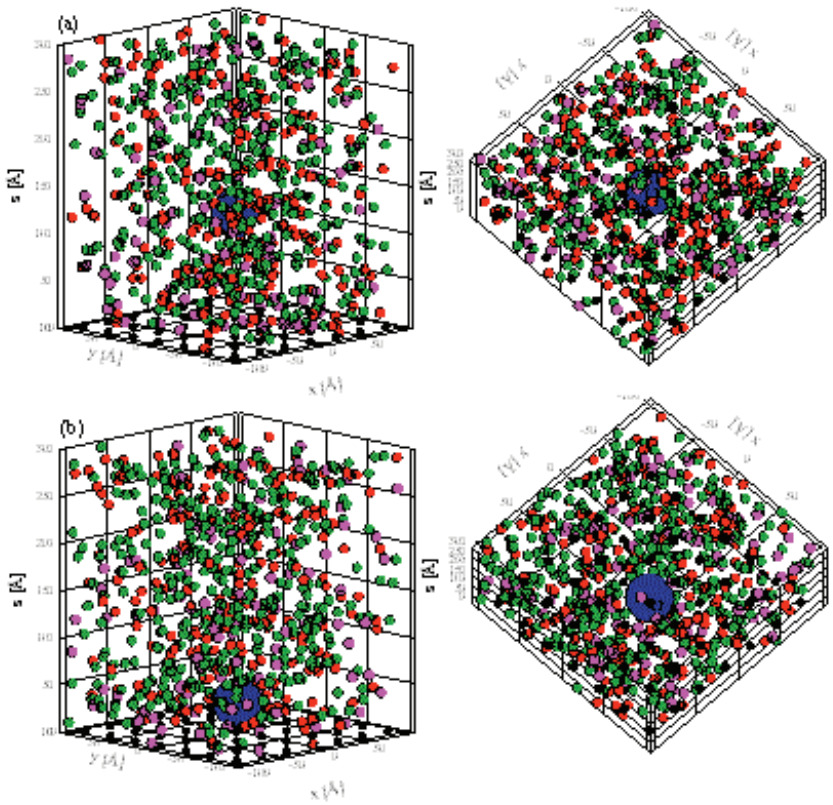

Figure 4.11 EDL structure during the interaction of the planar surface and the colloidal particle in a mixture of 2:1 and 1:1 electrolytes of ionic strength 0.05 M. The surface charge densities of the planar surface and the colloidal particle are –1.78 μC/cm^2 and –5.67 μC/cm^2, respectively, and the separation distances are: (a) 120 Å ($4d_M$), and (b) 30 Å (d_M).

Figure 4.12 presents the results for the mixture of 3:1 and 1:1 electrolytes. The low surface charge used in this case does not result in smaller number of counterions preferentially forming the EDL nor does it result in preferential exclusion of the trivalent counterions from the space between the charged surfaces although the diameter of the trivalent counterions is twice as large as the diameter of the monovalent counterions.

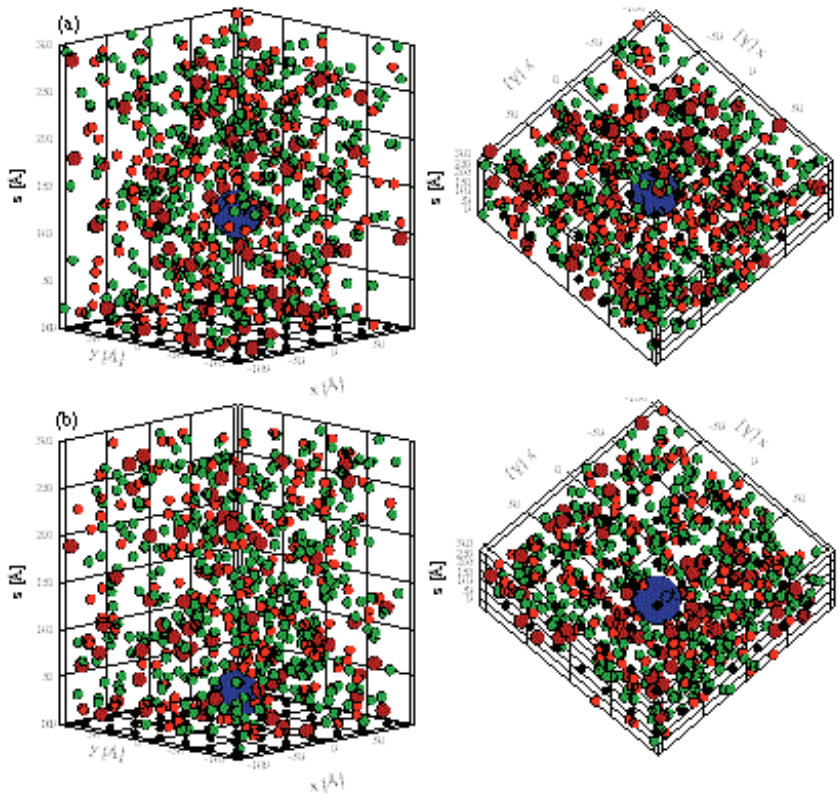

Figure 4.12 EDL structure during the interaction of the planar surface and the colloidal particle in a mixture of 3:1 and 1:1 electrolytes of ionic strength 0.05 M. The surface charge densities of the planar surface and the colloidal particle are –1.78 μC/cm^2 and –5.67 μC/cm^2, respectively, and the separation distances are: (a) 120 Å ($4d_M$), and (b) 30 Å (d_M).

Figure 4.13 presents the results for the mixture of 3:1, 2:1, and 1:1 electrolytes. As it can be seen, all the counterions participate in the formation of the independent EDLs at long separation distances, Figure 4.13(a), irrespectively of their size. All counterions are equally displaced from the space between the interacting surfaces before contact is made as it was observed in all the cases during weak repulsion or attraction. The fact that there are ions with different sizes in the electrolyte solution does not affect the results in great extent. Larger surface charge density values are required to detect size exclusion effects, i.e. preferential exclusion of ions from the space between the surfaces according to their size, as reported in Chapter 3.

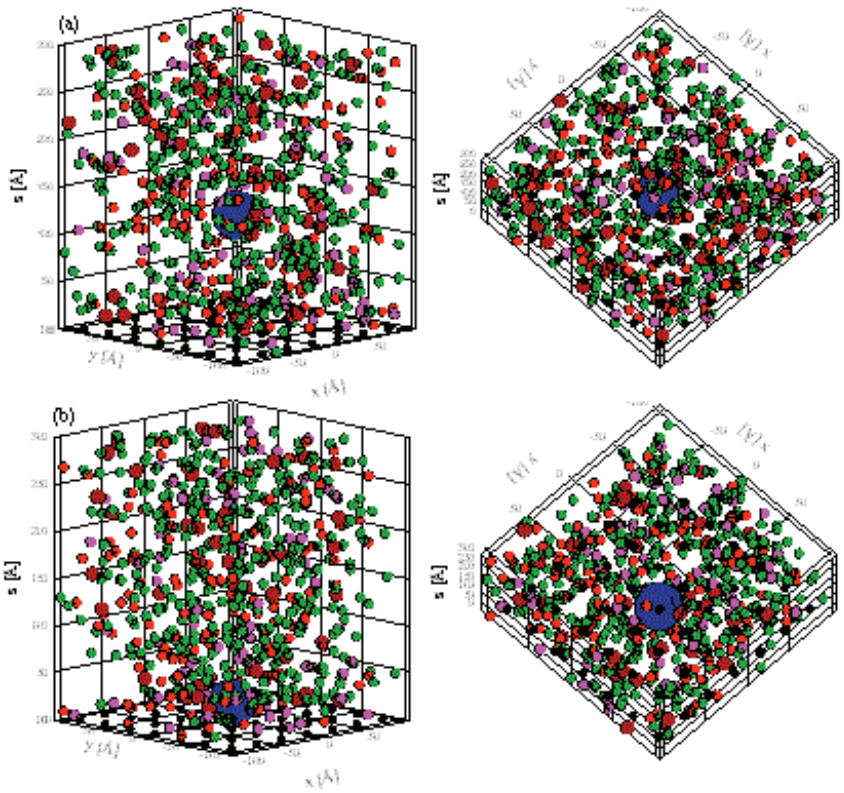

Figure 4.13 EDL structure during the interaction of the planar surface and the colloidal particle in a mixture of 3:1, 2:1 and 1:1 electrolytes of ionic strength 0.05 M. The surface charge densities of the planar surface and the colloidal particle are –1.78 μC/cm^2 and –5.67 μC/cm^2, respectively, and the separation distances are: (a) 120 Å ($4d_M$), and (b) 30 Å (d_M).

4.4.2 Intermediate repulsive interactions in mixtures of symmetric and asymmetric electrolytes

Figure 4.14 depicts the EDL structure during the interaction between the planar surface and the spherical particle in a mixture of 2:1 and 1:1 electrolytes at intermediate surface charge density values.

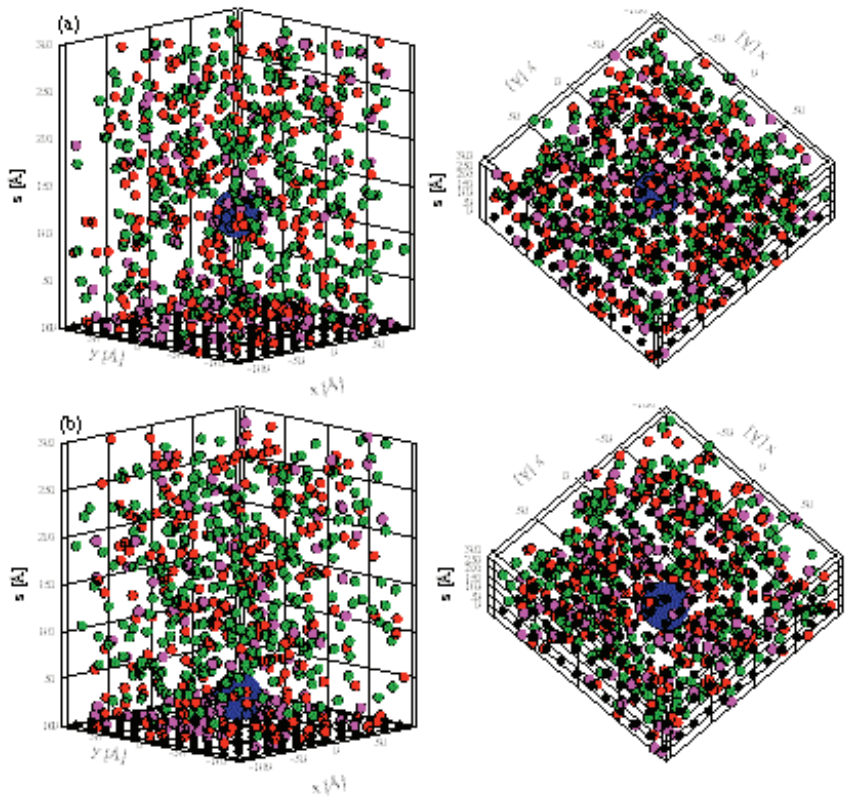

Figure 4.14 EDL structure during the interaction of the planar surface and the colloidal particle in a mixture of 2:1 and 1:1 electrolytes of ionic strength 0.05 M. The surface charge densities of the planar surface and the colloidal particle are –5.23 μC/cm^2 and –17.0 μC/cm^2, respectively, and the separation distances are: (a) 120 Å ($4d_M$), and (b) 30 Å (d_M).

Since the surface charge density values are relatively small, no size exclusion effect can be detected in the structure of the EDLs of the charged surfaces when there is no overlap [Figure 4.14(a)]. Both counterions, divalent and monovalent, are displaced from the region comprised between the interacting surfaces prior to contact in the same extent as the system that contained only 2:1 electrolyte. The extent of ions displacement from the region of interaction seems to scale with the larger valence of the counterions in the system.

Figure 4.15 presents the EDL structure during the interaction of the planar surface and the spherical particle in the case of a mixture of 3:1 and 1:1 electrolytes.

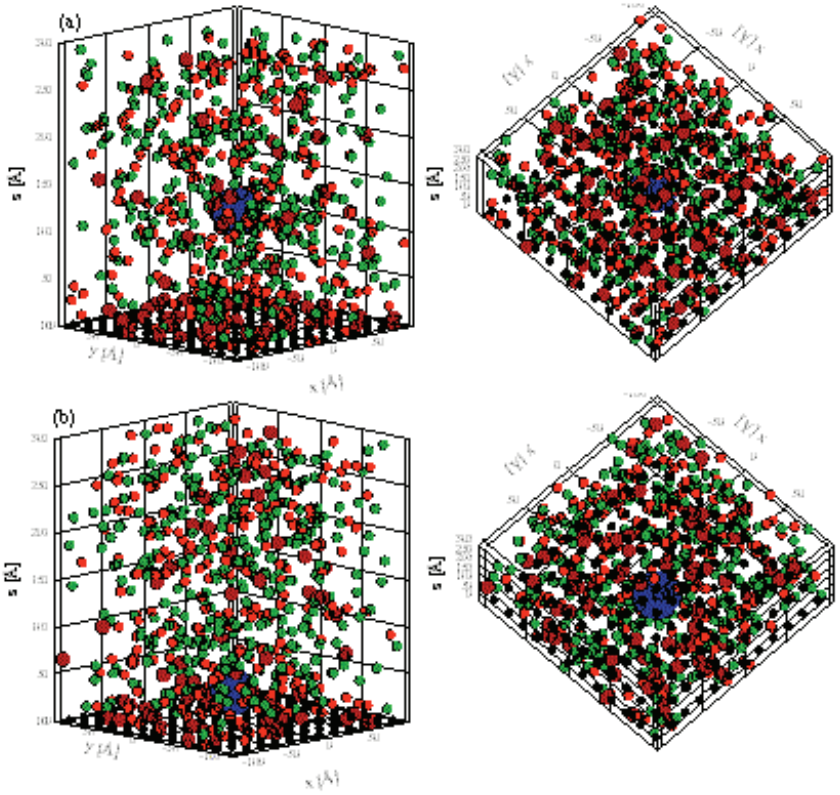

Figure 4.15 EDL structure during the interaction of the planar surface and the colloidal particle in a mixture of 3:1 and 1:1 electrolytes of ionic strength 0.05 M. The surface charge densities of the planar surface and the colloidal particle are –5.23 μC/cm^2 and –17.0 μC/cm^2, respectively, and the separation distances are: (a) 120 Å ($4d_M$), and (b) 30 Å (d_M).

Due to the relatively low values of surface charge densities chosen, the trivalent and monovalent counterions participate indistinctively in the structure of the EDL of both charged surfaces, Figure 4.15(a). As with previous cases, displacement of the ions from the region comprised between the interacting surfaces occur prior to contact. In the case of the mixture of 3:1 and 1:1 electrolytes, significant displacement of counterions can be observed even at separation distances of 60 Å ($2d_M$). The extent of displacement of the

ions from the region of interaction is definitely influenced by the counterion of larger valence present in the system.

Figure 4.16 presents a snapshot of the simulation results obtained for the interaction between the spherical particle and the planar surface in the mixture of 3:1, 2:1, and 1:1 electrolytes.

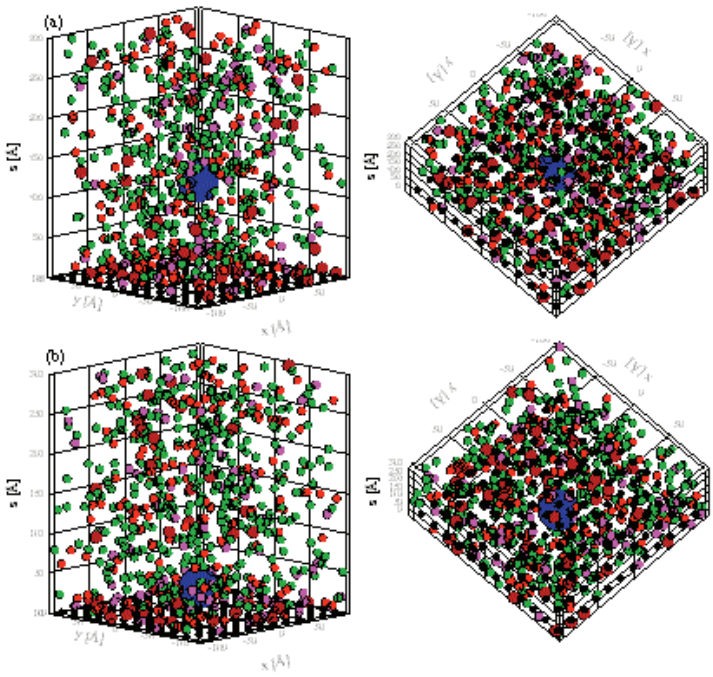

Figure 4.16 EDL structure during the interaction of the planar surface and the colloidal particle in a mixture of 3:1, 2:1 and 1:1 electrolytes of ionic strength 0.05 M. The surface charge densities of the planar surface and the colloidal particle are –5.23 μC/cm^2 and –17.0 μC/cm^2, respectively, and the separation distances are: (a) 120 Å ($4d_M$), and (b) 30 Å (d_M).

Ion displacement from the region of interaction occurs before the surfaces reach contact, as in the previous cases. However, the extent of the displacement of ions from the region between the surfaces is smaller than for the case of lower electrostatic coupling, as can be observed from the comparison between Figures 4.16 and 4.13.

4.5 Conclusions

Displacement of ions from the region between the interacting charged surfaces was observed in all the cases examined, even before the surfaces reached contact. The displaced ions accumulated behind the colloidal particle, resulting in slightly higher local concentrations than the ones observed prior to EDL overlap, when the surfaces develop their associated EDLs independently. The onset of displacement of the ions from the region of interaction coincided with the occurrence of EDL overlap whose range scaled with the diameter of the counterion. This observation was expected because the EDL range is determined by the size of the ion, as discussed in Chapter 3.

Additionally, the extent of displacement of ions from the region between the interacting surfaces diminishes as electrostatic coupling increases, i.e., as the values of surface charge density on both surfaces increase. This phenomenon seems to respond to a counterbalance between energy and entropic effects. Displacement of ions from the region of interaction is driven by increase in the entropy of the system, and results, as mentioned earlier, in depletion forces. However, as surface charge density increases, it is energetically costly not to neutralize the charges on the approaching surfaces. Therefore, displacement of ions from the region of interaction takes place at a lesser extent.

Finally, no ion exclusion effects were detected during the independent formation of the associated EDLs of the charged surfaces before EDL overlap. The values of surface charge density used in this part of the work were lower than the ones used in the study of

the EDL structure discussed in Chapter 3. Furthermore, no preferential displacement of ions from the region of interaction according to their size could be detected due to the same reason.

4.6 Summary

In this part of the work the behavior of the structure of the EDLs associated to a planar surface and a spherical colloidal particle were examined during their interaction.

The displacement of ions from the region of interaction was detected driven by entropic effects, even before the surfaces reached contact. The range for the onset of the displacement of ions was found to scale with the size of the counterions in the system. The extent of the displacement was found to diminish with increasing electrostatic coupling, i.e., higher values of surface charge density for the interacting surfaces. This phenomenon responds to a counterbalance of energetic and entropic effects.

In the same manner, an ordering of successive layers of fluid with higher and lower local concentrations could be detected in all the cases. The extent the ordering scaled with counterion valence, and its range, i.e. window of separation distances, decreased with increasing electrostatic coupling. The ordering effect took place within fewer layers of fluid as the surface charge densities or surface potentials increased.

The observations of the behavior of the EDL structures during interactions between the planar surface and the colloidal particle lead us to expect the presence of a depletion component in the interaction force between the surfaces that will be examined in Chapter 5.

CHAPTER 5

ELECTROSTATIC INTERACTION FORCES IN SYMMETRIC AND ASYMMETRIC ELECTROLYTES

5.1 Introduction

Electrostatic forces between charged surfaces are not only a direct consequence of the presence of surface charge. Their nature, range and magnitude are determined by the characteristics of the overlap of the associated electrical double layers (EDLs) to the charged surfaces, as discussed in Chapter 2.

In the case of colloidal particles and solid-liquid interfaces, surface charge can be manipulated either by applied external electric fields in the case of electrodes, or the chemistry of the solutions. Electrostatic interactions play an important role in many natural and engineered processes involving colloidal particles and solid-liquid interfaces.

Traditionally, the electrostatic interactions have been calculated within the framework of a mean-field, pseudo-one-component formulation known as the Derjaguin-Landau-Verwey-Overbeek (DLVO) theory. The classical calculation of the EDL forces involves the consideration of two main components: a purely electrostatic component and an

osmotic component due to the accumulation of ions in the region between the interacting surfaces (Elimelech et al., 1995; Hiemenz and Rajagopalan, 1997; Israelachvili, 1998; Belloni, 2000; Hunter, 2001). The discrepancies between classical theory predictions and experimental observations, reported in Chapter 1, have led to revisions of the DLVO theory and the statistical mechanics approach for certain specific geometries.

One of the most common revisions to the classical theory consists of the suitability of the Derjaguin approximation, which is employed during the calculation of interparticle interactions between charged spherical particles and between spherical particles and planar surfaces. This approximation, which uses linear expansions in the solution of the Poisson-Boltzmann (PB) equation for the EDL structure, is accurate for very low, constant surface potentials and very thin double layers when compared to the diameter of the spherical particles involved. The applicability of the DLVO theory can be extended to higher surface potentials and even to constant surface charge densities if non-linear expansions are employed in the solution of the PB equation, but the requirement of thin EDLs with respect to the dimensions of the interacting particles still prevails (Stankovich and Carnie, 1996; Nguyen et al, 2000).

Since the conception of the DLVO theory involves mean-field approximations and the application of the PB equation, not much can be done to increase its accuracy within its original framework. Therefore, much work has gone into applying statistical mechanics into the calculation of EDL forces through the determination of an effective interaction potential that will account for electrolyte and even solvent effects (Belloni, 2000). In the

1980's, numerical solutions of integral equations, especially with hypernetted-chain (HNC) theory closures, were employed to obtain effective interaction potentials within a framework of a primitive model and a pseudo one-component approximation (Patey, 1980; Kjellander et al., 1992; Chu and Wasan, 1996). One of the interesting findings from the application of the HNC solution for the potential between two identically charged colloidal particles was the detection of an attractive force associated to an interparticle potential minimum at relatively high surface charges (Patey, 1980).

Molecular dynamics (MD) and Monte Carlo (MC) simulations were introduced in order to overcome the pseudo one-component approximation and test the possibility of attraction of electrostatic origin between similarly charged solid-liquid interfaces.

Molecular modeling techniques present several challenges that have limited their application for the direct calculation of effective interaction potentials and effective interaction forces between charged surfaces (Belloni, 2000). Some of the challenges include the large number of particles required to maintain electroneutrality as charge asymmetry, i.e., surface charge, increases; the need for long run periods and small simulation steps due to the accumulation of ions in the vicinity of the charged surfaces; and, finally, the treatment of the long-range interaction potentials involved.

One of the first applications of molecular simulation techniques involved the study of the mechanical and thermodynamic properties of electrolyte solutions inside pores or inside thin planar slits, i.e. the interaction between infinitely uniformly charged planar surfaces

(Valleau et al., 1991; Kjellander, et al., 1992; Jamnik and Vlachy, 1993; Delville, 1994; Delville et al., 1997; Hribar and Vlachy, 2000). In the case of the interaction of infinite charged planar surfaces, the development of bulk conditions in the system is not necessary. The main property inside pores and planar slits obtained via molecular modeling techniques has been the osmotic pressure via the calculation of structure factors and pair distribution functions (Guldbrand et al. 1984; Hansen, 1986; Valleau et al., 1991; Delville, 1994; Belloni, 2000). One of the most striking findings of previous studies is the occurrence of minima in the osmotic pressure inside similarly charged walls, which can be associated with attractive interactions, for 2:2 and 2:1 electrolyte solutions at relatively low surface potentials (Guldbrand et al., 1984; Valleau et al., 1991; Delville, 1994; Delville, 1997) and for 1:1 electrolytes at high values of ionic strength (Kjellander et al., 1992). Most of this work was performed with ions modeled as point charges, or as charged hard spheres of diameters of 4.25 Å or less. Only size asymmetry among counterions was considered.

Several attempts have been performed in order to obtain effective pair interaction potentials between spherical colloidal particles (Crocker and Grier, 1996; Stevens et al., 1996; D'Amico and Löwen, 1997; Grønbech-Jensen et al., 1998; Lobaskin and Linse, 1998; Wu et al., 1999; Delville, 1999; Terao and Nakayama, 2001; Striolo et al., 2002; Angelescu and Linse, 2003; Feng and Ruckenstein, 2004), and even colloidal platelets (Meyer et al., 2001), based on structure factors and pair distribution functions. The objective of these simulations was to prove if effective electrostatic attraction between similarly charged particles might be possible. In fact, attractive interactions between

similarly charged surfaces were detected in the presence of divalent counterions (Valleau et al, 1991; Chu and Wasan, 1996; Grønbech-Jensen et al., 1998; Lobaskin and Linse, 1998; Delville, 1999; Wu et al., 1999; Meyer et al., 2001; Striolo et al., 2002; Angelescu and Linse, 2003), and when the colloidal particles were confined in small geometries (Crocker and Grier, 1996; Terao and Nakayama, 2001). In these studies, solutions containing pure monovalent or pure divalent counterions, modeled as either point charges or hard charged spheres of diameter up to 4.2 Å, were employed. No size asymmetry among counterions was considered.

The occurrence of attraction between similarly charged colloidal particles and solid-liquid interfaces, when divalent counterions are present in solution, might explain several of the discrepancies between the classical theory and experimental observations that were reported in Chapter 1. Although the calculation of an effective pair interaction potential demonstrates the existence of attraction between similarly charged surfaces when divalent counterions are present, the calculation involves an "averaging" procedure throughout the whole system that attempts to capture ion-ion correlation and other effects in one interaction term. In this part of the work, a simpler and more straightforward proof of the effect of ion-ion correlations and other effects neglected by the mean field approximation adopted within the DLVO theory is pursued. The force experienced by a spherical colloidal particle perpendicular to a discretely charged planar surface is calculated via Canonical Monte Carlo (CMC) simulations. Solutions of symmetric and asymmetric electrolytes and their mixtures are investigated in order to examine the specific effects of charge and size asymmetry on the interaction force. It is expected that

the direct calculation of the interaction force will not only capture effects like ion-ion correlations, but also will show the presence of other effects like the depletion forces expected from the analysis performed in Chapter 4. The choice of the system, i.e. a charged spherical colloidal particle interacting with a planar surface, is made for two reasons. First, the geometry can be related to natural or engineered processes such as transport of particles in porous media, filtration, deposition, membrane separations, and even particle aggregation. Second, the simulation scheme could be used later on to validate the molecular modeling results, against direct force measurements performed by atomic force microscopy (AFM), since the geometry is the same.

5.2 Simulations of the electrostatic force between a spherical particle and a planar surface

The system for the CMC simulations consisted of a quasi squared box with two impenetrable walls in the Z direction, one of them discretely charged, as described in Chapters 3 and 4. Boundary conditions were applied in the X and Y directions. Counterions, coions, and a colloidal particle were introduced into the system, as depicted in Figure 4.1.

5.2.1 Evaluation of the potential energy of the system

The potential energy was calculated as the sum of individual potential energies associated to each charged species (i.e., ions and colloidal particle), depending on its position inside

the simulation box, and the sum of the pairwise interaction energies among all species in the simulation box including the ions, charged groups on the wall and the colloidal particle (see equation 3.1). The ions, charged groups, and colloidal particle were modeled as charged hard spheres, and their pairwise interaction potential energies were calculated according to equations 3.2 and 4.1, which correspond to Coulomb's Law.

The long range corrections were performed via the association of a charged sheet of infinite dimensions to each ion and to each charged group inside the central simulation box. The colloidal particle did not have any charged sheet associated with it, since it did not possess images. This means that the particle was not replicated in the image boxes of the central simulation box. Following the discussion in Chapter 4, the effect of the occurrence of image EDLs associated to the colloidal particle in the image boxes of the central simulation box was neglected due to their small contribution to the total energy. Sizing the simulation box, in order to develop bulk conditions in all directions around the colloidal particle, contributed to minimize the effect of the images of the particle's EDL on the total energy.

5.2.2 CMC calculation of the interaction force

The net force experienced by a charged colloidal particle perpendicular to the discretely charged planar surface was calculated.

Three contributions were taken into consideration for the calculation of the force acting on the colloidal particle: (i) the force exerted on the particle by the charged groups on the planar surface, (ii) the force exerted on the particle by the ions comprising the EDL associated to the charged planar surface, and (iii) the force exerted on the particle by the ions comprising its own EDL, as depicted in equation 5.1:

$$F = F_{M-W} + F_{M-EDLW} + F_{M-EDLM} \qquad (5.1)$$

where F is the force acting on the colloidal particle in the direction perpendicular to the planar surface (Z direction), $F_{M\text{-}W}$ is the force in the Z direction exerted on the particle by the charged groups on the planar surface, $F_{M\text{-}EDLW}$ is the force in the Z direction exerted on the particle by the charged wall's EDL, and $F_{M\text{-}EDLC}$ is the force in the Z direction exerted on the particle by its own EDL.

In order to obtain the net force acting on the colloidal particle, the interaction force of the colloidal particle with each ion comprising the EDLs and each charged group on the surface was calculated and decomposed in the Z direction. A fictitious origin of coordinates was fixed at the center of the colloidal particle, as depicted in Figure 5.1:

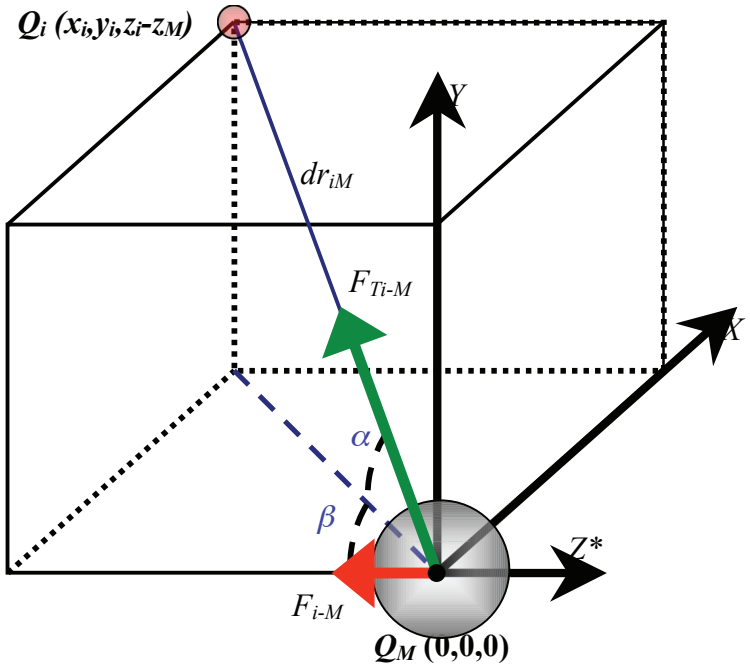

Figure 5.1 Schematic of the algorithm used to calculate the pair-wise interaction forces between the colloidal particle and ions or charged groups on the surface.

where Q_i and Q_M are the charges of an ion or a charged group and the colloidal particle respectively, (x_i,y_i,z_i-z_M) are the coordinates of an ion or a charged group with respect to the new origin (0,0,0), z_M is the original position of the colloidal particle in the Z^* direction, dr_{iM} is the distance between the center of the colloidal particle M and the ion or charged group i, α is the angle formed by dr_{iM} with the plane XZ*, β is the angle formed by the projection of dr_{iM} on the plane XZ* with the coordinate axis Z*, F_{Ti-M} is the force exerted on the particle M by the ion or charged group i, and F_{i-M} is the Z component of the force exerted on the particle M by the ion or charged group i, i.e. the component perpendicular to the charged surface. The colloidal particle is positioned at the center of the simulation box, so it's original coordinates are $(0,0,z_M)$.

The force, $F_{i\text{-}M}$, exerted on the particle M by an ion or a charged group i in the Z direction was calculated applying Coulomb's Law:

$$F_{i-M} = \frac{Q_i Q_M \bar{e}^2}{4\pi\varepsilon_0 \varepsilon\, dr_{iM}{}^2}\left[\cos\left(\arcsin\frac{y_i - y_M}{dr_{iM}}\right)\right]\left[\cos\left(\arctan\frac{x_i - x_M}{z_i - z_M}\right)\right]\left(\frac{z_M - z_i}{|z_M - z_i|}\right) \qquad (5.2)$$

where dr_{iM} is the distance between the centers of an ion or a charged group i and the colloidal particle M; Q_i and Q_M are the charges of ions i and the colloidal particle M, respectively; ε_0 and ε correspond to the permittivity of vacuum and relative permittivity of the solvent; x_M, y_M and z_M are the positions on the X, Y, and Z axes of the colloidal particle, respectively; and x_i, y_i, and z_i are the position of an ion or a charged group i on the X, Y, and Z axes, respectively. The last term in parenthesis corresponds to a vector with modulus equal to 1 that positions the point of action of the force experienced by the colloidal particle on its center.

The component in the Z direction of the force experienced by the colloidal particle when interacting with the charged planar surface, F, was calculated as the sum of the forces exerted on the colloidal particle by the ions conforming the EDLs associated to the planar surface and the colloidal particle and the forces exerted on the colloidal particle by the charged groups on the planar surface, $F_{i\text{-}M}$. The force experienced by the colloidal particle could bear two signs: (i) a negative sign when the force pointed towards the planar surface and was regarded as "attraction"; and (ii) a positive sign when the force pointed away from the planar surface and was regarded as "repulsion".

5.2.3 Simulation parameters

The planar surface was discretely charged by negatively charged groups of diameter of 3 Å, in a concentration equivalent to the following values of surface charge density: –1.78 $\mu C/cm^2$ and –5.23 $\mu C/cm^2$. These values, are much smaller than the ones used in Chapter 3, and satisfy the requirement to achieve bulk conditions in all directions surrounding the colloidal particle. Solutions of 1:1, 2:1 and 3:1 electrolytes were used. The coions were hydrated and monovalent, with a diameter of 4.25 Å, whereas the counterions had different hydrated diameters depending on their charge. Monovalent counterions were assumed to have a diameter of 4.25 Å, divalent counterions had a diameter of 6 Å, and trivalent counterions had a diameter of 9 Å. The colloidal particle had a diameter of 30 Å, and charges in its center equivalent to the following values of surface charge density: –5.67 $\mu C/cm^2$ and –17.0 $\mu C/cm^2$.

All the simulations were performed with 1000 to 2000 ions and charged groups in the system. Ratios of width to length (W/L) of 1.6 to 2.0, and acceptance ratios of less than 30 % were used. Averaging procedures were performed after 80% of the total run time was completed. Each force value was calculated from an average of at least two different simulations with a maximum absolute difference of $0.5x10^{-4}$ nN.

The simulations were performed by the code in Fortran 90/95 and an additional subroutine for the calculation of the interaction force. The code was run on high

performance computers (Origins 3000) under a Unix environment. Table 5.1 presents a summary of the simulations performed for this part of the work.

Table 5.1 Simulations performed for the calculation of the interaction force between a spherical colloidal particle and a discretely charged planar surface

Electrolyte	Planar surface charge density [$\mu C/cm^2$]	Colloidal particle charge density [$\mu C/cm^2$]	Separation distance, D [Å]
1:1	–1.78	–5.67	$5d_M$ $4d_M$ $3.5d_M$ $3d_M$ $2.5d_M$ $2d_M$ $1.5d_M$ d_M $0.8d_M$ $0.75d_M$ $0.6d_M$ $(d_w+d_M)/2$
	–5.23	–17.0	$5d_M$ $4d_M$ $3.5d_M$ $3d_M$ $2.5d_M$ $2d_M$ $1.5d_M$ d_M $0.8d_M$ $0.75d_M$ $0.6d_M$ $(d_w+d_M)/2$
2:1	Id	Id	Id
3:1	Id	Id	Id
2:1 + 1:1	Id	Id	Id
3:1 + 1:1	Id	Id	Id
3:1 + 2:1 + 1:1	Id	Id	Id

Id implies identical conditions as the ones described in the preceding cell of the table.

Two simulations were performed for each condition in order to obtain average values. The position of the colloidal particle in the Z direction, i.e., its distance from the planar surface was maintained constant in each simulation. Thermodynamic equilibrium was achieved, and the interaction force was calculated as an ensemble average over the last 20 % of the simulation run.

Initially, cutoff distances around the colloidal particle and the planar surface were introduced in order to include only the interaction forces of the colloidal particles with ions associated with any of the two EDLs in the system. Therefore, ion distribution functions were initially used to evaluate the thickness of the double layer, label the ions in the system as "EDL ions" or "non-EDL ions", and include or exclude them from the force calculation algorithm. This procedure, besides being computationally costly, could result in cut-offs distances of arbitrary nature in some cases. Trial simulations were performed including all the ions in the force calculation algorithm, based on the premise that the net force exerted on the particle by the ions comprising the bulk solution should be zero. Comparisons between simulations considering a cutoff distance for the EDL thickness and simulations including all the ions in the system did not present differences. In fact, for large separation distances, where no EDL overlap was expected, the simulations including all the ions in the system gave a clean value of 0 for the force experienced by the colloidal particle, as expected. Therefore, the results discussed in this work are the ones obtained from simulations where all the ions in the system were included in the calculation of the force experienced by the colloidal particle while interacting with the charged planar surface.

For purposes of discussion, the results are presented as force curves, i.e., force experienced by the colloidal particle as a function of the separation distance between the planar surface and the closest point of the spherical surface. The same scale in the force axes is employed in all cases in order to facilitate comparisons.

5.2.4 Classical calculation of the interaction force between a spherical particle and a planar surface in a 1:1 electrolyte

The CMC simulation results for the interaction force in terms of separation distance between the spherical colloidal particle and the planar surface were compared to DLVO predictions of the electrostatic interparticle force at identical conditions in the case of the solutions of 1:1 electrolytes. The objectives of the comparisons of CMC calculations with DLVO predictions are to test the reliability of the simulation scheme and to establish the specific differences between the two approaches, i.e., establish the consequences of the application of the mean-field, pseudo-one-component approximation within the framework of the DLVO theory, which is based on the PB equation for the EDL.

Analytical expressions based on the PB equation for the electrostatic interactions between a spherical particle and a planar surface, in the case of constant surface charge, are not readily available, especially without additional approximations to those considered in the formulation of the PB equation. Therefore, an expression for the electrostatic interaction force between two spherical charged particles was chosen as a starting point for the

derivation of an analytical expression for the sphere – planar surface system. The expression was originally derived with the following approximations: (i) it can be applied to conditions of constant surface charge (most of the models are applicable to constant surface potential), (ii) a linearized series expansion of the PB equation has been employed, and (iii) the expression was obtained via Derjaguin integration methods (Wiese and Healy, 1970; Usui, 1973). The interaction potential, $V(D)$, between two charged spheres as a function of separation distance, D, is given by:

$$V(D) = \frac{2\pi a_1 a_2 n_\infty k_B T}{(a_1 + a_2)\kappa^2}\left(\Phi_1^2 + \Phi_2^2\right)\left[\frac{2\Phi_1\Phi_2}{\Phi_1^2 + \Phi_2^2}\ln\left(\frac{1+\exp(-\kappa D)}{1-\exp(-\kappa D)}\right) - \ln\left(1-\exp\left(1-\exp(-2\kappa D)\right)\right)\right] \quad (5.3)$$

where a_1 and a_2 correspond to the radii of the spherical colloidal particles, n_∞ corresponds to the ionic strength of the bulk solution, k_B is the Boltzmann constant, T is the absolute temperature, Φ_1 and Φ_2 are the reduced potentials at the surface equivalent to certain values of surface charge density, and κ is the Debye length, defined by equation 2.9.

The reduced potentials, Φ_i, are related to the potentials at the surface, ψ_i, via the following expression:

$$\Phi_i = \frac{\bar{e}\psi_i}{k_B T} \quad (5.4)$$

where □ is the charge of the electron, k_B is the Boltzmann constant, and T is the absolute temperature. The potential at the surface and the surface charge density are related through the following electroneutrality condition:

$$\sigma_0 = -\varepsilon_0 \varepsilon_r \left(\frac{d\psi}{dz} \right)\Bigg|_{z=0} \qquad (5.5)$$

where σ_0 is the surface charge density, ε_0 and ε_r are the permittivity of vacuum and the permittivity of water respectively, and ψ is the electrical potential.

The electrostatic force $F(D)$, at a given separation distance D, is related to the interaction potential between two surfaces through the following expression:

$$F(D) = -\frac{dV}{dz}\Bigg|_{z=D} \qquad (5.6)$$

where V is the interaction potential between two charged surfaces, given by equation 5.3.

In the case of a spherical particle interacting with a planar surface, one can approximate the interaction to the one between two spherical particles with one of the particles having a curvature tending to infinite. Therefore, the limit when a_2 (the radius of the planar surface) tends to infinite was applied to equation 5.3. Then, the resulting expression was derived with respect to separation distance in order to apply equation 5.6. The following

expression for the electrostatic force, *F(D)*, between a charged spherical particle and a charged planar surface as a function of separation distance *D*, was obtained:

$$F(D) = \frac{4\pi d_M n_\infty k_B T}{\kappa} \frac{\left(\Phi_M^2 + \Phi_W^2\right)}{1 - \exp(-2\kappa D)} \left[\frac{2\Phi_M \Phi_W}{\left(\Phi_M^2 + \Phi_W^2\right)} \exp(-\kappa D) + \exp(-2\kappa D) \right] \quad (5.7)$$

where d_M corresponds to the diameter of the spherical colloidal particle, n_∞ corresponds to the ionic strength of the bulk solution, k_B is the Boltzmann constant, T is the absolute temperature, Φ_M and Φ_W are the reduced potentials at the surface for the colloidal particle and the planar surface respectively, and κ is Debye length, defined by equation 2.9.

Equation 5.7 was used to predict the electrostatic interaction force between the planar surface and the spherical particle as a function of distance for all the comparisons with the CMC simulation results at identical conditions for the 1:1 electrolyte solutions. Equation 5.5 was applied to estimate the values of the reduced potentials at the surface with the values of surface charge employed in the CMC simulations. Comparisons of the behavior of the force curves obtained by the classical approach and the CMC simulations are performed in terms of interaction force as a function of reduced separation distance in terms of the radius of the colloidal particle R_M.

5.3 Interaction force between a spherical particle and a planar surface in a single electrolyte solution

Simulations with solutions of the same ionic strength containing a single 1:1, 2:1, or 3:1 electrolyte were performed in order to assess the effect of the size and the charge of the counterion on the force experienced by a spherical colloidal particle as it approaches a discretely charged planar surface.

5.3.1 Electrostatic force at low surface charge densities

One of the limitations of the DLVO theory, which was pointed out via comparisons to experimental data, is its applicability to cases of low surface potential or low surface charge density (Elimelech et al., 1995; Hiemenz and Rajagopalan, 1997; Israelachvili, 1998; Hunter, 2001). The classical expressions for the electrostatic interparticle force between charged surfaces are able to predict the behavior of real surfaces in 1:1 electrolytes when the thickness of the EDLs involved is smaller than the characteristic size of the system, e.g. the diameter of spherical particles involved. Therefore, comparisons of CMC simulations with DLVO theory predictions of the electrostatic interaction force at low surface potentials can be helpful in revealing some specific predictive limitations of the classical theory associated to the mean-field, pseudo one-component approximation. The values of the surface charge density selected for the spherical colloidal particle and the planar surface were –5.67 μC/cm^2 (surface potential, ψ_M = –103.9 mV) and –1.78 μC/cm^2 (surface potential, ψ_W = –32.6 mV), respectively.

5.3.1.1 CMC simulations vs DLVO theory: the case of a 1:1 electrolyte

Figure 5.2 presents the results for the electrostatic interaction force curve experienced by a spherical colloidal particle interacting with a discretely charged planar surface.

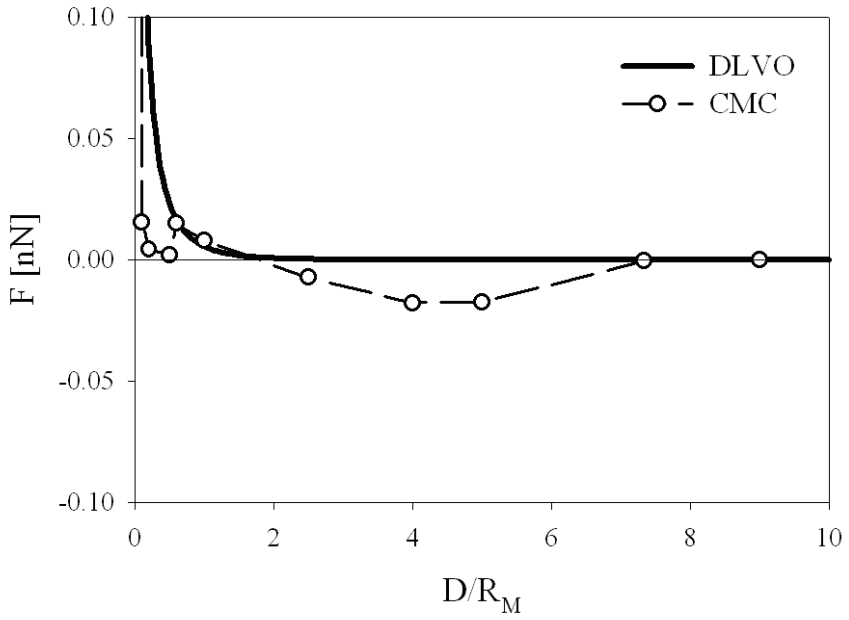

Figure 5.2 Force experienced by a colloidal particle as a function of reduced distance when interacting with a planar surface obtained by classical DLVO theory calculations and CMC simulations. The surface charge density of the spherical particle and the planar surface are equivalent to –5.67 μC/cm^2 (ψ_M = –103.9 mV) and –1.78 μC/cm^2 (ψ_W = –32.6 mV), respectively. A 1:1 electrolyte solution of ionic strength equal to 0.05 M is employed.

Figure 5.2 presents some qualitative agreement between the predictions of the DLVO theory and the CMC simulations for the interaction force between a spherical colloidal particle and a planar surface. The DLVO theory always predicts a repulsive interaction between two similarly charged surfaces at all conditions of ionic strength and values of surface charge density (Elimelech et al., 1995; Hiemenz and Rajagopalan, 1997; Israelichvili, 1998; Hunter, 2001). The strengths of the surface charge and the solution

ionic strength only affect the magnitude and the range of the repulsive interaction force. The CMC simulation results on the other hand show an interaction force that is oscillatory in nature as it can be seen in Figure 5.2. There is a shallow attractive zone between the separation distances of 1.67 to 7.00 (25 to 105 Å), and an abrupt short range decay or minimum in the interaction force almost at contact between 0.1 and 0.6 (1.5 and 9.0 Å). In the case of the short range decay, although still repulsive in nature, the magnitude of the minimum force is almost zero (2.09×10^{-3} nN at 0.5, 7.5 Å, of separation distance between the surfaces).

Molecular modeling works on the calculation of the effective interaction potentials between similarly charged surfaces embedded in 1:1, 2:1, and 2:2 electrolytes report the existence of two types of attractive effective interaction potential between surfaces: a short-range depletion interaction of attractive nature and a long-range attractive interaction potential of electrostatic origin (Valleau et al., 1991; Chu and wasan, 1996; Wu et al., 1999; Striolo et al., 2002). The origin for the depletion interaction is believed to be entropic due to excluded volume effects, which are a direct consequence of the consideration of ions with finite size (Valleau et al, 1991, Wu et al., 1999; Striolo et al, 2002; Oettel, 2004). The origin for the long-range attractive interaction is believed to reside in the ion-ion correlation effects (Valleau et al., 1991; Delville et al., 1997; Meyer et al., 2001; Striolo et al., 2002). Specifically, the occurrence of long-range attractive effective interaction potentials is believed to correspond to the "attraction from intervening counterion layers and the correlated density functions in the EDLs

surrounding both particles" (Wu et al., 1999) or to the influence of many body effects on the effective interaction potential (Feng and Ruckenstein, 2004).

Although the force experienced by a colloidal particle when interacting with a charged planar surface was calculated in this work, the two types of interaction reported in the literature during the calculation of effective pair interaction potentials between spherical colloidal particles can be detected. As discussed in Chapter 4, the analysis of the structure of the interacting EDLs showed that ions are displaced from the region between the interacting surfaces as they approach each other. This behavior is depicted in Figure 4.5, which displays results at the same conditions used in Figure 5.2. The displacement of ions from the interaction region starts taking place at a separation distance equivalent to one particle radius (15 Å). In Figure 5.2, this separation distance is the one at which the interaction force reaches a repulsive local maximum (1.48×10^{-2} nN), before it drops significantly to a minimum. Therefore, the short range decrease of the magnitude of the force experienced by the colloidal particle corresponds to depletion forces.

The particle experiences a long-range weak attractive force, most probably due to ion-ion correlation effects. The analysis of the structure of the EDLs during the interaction of the charged surfaces, performed in Chapter 4, shows that the surfaces develop independent EDLs and bulk conditions are achieved in the space between the two surfaces at long separation distances. However, as the surfaces get closer, the zone of bulk conditions decreases and, as EDL overlap occurs, layers of fluid with counterions and coions are squeezed out of the space between the interacting surfaces, resulting in a slight ordering

of layers of fluid with consecutive high local concentrations of counterions or coions. This partial ordering, which is a result of the interactions between the ions located in the space between the charged surfaces, may result in some degree of charge neutralization between adjacent layers of fluid in the region between the two surfaces and in the net shallow attractive interaction observed in figure 5.2 if the number of counterions is higher than the coions. This phenomenon corresponds to the ion-ion correlation effects that are not taken into consideration during the formulation of the DLVO theory. One must also note that volume exclusion effects take place as well as layers of fluid and ions are being squeezed out of the space between the surfaces. However, ion exclusion effects occur to a lesser extent than the ones observed as the surfaces get very close to contact since screening of charge is limited to fewer layers of fluid.

5.3.1.2 CMC simulations of asymmetric electrolytes: 2:1 and 3:1 electrolytes

Figure 5.3 presents the results of the forces experienced by the colloidal particle when it is embedded in a 1:1 electrolyte solution, a 2:1 electrolyte solution, and a 3:1 electrolyte solution. Although the ionic strength and the surface potentials are the same in all cases, 0.05 M, the effects of charge and size asymmetry on the interaction force can be observed. The trivalent ions are assumed to have a diameter of 9 Å, while the diameter of the divalent ions and the monovalent ions corresponds to 6 Å, and 4.25 Å, respectively. The depletion force can be detected in all three cases depicted in Figure 5.3, although the magnitude of the minimum value of the force and the force – distance profiles vary.

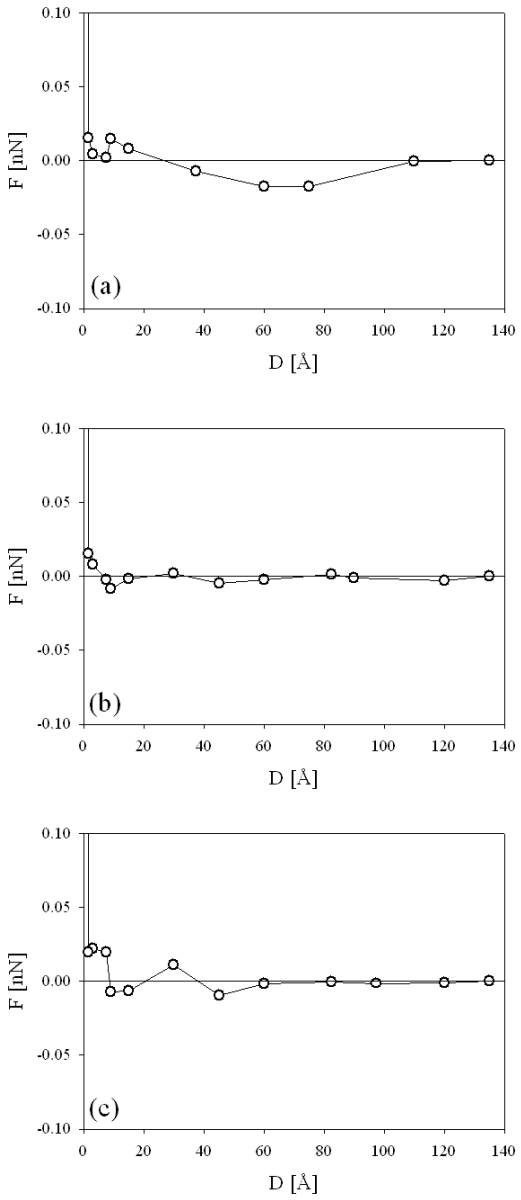

Figure 5.3 Force experienced by a colloidal particle as a function of distance when interacting with a planar surface. The surface charge densities of the spherical particle and the planar surface are equivalent to –5.67 μC/cm^2 (ψ_M = –103.9 mV) and –1.78 μC/cm^2 (ψ_W = –32.6 mV) respectively. Solutions of ionic strength 0.05 M are employed, containing (a) 1:1 electrolyte, (b) 2:1 electrolyte, and (c) 3:1 electrolyte.

In the case of the 1:1 electrolyte, Figure 5.3(a), the depletion effect occurs at separation distances between contact and 9 Å with a repulsive local minimum force of 2.02x10^{-3} nN at 7.5 Å of separation distance. In the case of the 2:1 electrolyte, depicted in Figure

5.3(b), the depletion effects are displaced further away from the surface, i.e., at separation distances between 7.5 and 15 Å with an attractive local minimum force of -8.5×10^{-3} nN at 9 Å from the planar surface. In the case of the 3:1 electrolyte, Figure 5.3(c), it is hard to determine which minimum corresponds to the depletion effect. There are three noticeable local minima in the interaction force, two of them attractive and one of them repulsive. At first impression, one might consider that the depletion effect takes place further away from the planar surface, at separation distances between 9 and 15 Å, and with an associated attractive local minimum force of -7.16×10^{-3} nN at 9 Å from the planar surface. However, we should keep in mind that there is a local minimum force of repulsive nature with a magnitude of 1.97×10^{-2} nN at 1.5 Å from the planar surface.

The depletion component of the interaction force is attractive in nature (Valleau et al, 1991, Wu et al., 1999; Striolo et al, 2002; Oettel, 2004), thus, it diminishes the magnitude of the repulsion at short separation distances, or, it may even result in short-range attractive interaction forces (Wu et al., 1999; Striolo et al., 2002). The magnitude of the contribution of the depletion force to the net interaction force is a function of the displaced volume, or a function of the size of the ions being displaced. The displacement of divalent and trivalent ions that are larger than the monovalent counterions seems to result in larger magnitudes of depletion contribution to the net interaction force, with divalent ions resulting in a maximum value of depletion force at these conditions of surface charge density. One should also consider that the number concentration of counterions required for screening the surface charge decreases as the ion valence increases, and that contributes to diminish the amount of excluded volume.

The long-range electrostatic attraction is very noticeable in the case of 1:1 electrolyte, Figure 5.3(a). In the case of the 2:1 and 3:1 electrolytes, Figures 5.3(b) and 5.3(c), the force seems to oscillate between slightly repulsive and slightly attractive values at long separation distances. As discussed in Chapter 3, divalent and trivalent counterions are more effective in terms of screening surface charge, and they present more noticeable ordering of successive layers of fluid with accumulation or depletion of counterions and coions in the EDL (e.g. Figure 3.4) but at distances closer to the charged surface. Therefore, a more effective screening of the charge in the region between the surfaces takes place, which results in long-range attractive effects of lesser magnitude. Although the oscillations of the force at large separation distances have a smaller magnitude for 3:1 electrolytes than for 2:1 electrolytes, a relatively large oscillation of the force experienced by the colloidal particle occurs between the separation distances of 30 Å and 9 Å in the case of the 3:1 electrolyte. The large size of the trivalent counterions may have induced some excluded volume effects not only at contact, but as the particles get closer. Furthermore, the large charge and size asymmetry between counterions and coions might as well enhance the ion-ion correlation effects: the counterions bear three times the charge of the coions, and they are twice as large. In Chapter 3, we reported a high degree of oscillations in terms of local concentrations in the case of 3:1 electrolytes, which resulted from successive accumulation of trivalent counterions and monovalent coions in adjacent layers of fluid to the charged surface, as can be seen in Figure 3.4.

5.3.2 Electrostatic force at intermediate surface charge densities

As the surface charge densities or surface potentials of two interacting surfaces increase, the predictive capabilities of the DLVO theory diminish because the size of the interacting EDLs becomes comparable to the characteristic size of the system (Elimelech et al., 1995; Hiemenz and Rajagopalan, 1997; Israelachvili, 1998; Hunter, 2001). Therefore, more noticeable differences between the CMC simulations and the DLVO theory predictions are expected.

A comparison between the predictions of the interaction force for a 1:1 electrolyte at the same ionic strength, depicted in Figure 5.2, will be performed in this section. The effects of charge and size asymmetry of the electrolyte comprising the EDLs of the interacting surfaces will be addressed in this section as well.

5.3.2.1 DLVO theory vs CMC simulations in the case of a 1:1 electrolyte

Figure 5.4 presents the results for the force experienced by a spherical colloidal particle interacting with a planar surface embedded in a 1:1 electrolyte at an ionic strength of 0.05 M. The diameter of the monovalent ions corresponds to 4.25 Å.

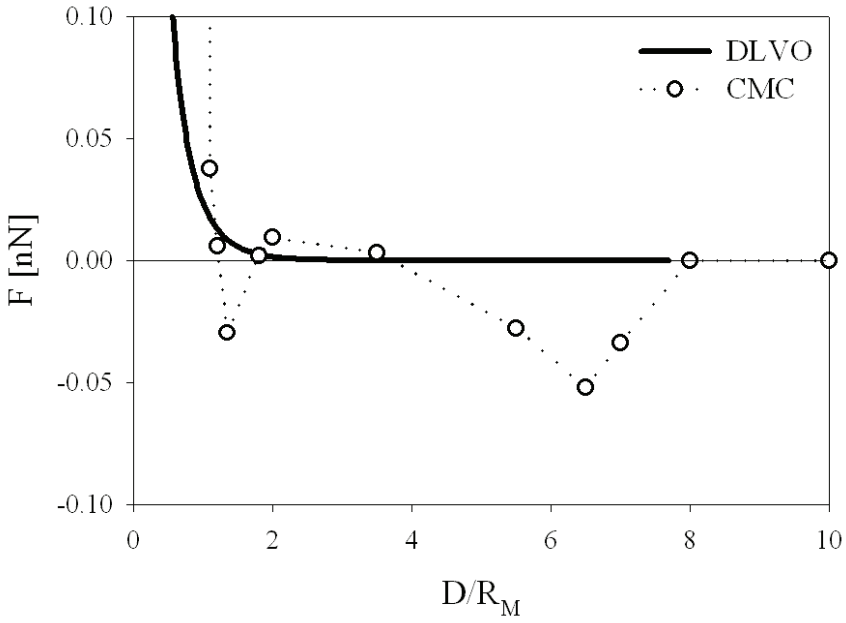

Figure 5.4 Force experienced by a colloidal particle as a function of reduced separation distance when interacting with a planar surface, obtained by classical DLVO theory calculations and CMC simulations. The surface charge densities of the spherical particle and the planar surface are equivalent to –17.0 μC/cm^2 (ψ_M = –311.5 mV) and –5.23 μC/cm^2 (ψ_W = –95.8 mV) respectively. A 1:1 electrolyte solution of ionic strength equal to 0.05 M is employed.

In the case of intermediate charge densities, the two effects already detected at lower potentials are detected as well, there is a short-range depletion force and a long-range attractive electrostatic force. The excluded volume or depletion contribution results in an attractive minimum of -2.96×10^{-2} nN at a reduced separation distance of 0.37 (5.5 Å) from the surface as depicted in Figure 5.4. However, the window of separation distances where the depletion effects are noticeable is narrower in the case of intermediate surface charge densities, Figure 5.4, than in the case of lower ones, Figure 5.2. In the same manner, the long-range electrostatic attraction takes place in a narrower range of separation distances at intermediate surface potentials than at lower ones, i.e. 4.33 to 6.33 (65 to 95 Å) in the higher-potential case compared to 1.67 to 7.00 (25 to 105 Å) in the lower-potential case (Figure 5.2). The long-range electrostatic attraction reaches a deep

minimum (attractive force) of -5.21×10^{-2} nN at 5.5 (82.5 Å) in the case of higher surface potentials as depicted in Figure 5.4.

Higher surface charge or surface potentials result in higher local concentrations of counterions in the first couple of layers of fluid adjacent to charged surfaces, as discussed in Chapter 3. In some cases, counterions might even collapse or condense on the first layer of fluid adjacent to a charged surface at sufficiently high surface charges (Delville et al., 1997). It was shown in Chapter 3 that the screening of surface charge takes place in the first two or three layers of fluid adjacent to the surface at very high surface charge densities. Therefore, a larger excluded volume effect at smaller separation distances is expected as the charge densities or potentials of the interacting surfaces increase. As mentioned in Chapter 4, the onset of the displacement of the ions from the region comprised between the interacting surfaces occurs at smaller separation distances for higher surface charges, which relates to the narrower window of separation distances for the depletion effect detected in Figure 5.4. Additionally, the magnitude of the attractive long-range interactions at intermediate values of the surface potential is much higher than the one at low surface charges. This behavior was expected, since higher values of local concentrations of counterions and lower values of local concentration of coions are expected at higher surface charge densities.

5.3.2.2 CMC simulations of asymmetric electrolytes: 2:1 and 3:1 electrolytes

Figure 5.5 presents the results for the CMC calculations of the force experienced by the colloidal particle at intermediate surface charge densities and the same conditions of ionic strength depicted in Figure 5.3. As discussed in section 5.3.2.1, in the case of the 1:1 electrolyte, the excluded volume or depletion contribution results in an attractive minimum of -2.96×10^{-2} nN at a distance of 5.5 Å from the surface, and the window of separation distances of the long-range attraction lies between 65 to 95 Å [see Figure 5.5(a)]. The long-range electrostatic attraction reaches a deep minimum (attractive force) of -5.21×10^{-2} nN at 82.5 Å, as also depicted in Figure 5.5(a). In the case of the 2:1 electrolyte [Figure 5.5(b)], what seems to be the excluded volume or depletion contribution results in a local attractive minimum force of -1.32×10^{-2} nN at a distance of 7.5 Å from the surface, and the window of separation distances of the long-range attraction lies between 20 to 95 Å. However, a minimum force of repulsive nature takes place close to contact (4.34×10^{-2} nN at a distance of 1.5 Å). The long-range electrostatic attraction reaches two deep minima (attractive force) with magnitudes of -9.66×10^{-2} nN and -7.10×10^{-2} nN at 75.0 Å and 30.0 Å, respectively, as depicted in Figure 5.5(b).

Finally, in the case of the 3:1 electrolyte [Figure 5.5(c)], what we believe to be the excluded volume or depletion contribution results in two local attractive minima of -3.40×10^{-3} nN at a distance of 1.5 Å from the surface, and of -2.65×10^{-2} nN at 10.5 Å. The window of separation distances of the long-range attraction lies between 35 to 85 Å [Figure 5.5(a)]. The long-range electrostatic attraction reaches one minimum (attractive

force) with a magnitude of -2.75×10^{-2} nN at 30.0 Å of separation distance, as depicted in Figure 5.5(c).

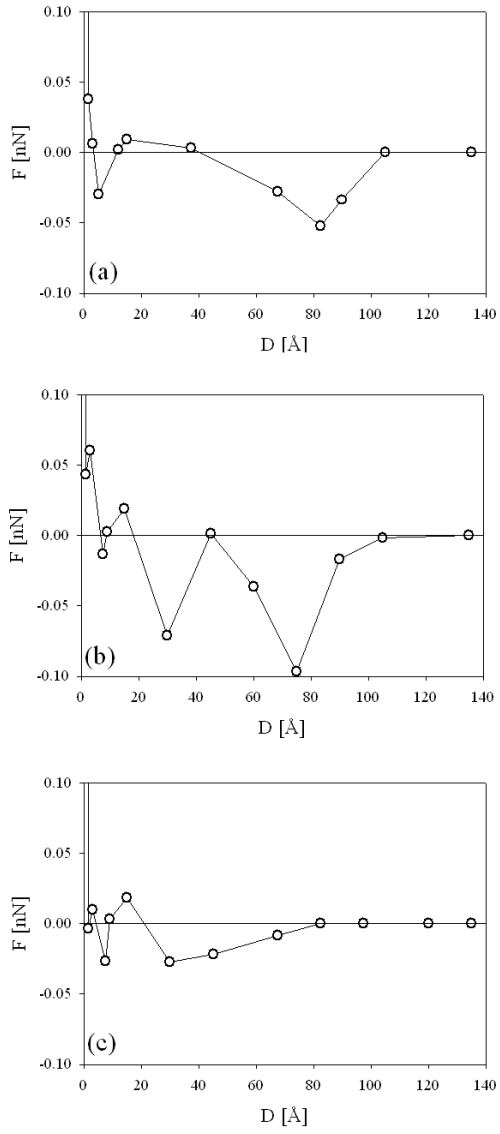

Figure 5.5 Force experienced by a colloidal particle as a function of separation distance when interacting with a planar surface. The surface charge densities of the spherical particle and the planar surface are equivalent to -17.0 μC/cm^2 ($\psi_M = -311.5$ mV) and -5.23 μC/cm^2 ($\psi_W = -95.8$ mV) respectively. Solutions of ionic strength 0.05 M are employed, containing (a) 1:1 electrolyte, (b) 2:1 electrolyte, and (c) 3:1 electrolyte.

As in the case of low surface charge densities, the oscillations of the interaction force are of lesser magnitude in the case of 3:1 electrolytes than in the case of 2:1 electrolytes, and

they tend to occur at shorter separation distances between both surfaces. As discussed in Chapter 3, the more effective screening of charge by higher valence ions results in fewer layers of fluid involved in the EDL, and that may explain the fact that the range of the long-range attractive effects becomes shorter as the counterion valence increases.

The fact that there seem to be two depletion minima in the case of 2:1 and 3:1 electrolytes is very interesting. The local minima occur at a separation distance of 1.5 Å in the case of 2:1 electrolyte at intermediate surface charge densities, and in the cases of 3:1 electrolyte at low and intermediate surface charge densities. A possible explanation may be linked to the displacement of ions from layers of fluid adjacent to the sides of the spherical particle as the surface reaches contact.

One should also note that, among the three electrolytes selected, trivalent counterions present the negative interaction minima of smaller magnitude, especially at intermediate surface charge densities.

5.4 Interaction between a spherical colloidal particle and a planar surface in mixtures of symmetric and asymmetric electrolytes

Following the same rationale behind the planning of simulation experiments employed in Chapters 3 and 4, we examined the behavior of the net force experienced by a charged spherical colloidal particle that interacts with a charged planar surface for mixtures containing 1:1, 2:1 and 3:1 electrolytes. The ionic strength of all the solutions was 0.05

M, and the two cases of low and intermediate sets of values of surface charge densities, discussed in the previous section of this Chapter, were examined here as well.

5.4.1 Low surface charge densities

Figure 5.6 presents the results for the force experienced by the spherical colloidal particle when it is embedded in a solution of 1:1 and 2:1 electrolytes of ionic strength 0.05 M.

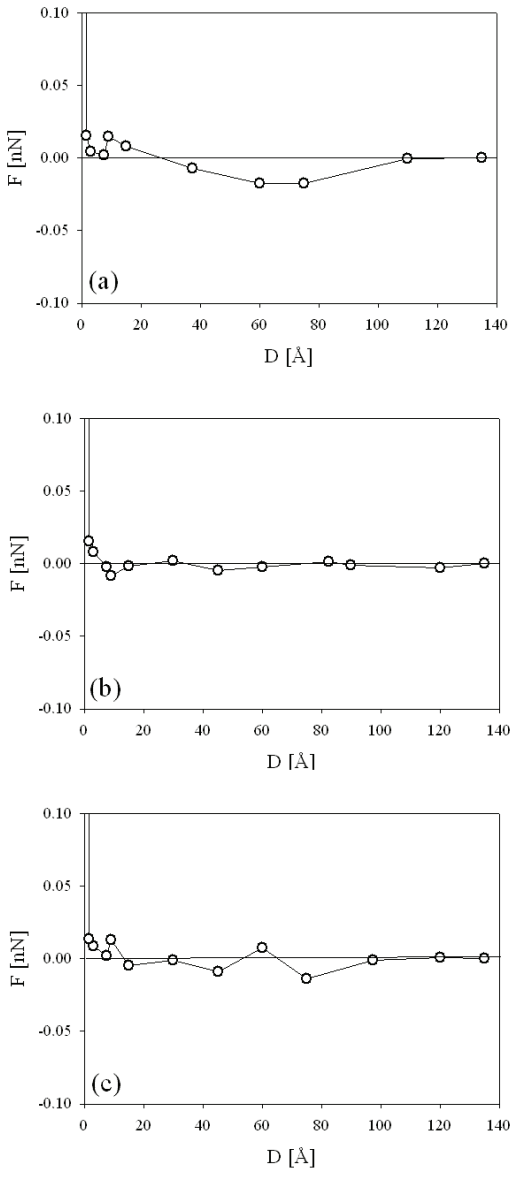

Figure 5.6 Force experienced by a colloidal particle as a function of distance when interacting with a planar surface. The surface charge densities of the spherical particle and the planar surface are equivalent to –5.67 μC/cm^2 (ψ_M = –103.9 mV) and –1.78 μC/cm^2 (ψ_W = –32.6 mV) respectively. Solutions of ionic strength 0.05 M are employed, containing (a) 1:1 electrolyte, (b) 2:1 electrolyte, and (c) mixture of 2:1 and 1:1 electrolytes.

For the purpose of discussion, the behavior of the force curves obtained in solutions of a single 1:1 electrolyte and a single 2:1 electrolyte at the same conditions of ionic strength and at the same values of surface charge density are displayed in Figures 5.6(a) and

5.6(b), respectively. Figure 5.6(c) presents the results for the mixture of 2:1 and 1:1 electrolytes. A local minimum in the interaction force of slightly repulsive nature ($1.95x10^{-3}$ nN), related to depletion effects, takes place at a separation distance of 7.5 Å. This separation distance coincides with the separation distance of the local minimum force related to depletion effects reported for 1:1 electrolytes, and the magnitudes of the two force minima differ only in $0.14x10^{-3}$ nN. There is no shallow long-range attractive interaction in the case of the mixture of 2:1 and 1:1 electrolytes, as can be seen in Figure 5.6(c), but rather an oscillatory behavior between slightly attractive and repulsive values similar to the one observed for the single 2:1 electrolyte case, depicted in Figure 5.6(b). However, the oscillations in the case of the mixture are of a slightly larger magnitude.

The results observed in Figure 5.6 point to the conclusion that there seems to be a combination of behaviors of the single 1:1 and 2:1 electrolytes in the resulting behavior of the mixture of these electrolytes. At short separation distances, the monovalent counterions seem to dominate the behavior of the interaction force. On the other hand, the divalent counterions seem to dominate the long-range interactions. However, no preferential screening of charge by divalent counterions or monovalent counterions could be detected in Chapter 4.

Figure 5.7 presents the results for the mixture of 3:1 and 1:1 electrolytes at an ionic strength of 0.05 M and low values of surface charge density.

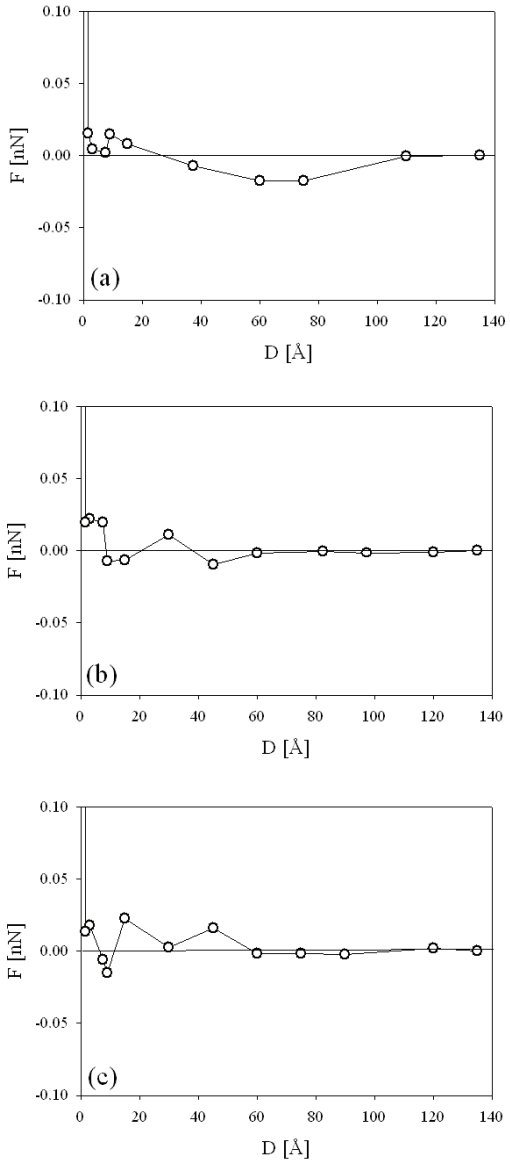

Figure 5.7 Force experienced by a colloidal particle as a function of distance when interacting with a planar surface. The surface charge densities of the spherical particle and the planar surface are equivalent to –5.67 μC/cm^2 (ψ_M = –103.9 mV) and –1.78 μC/cm^2 (ψ_W = –32.6 mV), respectively. Solutions of ionic strength 0.05 M are employed, containing (a) 1:1 electrolyte, (b) 3:1 electrolyte, and (c) mixture of 3:1 and 1:1 electrolytes.

Once again the behavior of the force curves obtained in solutions of a single 1:1 electrolyte and a single 3:1 electrolyte at the same conditions are displayed in Figures 5.7(a) and 5.7(b), respectively. In Figure 5.7(c), there are two local minima close to contact: a local minimum in the interaction force of slightly repulsive nature (1.34x10^{-3}

nN) takes place at a separation distance of 1.5 Å. This separation distance coincides with the separation distance of the local minimum force reported for the single 2:1 electrolyte at intermediate surface charge densities depicted in Figure 5.5(b), and for the single 3:1 electrolyte at both low and intermediate values of surface charge densities depicted in Figures 5.3(c) and 5.5(c), respectively. A second minimum of attractive nature ($-1.50 \bullet 10^{-2}$ nN) takes place at a separation distance of 9.0 Å. There is no shallow long-range attractive interaction in the case of the mixture of 3:1 and 1:1 electrolytes, as can be seen in Figure 5.7(c), but rather an oscillatory behavior displaced towards the repulsive region that resembles the single 3:1 electrolyte case, depicted in Figure 5.7(b).

Although a combination of behaviors of the single 1:1 and the single 3:1 electrolytes can be noticed in Figure 5.7, the range of influence of each kind of electrolyte in terms of separation distance cannot be clearly established. However, the fact that long-range weak attractive interactions are absent at separation distances larger than 55Å for the mixture of electrolytes implies that, at those long separation distances, the trivalent counterion determines the behavior of the interactions.

Figure 5.8 presents the behavior of the force experienced by the colloidal particle interacting with the planar surface in a mixture of 1:1, 2:1, and 3:1 electrolytes.

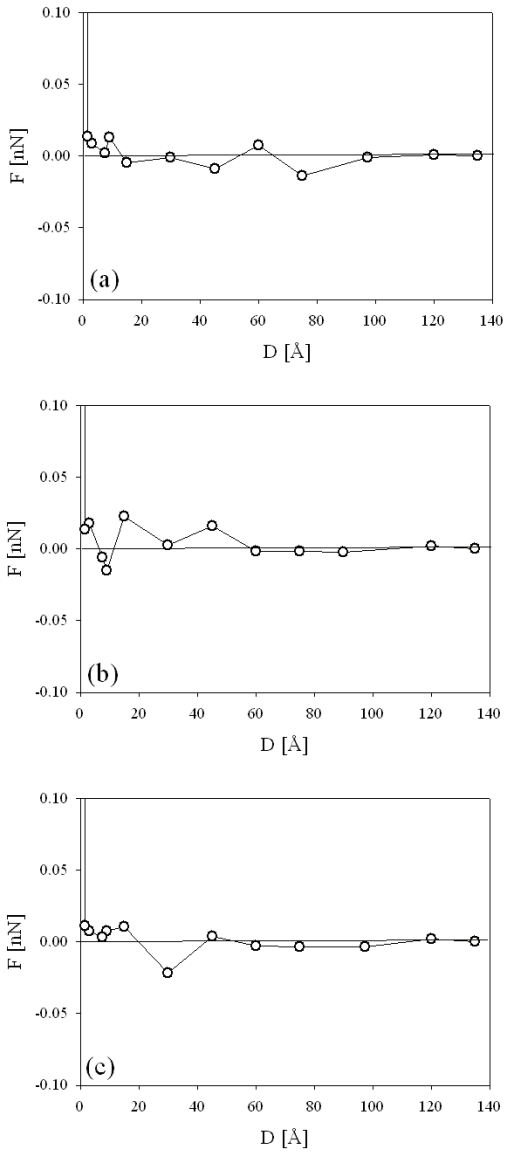

Figure 5.8 Force experienced by a colloidal particle as a function of distance when interacting with a planar surface. The surface charge densities of the spherical particle and the planar surface ARE equivalent to –5.67 μC/cm^2 (ψ_M = –103.9 mV) and –1.78 μC/cm^2 (ψ_W = –32.6 mV), respectively. Solutions of ionic strength 0.05 M are employed, containing mixtures of (a) 2:1 and 1:1 electrolytes, (b) 3:1 and 1:1 electrolytes, and (c) 3:1, 2:1 and 1:1 electrolytes.

For the purpose of discussion, the behavior of the force curves obtained in mixtures of 2:1 and 1:1 electrolytes, and 3:1 and 2:1 electrolytes at the same conditions of ionic strength and at the same values of surface charge density are displayed in Figure 5.8(a) and Figure 5.8(b), respectively. Figure 5.8(c) presents the results for the mixture of 3:1,

2:1, and 1:1 electrolytes. A local minimum in the interaction force of slightly repulsive nature (3.09×10^{-3} nN), related to depletion effects, takes place at a separation distance of 7.5 Å. This separation distance coincides with the separation distance of the local minimum force related to depletion effects as reported for the single 1:1 electrolyte (Figure 5.2), and the mixture of 2:1 and 1:1 electrolytes depicted in Figure 5.8(b). The behavior of the force for the mixture of 3:1, 2:1, and 1:1 electrolytes does not present shallow long-range attractive interaction, as can be seen in Figure 5.8(c), but rather an oscillatory behavior between slightly attractive and repulsive values similar to the one observed for the single 2:1 electrolyte and the single 3:1 electrolyte cases [Figures 5.3(b) and 5.3(c), respectively].

Although no clear distinction can be made on which counterion determines the behavior within which window of separation distances, it seems that the monovalent counterion determines the behavior at short separation distances (lower than 15 Å to contact), and the divalent and trivalent counterions determine the behavior at long separation distances. This observation correlates well with the observation that at short distances, the monovalent counterions carry most of the charge screening due to their smaller size. On the other hand, at long distances, higher-valence counterions require that fewer layers of fluid be involved in the EDLs because they are more effective in screening the surface charge. This behavior allows higher-valence counterions to control the electrostatic interaction at larger separation distances, and narrow the range of the long-range attractive forces.

5.4.2 Intermediate values of surface charge densities

In the previous section, we observed that the magnitude and number of deep minima in the interaction force curve increase with increasing surface potential. This behavior is further explored in this section with mixtures of electrolytes at the same ionic strength.

Figure 5.9 presents the results for the mixture of 2:1 and 1:1 electrolytes:

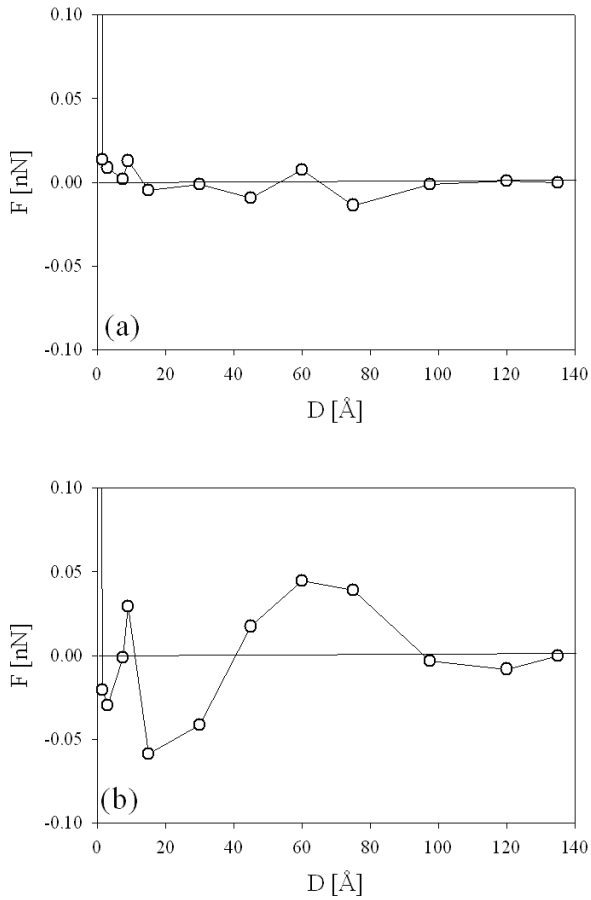

Figure 5.9 Force experienced by a colloidal particle as a function of distance during the interaction with a planar surface. Solutions of ionic strength 0.05 M containing a mixture of 2:1 and 1:1 electrolytes are employed. The surface charge densities of the spherical particle and the planar surface are equivalent to: (a) –5.67 μC/cm^2 (ψ_M = –103.9 mV) and –1.78 μC/cm^2 (ψ_W = –32.6 mV) respectively, and (b) –17.0 μC/cm^2 (ψ_M = –311.5 mV) and –5.23 μC/cm^2 (ψ_W = –95.8 mV) respectively.

Figure 5.9(a) presents the results obtained for the mixture of 2:1 and 1:1 electrolytes at low surface charge densities. In Figure 5.9(b), two steep local attractive minima, a local repulsive maximum and a shallow attractive minimum can be seen. The excluded volume effect seems to be related to the steep attractive minimum of the force (-2.98×10^{-2} nN) located at 3 Å of the surface. The steep attractive minimum with a magnitude of -5.86×10^{-2} nN at 15 Å seems to correspond to an electrostatic effect. There is maximum in the force of repulsive character (4.47×10^{-2} nN) at 60 Å followed by a shallow minimum that resembles the one for single 1:1 electrolyte.

Figure 5.10 presents the results for the mixture of 3:1 and 1:1 electrolytes of ionic strength equal to 0.05 M, at intermediate values of surface charge densities.

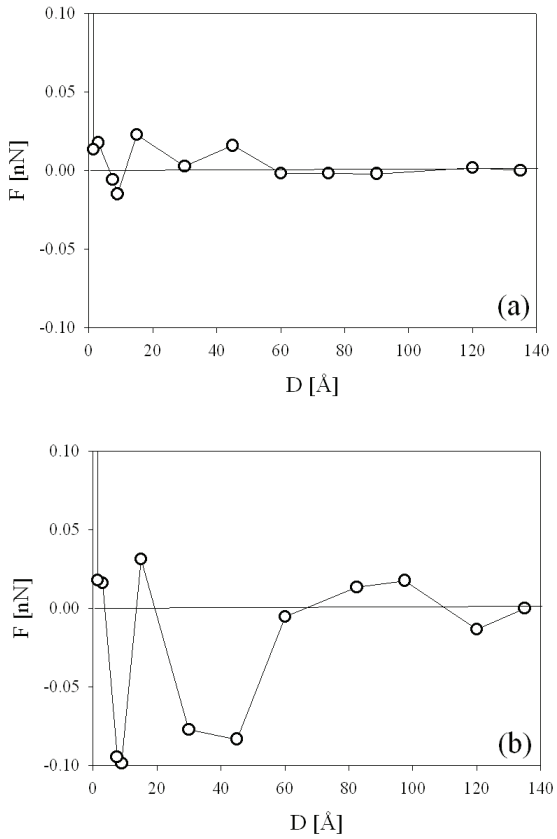

Figure 5.10 Force experienced by a colloidal particle as a function of distance during the interaction with a planar surface. Solutions of ionic strength 0.05 M containing a mixture of 3:1 and 1:1 electrolytes are employed. The surface charge densities of the spherical particle and the planar surface are equivalent to: (a) –5.67 μC/cm^2 (ψ_M = –103.9 mV) and –1.78 μC/cm^2 (ψ_W = –32.6 mV) respectively, and (b) –17.0 μC/cm^2 (ψ_M = –311.5 mV) and –5.23 μC/cm^2 (ψ_W = –95.8 mV) respectively.

Again, Figure 5.10(a) presents the results obtained for the mixture of 3:1 and 1:1 electrolytes at low surface charge densities. Figure 5.10(b) presents a similar behavior to the one observed for mixtures of 2:1 and 1:1 electrolytes: two steep local attractive minima, a local repulsive maximum, and a shallow attractive minimum can be seen. The excluded volume effect seems to be related to the steep attractive minimum of the force ($–9.84x10^{-2}$ nN) located at 9 Å of the surface. The steep attractive minimum with a magnitude of $–8.32x10^{-2}$ nN at 45 Å seems to correspond to an electrostatic effect. There

is a maximum in the force of repulsive character ($1.75x10^{-2}$ nN) at 97 Å followed by a shallow minimum that resembles the one for single 1:1 electrolyte.

The behavior of the mixtures of electrolytes at intermediate values of surface charge densities is unexpected. The slight oscillatory behavior between repulsion and attraction detected at low surface charge densities seems to be enhanced by larger values of surface potential.

The possibility of instability of the system during the simulations was investigated via the repetition of the calculations. The behavior does not seem to be associated to the calculation procedure or to any numerical errors, since the difference between the values of force in each point obtained in different simulations did not exceed $\pm 0.5x10^{-4}$ nN, which corresponds to the maximum difference between all the repetitive simulations performed.

5.5 Conclusions

The force experienced by a charged spherical particle interacting with a charged planar surface was calculated in this part of the work. The behavior of the force observed coincides with the behavior reported in literature for the effective pair interaction potential between spherical particles and colloidal platelets, obtained via molecular modeling or hypernetted-chain (HNC) theory calculations. Attractive depletion effects and long-range electrostatic attraction between similarly charged surfaces do take place.

The presence of a short-range, abrupt minimum in the force experienced by the spherical particle was detected for all electrolytes. The phenomenon responds to depletion or excluded volume effects, whose contribution to the net force is always attractive, and is a direct consequence of the consideration of the size of the ions comprising the electrolyte solutions. As expected, the magnitude of the contribution of the depletion force to the net force increases with ion size. In our model system, the size of the ions increases as their valence increases. The contribution of the depletion effects to the net interaction force reaches a maximum for divalent counterions, diminishing for trivalent counterions, because as the valence of the counterion increases, the local number concentration of counterions required to screen the surface charge diminishes. In the case of single 2:1 electrolyte solutions at intermediate surface charge densities, single 3:1 electrolyte solutions at low and intermediate surface charge densities, and of mixtures of electrolytes at low surface charge densities, two depletion effects can be detected. The local minimum of interaction force closest to the surface occurs at consistently the same separation distance for all the cases mentioned above.

A long-range attractive electrostatic effect was detected in all cases. In the case of the single 1:1 electrolyte, the electrostatic attractive forces present a shallow minimum at long separation distances. As the surface charge increases, the attractive forces of electrostatic origin present a steep minimum and their range of action gets displaced towards lower separation distances. As electrostatic coupling increases, i.e., the valence of the counterion present in the system increases, the range of the electrostatic attractive

effects on the interaction force is also displaced towards lower separation distances. This phenomenon is a direct consequence of the more effective screening of the surface charges performed by higher-valence counterions, i.e., fewer layers of fluid are involved in the EDLs. At low electrostatic potentials and high electrostatic coupling only a slightly oscillatory behavior of the force between mild attraction and mild repulsion at large separation distances can be observed. At high electrostatic potentials and high electrostatic coupling, steep attractive minima of the interaction force that have an electrostatic origin can be detected in all the cases. It is interesting to note that, while the case of single 2:1 electrolyte presents two minima of electrostatic origin, the case of single 3:1 electrolyte presents only one. The divalent electrolyte seems to depict the worst case in terms of deviations of the behavior of the interaction force with respect to the predictions of the classical theory.

The behavior of the interaction force in mixtures of electrolytes seems to respond to a combination of the behaviors of the single electrolytes the mixture is composed of especially at low surface charge potentials. The higher-valence counterions seem to determine the behavior of the force at long separation distances since no long-range attractive shallow minima were detected at low surface charge densities. Finally, at intermediate values of surface charge densities, the force in mixtures of electrolytes presents an atypical behavior, difficult to explain.

The occurrence of attractive interactions between similarly charged surfaces cannot be predicted by the classical theory due to the mean-field, pseudo-one-component

approximation within its conception. These phenomena might be responsible for the differences between the predictions of classical theory and experimental observations widely reported in literature.

5.6 Summary

In this part of the work, the force experienced by a charged spherical colloidal particle when interacting with a discretely charged planar surface was calculated.

The presence of a depletion effect and a long-range electrostatic effect of attractive nature were detected in agreement to similar molecular modeling work focused on the calculation of the effective pair interaction potential between charged spherical colloidal particles and platelets. The depletion effects escalate with electrostatic coupling since the size of the counterions and the charge increase simultaneously in our model system. The electrostatic effects are enhanced by larger values of surface charge densities. Minima in the force are detected at several separation distances between the interacting surfaces.

Up to this point the work focused on indifferent electrolytes, so all the phenomena observed were limited to the EDLs of the charged surfaces. In the next Chapter, the effects of asymmetric, non-indifferent electrolytes will be examined. In that case, the influence of charge asymmetry is expected to go beyond the EDLs, resulting in modifications of surface charges.

CHAPTER 6

INTERPARTICLE INTERACTIONS IN NON-INDIFFERENT ELECTROLYTES: SURFACE CHARGE MODIFICATION

6.1 Introduction

Colloidal particles and surfaces acquire surface charge in aqueous electrolyte solutions via chemical processes, such as protonation and deprotonation of surface groups, as well as adsorption of metal ions or other molecules. The surface charge may be nonuniformly distributed on the surface, depending on its characteristics and the distribution of active sites for the charging process. Furthermore, the presence of non-indifferent electrolytes in the electrical double layer (EDL), e.g., some metal ions and organic electrolytes, or simply organic molecules and polymers can result in a modification of the surface charge, and therefore in the characteristics of the interparticle interactions.

In the case of inorganic particles, selective ion adsorption of non-indifferent electrolytes to different crystal planes or association with different surface charged groups may occur (Feick et al., 2004). In fact, the association of such contaminants as heavy metal ions, radioactive materials, or organic molecules with soil particles via adsorption is

responsible for the translocation of these species in soils, groundwater aquifers, and fracture rocks (Ryan and Elimelech, 1996; Kretzschmar et al., 1996).

In the case of biological systems, bacteria and other particles including protein complexes have different chemical groups on their surfaces that may also lead to charge heterogeneity (Hartley et al., 1998; Keslarek et al., 2002).

The hypothesis that surfaces may not be uniformly charged has been proposed as an explanation for the discrepancies between the classical theory and the experimental observations reported in literature. In terms of distribution of surface charge, three possibilities have been contemplated: nonuniformity of charge distribution, nonrandomness of charge distribution, and surface charge heterogeneities (Miklavic et al., 1994; Ryan and Elimelech, 1996; Kretzschmar et al., 1996; Behrens et al., 2000; Velegol and Thwar, 2001; Shellenberger and Logan, 2002). Initial experimental and theoretical analyses have assessed the contribution of nonuniformity and nonrandomness of charge to deviations in the behavior of colloidal particles with respect to theoretical predictions (Miklavic et al., 1994; Ryan and Elimelech, 1996; Velegol and Thwar, 2001). However, the occurrence of surface charge heterogeneity, which is a direct consequence of the presence of non-indifferent electrolytes in the EDL, is still to be explored.

Atomic force microscopy (AFM) has been used to provide images of planar surfaces at the nanoscale, as well as direct measurements of interaction forces between a cantilever tip and a planar surface of hard or soft materials (Ishino et al., 1997; Behrens et al., 2000;

Camesano and Logan, 2000). Direct force measurements of interaction forces between a planar surface and a tip have been used to assess the surface charge of the planar surface (Butt, 1992; Heinz and Hoh, 1999). Changes in topography and interaction forces resulting from adsorption have also been investigated via AFM (Larson and Pugh, 1998). Furthermore, force-volume AFM has been used to combine force measurements with precise tip positioning on the surface in order to provide two-dimensional arrays of force curves (Rotsh and Radmacher, 1997; Johnson et al., 2003).

AFM has been used to detect the spatial distribution of polar functional groups on modified silica surfaces by associating the functional groups with specific images of the adhesion force. Force imaging has also been used to monitor two-dimensional partial adsorption of cationic polyelectrolytes on an oxidized silicon wafer. The location of sites covered by electrolyte could be directly related to regions on the surface where strong adhesive forces were detected during tip retraction. Furthermore, adsorption of mixtures of polyelectrolytes could lead to a heterogeneous surface with different adhesive forces associated with regions bearing different functional groups (Kramer et al., 1998; Estel et al., 2000). Indentation curves of commercially available elastomers were studied by the application of force-imaging AFM, and the location of calcium carbonate inclusions was detected through the change in the adhesive force. Applications of scanning electron microscopy/energy-dispersive X-ray analysis (SEM/EDX) showed that the “pits” and “holes” observed during force imaging could be directly linked to calcium inclusions (Terán-Arce et al., 2003).

In this part of the work, a mixture of an indifferent and a non-indifferent electrolyte was selected in order to experimentally assess the effect of non-indifferent electrolytes on the EDL and on the interparticle interactions. Most non-indifferent electrolytes are comprised of divalent or trivalent ions. Therefore, the electrolyte mixture used in this part of the work also contemplates asymmetry in size and charge.

Most of the studies using conventional AFM have focused on mapping the adsorption sites of long organic molecules by monitoring adhesive forces. The same principle is applied in that the net interaction forces are monitored to detect the presence and location of chemical groups bearing different charges on the surface. Copper ions were selected as non-indifferent electrolyte, since it is well known that copper adsorbs onto silica surfaces. Furthermore, AFM measurements of the interaction forces during adsorption of copper ions onto silica particles have shown that adsorption results in charge reversal, which implies change in the direction of the interaction force (Chin et al., 2002b; Vithayaveroj et al., 2003). Force-volume AFM is employed in an attempt to detect local changes in the interaction force due to the presence and adsorption of copper ions in the system.

6.2 Procedure for the experimental determination of interparticle forces

The system of study consisted of a fused silica plate and a standard silicon nitride tip embedded in background electrolyte. Silica was selected as a model surface because its charging process, i.e., protonation and deprotonation of silanol groups on the surface, can be controlled by adjusting the pH of the solution. Additionally, silica constitutes a good

model system for solids encountered in environmental systems. The requirement for high lateral resolution was met by using standard silicon nitride cantilever tips. The conditions of pH and ionic strength were selected according to three criteria: surface charge of the silica substrate and the silicon nitrite tip, predominance of electrostatic forces over Van der Waals forces, and absence of precipitated copper species. The specific concentrations of copper ion solutions injected into the systems were selected to ensure partial adsorption onto the silica surface, under the premise that copper ion adsorption might be responsible for surface charge heterogeneities.

6.2.1 Silica surfaces and standard silicon nitride tips

The substrate consisted of fused silica plates. The silica plate (Ted Pella, Inc., Redding, CA) was cleaned by soaking it for more than 12 h in a concentrated H_2SO_4 solution (Fisher Scientific, Fair Lawn, NJ). Each silica plate was rinsed with deionized (DI) water before each experiment. The topographic smoothness of the surface was determined via AFM height-images obtained using a standard NP silicon nitride tip (Digital Instruments, Santa Barbara, CA) that is constituted of a single crystal of silicon nitride of a cast shape (a tetrahedral with a rounded tip). The manufacturers report a tip radius of 20 nm for the half sphere on the edge of the silicon nitride crystal. The probe contains four cantilevers of triangular shape. In order to have the maximum sensitivity, cantilevers with a nominal spring constant of 0.06 N/m and 0.12 N/m were selected for all the experiments. The values of spring constant reported by the manufacturer were tested via the application of the method described by Cleveland et al. (Cleveland et al., 1993) that was also used in

previous work (Chin et al., 2002b). The silicon nitride tip was sequentially rinsed with DI water, hydrochloric acid, DI water, methanol, and DI water. The tip was then gently blown dry with nitrogen gas before use. The goal of the cleaning process was to remove any organic contaminants.

6.2.2 Solutions of indifferent and non-indifferent electrolytes

Water of 18-MΩ/cm resistivity at 25 ºC, prepared by an E-pure system (model D4631, Barnstead Thermolyne Co., Dubuque, IA), was used for the cleaning procedures and for the preparation of solutions. Copper ion solutions were prepared from copper nitrate (Fisher Scientific, Fair Lawn, NJ). A solution of hydrochloric acid of concentration 1 N (Fisher Scientific, Fair Lawn, NJ) was used for the adjustment of the pH of the solutions and for the cleaning procedures. Different sets of experiments involved the filtration of the copper solutions during injection of the AFM cell with Acrosdisic 13-mm syringe filters with 0.2-μm nylon membranes (Pall Life Sciences, East Hills, NY) in order to avoid the possibility of introducing particles or precipitates into the system that might affect the results. The background electrolyte solutions for adjusting the ionic strength were prepared from enzyme grade (Fisher Scientific, Fair Lawn, NJ) sodium chloride, which is regarded as an indifferent electrolyte.

6.2.3 Determination of the surface charge of the silica surfaces and the silicon nitride tips

Measurements of the zeta potential of both silica and silicon nitride surfaces were performed with a zeta meter (Zee Meter; Pen Kem, Inc., Bedford Hills, NY) using sodium chloride solutions as background electrolyte and dilute hydrochloric acid solutions for adjusting the pH. The Zee Meter measures the zeta potential of particles by determining the rate at which these particles move in a known electric field. The method is commonly referred to as microelectrophoresis. Silicon nitride crystals of alpha phase, electronic grade (94 % alpha phase) and beta phase from Alfa Aesar (Ward Hill, MA) and nonporous 3-μm silica particles from Bangs Laboratories, Inc. (Fishers, IN) were used during these measurements.

6.2.4 AFM force measurements

The interaction forces were measured by a Nanoscope IIIa atomic force microscope (Digital Instruments, Santa Barbara, CA) equipped with a fluid cell. Force-volume mode was used in this work because it provides not only an image and a single interaction force curve but also complete force vs distance curves at different points on the surface. In this mode, force curves are obtained while the AFM tip scans the sample surface. Therefore, a two-dimensional array of force vs distance curves is acquired. Each curve can be analyzed, and several quantities characterizing the interaction forces curve can be

calculated. The force at a constant distance from the surface can be displayed and analyzed for the whole array, and an image of the interaction forces can be created.

The imaging capability of AFM is the result of the logic of a control loop. The control loop works based on the difference of measured values of height (distance between the tip and the surface) and deflection of the cantilever with respect to set-point values. The set-point values can be either automatically defined by the AFM software or manually defined by the user.

In the case of height-imaging (normal AFM imaging), the topography of the surface is reproduced by the analysis of the data of the upward/downward movements of the sample with respect to the tip that aim to comply with the set-point height. Since there are interaction forces between the tip and the surface, recording cantilever deflection during upward/downward (extension/retraction) movements allows the acquisition of interaction force data.

During force-volume imaging, the set-point parameter is a constant value of deflection of the cantilever (i.e., constant force acting on the cantilever). The difference between the measured deflection of the cantilever and the set-point value causes the sample to be displaced away from the tip. The distance traveled by the sample is associated with the strength and direction of the interaction force. The upward/downward movements of the sample with respect to the tip allow the construction of a map of interaction forces, or a "force-topography" image. Because of the limitation of accumulated data, the force-

image obtained is not as sharp as the conventional AFM image. Instead, the image resembles mosaics of force data collections. Force measurements at different spots on the surface can be carried out only at a resolution of 64 × 64 spots, and the number of data points per force curve is limited to 64 at this resolution during extension and retraction. A maximum value of 1 Mb of data can be stored during this process. The resolution chosen and the amount of data recorded during each force curve measurement are interrelated; therefore, the resolution can be diminished in order to increase the amount of data per force curve. In this study, only 32 × 32 surface points were examined covering a surface of 12.5 x 12.5 μm. However, 256 data points per force curve, including extension and retraction, were recorded in order to acquire a higher resolution in the force curve data.

6.2.5 Surface analysis: determination of the presence of non-indifferent electrolyte on the silica surface

X-ray photoelectron spectroscopy (XPS) analyses were performed with a Phi model 5600LS X-ray Photoelectron spectrometer (Physical Electronics USA, Chanhassen, MN) in order to confirm the presence of copper ions on the silica surface after AFM measurements. The X-ray source utilized was Mg k-alpha (non-monochromatic). The angle between the source and the sample normal was 45 degrees, and the angle between the electron analyzer and the sample normal was 45 degrees. The experiments were performed at a base pressure of 1 x 10^{-9} torr. Survey scans (i.e., wide region scans) were

performed at an analyzer pass energy of 93.9 eV, and core level data (i.e., narrow region scans) were performed at an analyzer pass energy of 117.4 eV.

6.3 Interaction between silica and silicon nitride in a 1:1 indifferent electrolyte solution

Because the charging mechanisms of silica and silicon nitride depend on pH, it was necessary to characterize the interaction of these surfaces under different conditions of pH. This information was useful to anticipate the direction of the interaction force between silica and silicon nitride prior to the injection of copper ions into the system. Sodium chloride is used as the 1:1 indifferent electrolyte or background electrolyte.

The silicon nitride crystal serving as the tip could not be detached from the cantilevers; therefore, electrokinetic experiments with three types of commercially available silicon nitride crystals and silica particles were performed using a Zee Meter in order to determine the behavior of the zeta potential of the surfaces of interest and juxtapose that information with direct interaction force measurements. The measurements were performed in solutions of sodium chloride at an ionic strength 0.05 M, 0.005 M, and 0.0005 M. The results of the zeta potential measurements for silicon nitride and alpha phase at an ionic strength of 0.005 M are presented in Figure 6.1(a). The alpha-phase silicon nitride crystals have an isoelectric point of 7.2. This value falls in the range of 6 to 8.5 for the isoelectric point of silicon nitride tips reported in the open literature (Senden and Drummond, 1995; Miyatani et al., 1998; Behrens et al., 2000; Ziegler et al.,

2002). We consider the silicon nitride tip to behave as the commercially available alpha phase silicon nitride during this work. The isoelectric point of silica corresponds to pH 3 (see Figure 6.1).

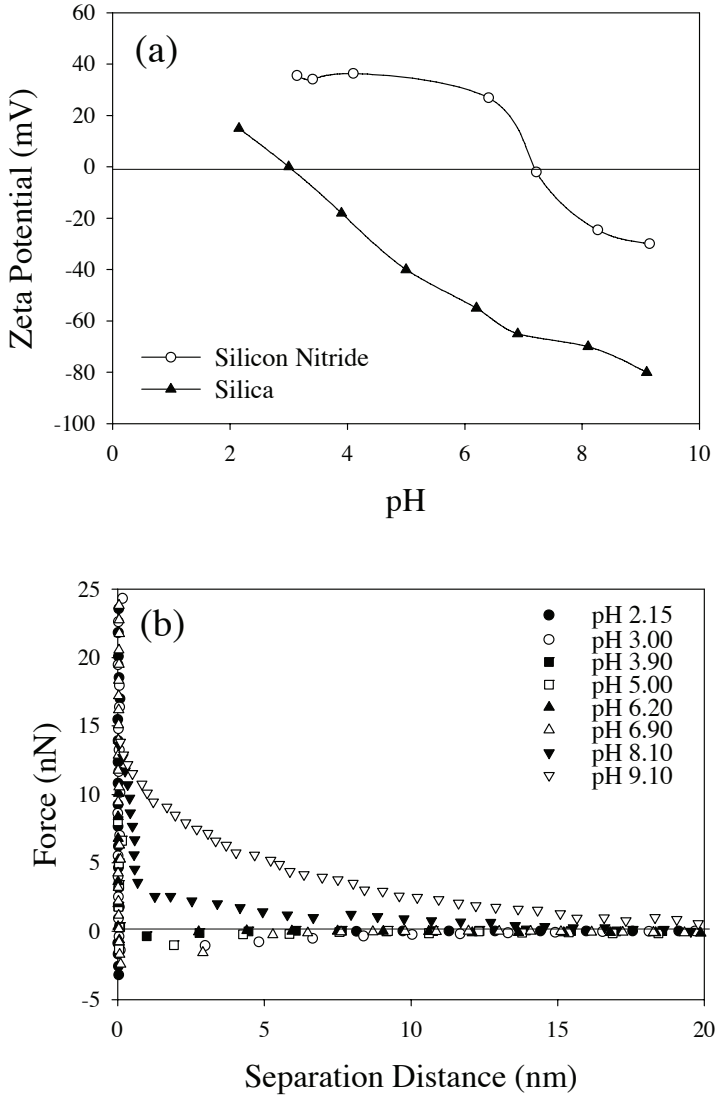

Figure 6.1 (a) Zeta potential of silicon nitride and silica for different pH values, measured by Zee Meter, in NaCl solutions of ionic strength 0.005 M. (b) Interaction force curves between silicon nitride and silica as a function of pH, measured by AFM, in NaCl solutions of ionic strength 0.005 M. *(Taboada-Serrano et al., 2005a)*

The measurements of zeta potential were combined with measurements of the overall interaction force between silica and silicon nitride at different pH conditions and at the three conditions of ionic strength used in the zeta potential measurements. The results for the ionic strength of 0.005 M are presented in Figure 6.1(b). At pH values of 2.15 and 3, the overall interaction forces between the silicon nitride tip and the silica surface are attractive because these pH values are very close to the isoelectric point of silica and, under such conditions, the van der Waals attractive forces are expected to dominate over the weak electrostatic forces. At the pH range of 3.90 to 6.90, the measured forces were strongly attractive, a finding that agrees with the fact that silicon nitride and silica are oppositely charged in this pH range. Repulsive forces can be detected from pH values of 8.10 to 9.10, in agreement with the electrokinetic measurements. These results provide some qualitative information on the direction of the interaction force between silica and silicon nitride that should be expected at different pH conditions due to the protonation/deprotonation surface-charging mechanisms.

Table 6.1 presents a summary of the experiments performed in terms of force-volume imaging in this work. Two pH conditions and three copper ion concentrations were examined. All the surfaces were analyzed prior copper ion injection (sets listed under $[Cu]_T = 0$). In each experiment, four kinds of measurements were performed: a height-image scan of the surface to analyze topography and surface roughness, a test of the scope trace to discard the occurrence of noise or vibration, a single force measurement to assess sensitivity and other parameters required for force-volume imaging, and force volume imaging. Between 20 and 30 pairs of extension/retraction data were

independently imported and analyzed in each case of the 1024 deflection data acquired in each measurement associated with force-imaging. The extension data of cantilever deflection as a function of distance were converted to force data by the application of Hooke's Law (Chin et al., 2002a). In order to facilitate the visualization of results, only three force curves of each set of data are depicted in all the figures from 0 nm to 30 nm of separation distance. For distances longer than 30 nm, the net interaction force is 0.

Table 6.1 Summary of the force-imaging experiments

Copper Ion Concentration	pH = 4.5	pH = 5.5
$[Cu]_T = 0.0000$ M	6 sets of experiments	6 sets of experiments*
$[Cu]_T = 0.0016$ M	2 sets of experiments	2 sets of experiments
$[Cu]_T = 0.0076$ M	2 sets of experiments	4 sets of experiments*
$[Cu]_T = 0.0304$ M	2 sets of experiments	No experiments

All the experiments were performed at an ionic strength of 0.1 M, except for 2 sets, in the groups marked with *, that were performed at an ionic strength of 0.5 M.

Since the blank experiments (i.e., force-images of surfaces in the 1:1 indifferent electrolyte prior to copper ion injection) present similar behavior, only one result is presented for purposes of discussion.

Figure 6.2 presents the force image of the interaction force between the silica surface and the silicon nitride tip at pH 5.5. The interaction forces measured along the surface are attractive (according to the convention adopted in Chapter 5, negative sign in force vs distance curves denotes attraction), although of different magnitude in each region. This

behavior can be inferred by the shades exhibited by the different sections of the surface. The three force curves selected for the purpose of illustration confirm this result.

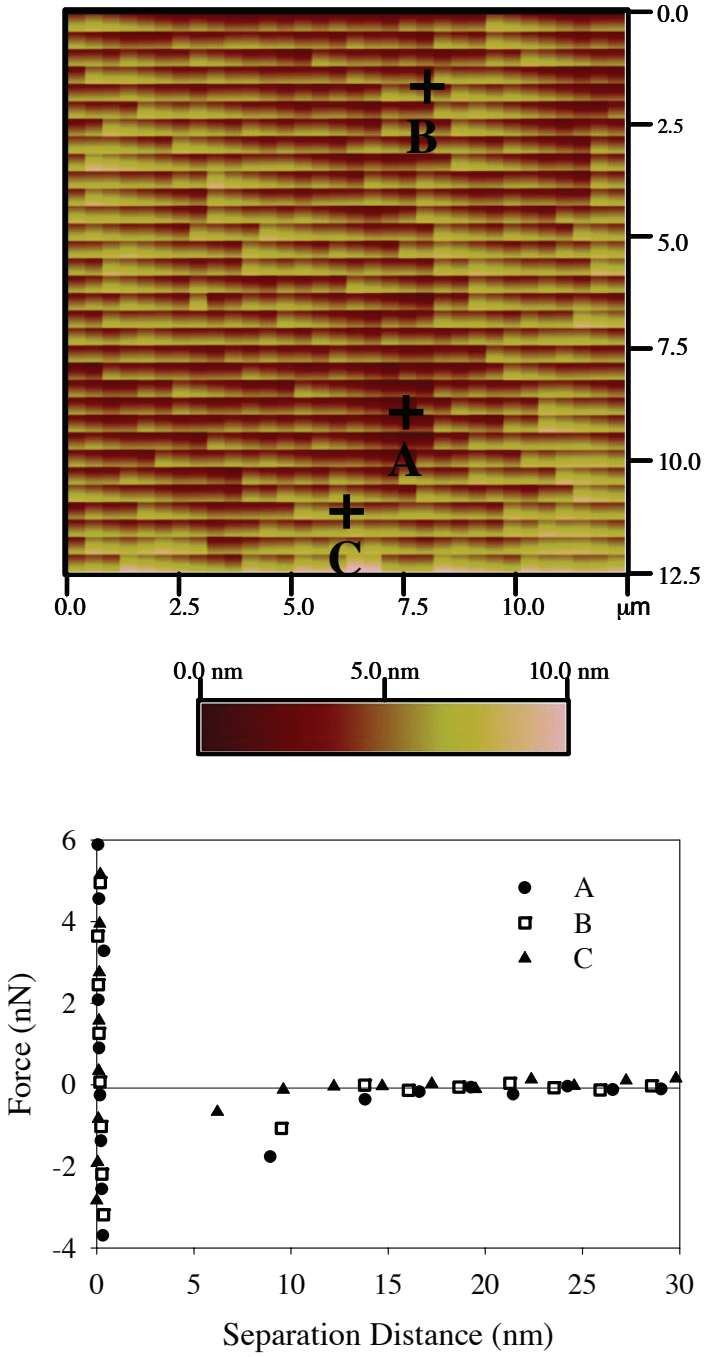

Figure 6.2 Force image and interaction force curves for silica and silicon nitride at pH 5.5 and ionic strength of 0.1 M (NaCl used as 1:1 indifferent electrolyte or background electrolyte). *(Taboada-Serrano et al., 2005a)*

The magnitude of the attractive well of the forces ranged from –4 to –2 nN. Darker spots are associated with strong attractive forces (almost -4 nN in magnitude in the case of curve A), whereas lighter spots are associated with weaker attractive forces (around –2.8 nN in magnitude, curve C). The regions bearing different magnitudes of attractive forces are nonuniformly distributed on the surface. The silica surface is overall negatively charged and the interaction force with the silicon nitride tip is overall attractive; however, the distribution of charge is definitely nonuniform.

6.4 Interaction between silica and silicon nitride in a 2:1 non-indifferent electrolyte solution

As stated earlier, copper nitrate was selected as the non-indifferent asymmetric electrolyte. The behavior of copper ion in electrolyte solutions and its possible interactions with both surfaces demanded a careful selection of experimental conditions.

Copper ion adsorption occurs on silica and on silicon nitride depending on conditions of pH. Copper ion uptake by silica begins to occur at pH 3, and, for relatively low concentrations, complete coverage of the surface occurs at a pH of ~7. The solubility limit of copper as tenorite (CuO) decreases drastically beyond pH 6 (Subramaniam et al., 2003). Experimental studies on copper ion adsorption onto silicon nitride via AFM measurements report that no adsorption occurs at pH values lower than 7.5 (Larson and Pugh, 1998). Therefore, the pH values of 4.5 and 5.5 were chosen to promote partial copper ion adsorption onto the silica surface. We assumed that the injection of copper

ions into the system would modify only the silica surface and no adsorption of copper ions onto the silicon nitride tip would occur.

If copper ion adsorption is the mechanism leading to generation of surface charge heterogeneities, it is expected that the extent of surface charge heterogeneity would be larger at pH 5.5 than at pH 4.5. The adsorption front of copper ions on silica, as a function of concentration of copper ion in liquid, shifts towards lower concentrations with increasing pH (Subramaniam et al., 2003). A similar behavior can be observed in curves of copper ion adsorbed as a function of pH; the copper uptake curve is shifted to lower pH values as the concentration of copper ions in liquid increases (Subramaniam et al., 2003).

Three copper ion concentrations (i.e., total copper ions introduced to the system) were selected in order to produce different degrees of surface charge heterogeneity: 0.0016 M (100 ppm), 0.0076 M (500 ppm), and 0.0304 M (2000 ppm). After the copper ion solution was introduced to the AFM cell, it was allowed to sit for a few hours so that the system would reach equilibrium. Force-volume images were taken after equilibration, and extension and retraction force curves associated with different sections of the surface were stored. The information for each force curve was imported independently and converted into force data via the application of Hooke's Law (Chin et al., 2002a). Since the force-image allows the identification of the regions that are heterogeneously charged, the data corresponding to those regions (i.e., force curves) were analyzed. Additionally, randomly sampled force curves of regions that do not present heterogeneities were also

obtained. These regions are depicted in darker colors. Due to the extensive amount of data, only three extension force curves were selected from the set of sampled force data in each case for discussion.

At pH 4.5 and a total copper ion concentration of 0.0016 M (results not shown), no regions of charge reversal can be detected. The silica surface still presents regions of randomly distributed shades and associated attractive forces. However, on average, a decrease of 1.5 nN in the magnitude of the attractive well of the interaction forces occurs in all the regions after the injection of copper ions in relation to the interaction forces between silica and silicon nitride without the presence of copper ions. This fact was stated through comparison of force images and randomly sampled force curves associated with them right before copper ion injection and after the equilibration period of the system with copper solution.

Figure 6.3 presents the force image of the interaction of silica and silicon nitride after the injection of 0.0076 M total copper ion concentration into the system at pH 4.5. In this case, no regions of charge reversal are detected on the surface. However, as in the previous case, a reduction in the magnitude of the attractive well of the interaction forces by 2.5 to 3.5 nN can be detected in all the regions with respect to the magnitude of the attractive forces measured prior to copper injection. In both cases, the force images depict regions of associated forces of different magnitudes randomly distributed on the surface. The surface is nonuniform, but the difference in the magnitude of the attractive forces in different regions is very small (approximately 0.3 nN). The decrease in

magnitude of the attractive forces (i.e., the depth of the attractive well) is believed to occur due to limited adsorption of copper ions.

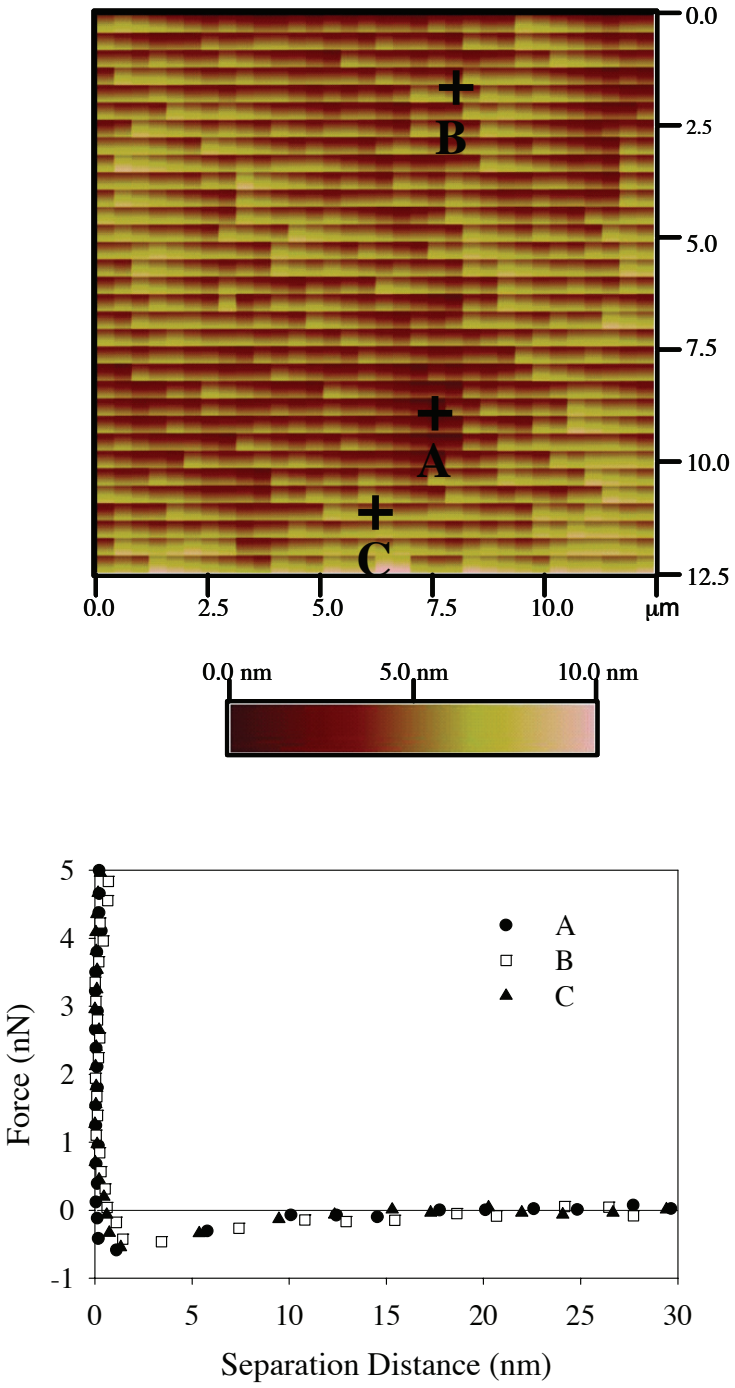

Figure 6.3 Force image and interaction force curves for silica and silicon nitride at pH 4.5, ionic strength of 0.1 M (NaCl used as background electrolyte), and total copper ion concentration of 0.0076 M. *(Taboada-Serrano et al., 2005a)*

The limited adsorption under the conditions depicted in figure 6.3 is insufficient to result in charge reversal that can be detected by the instrument.

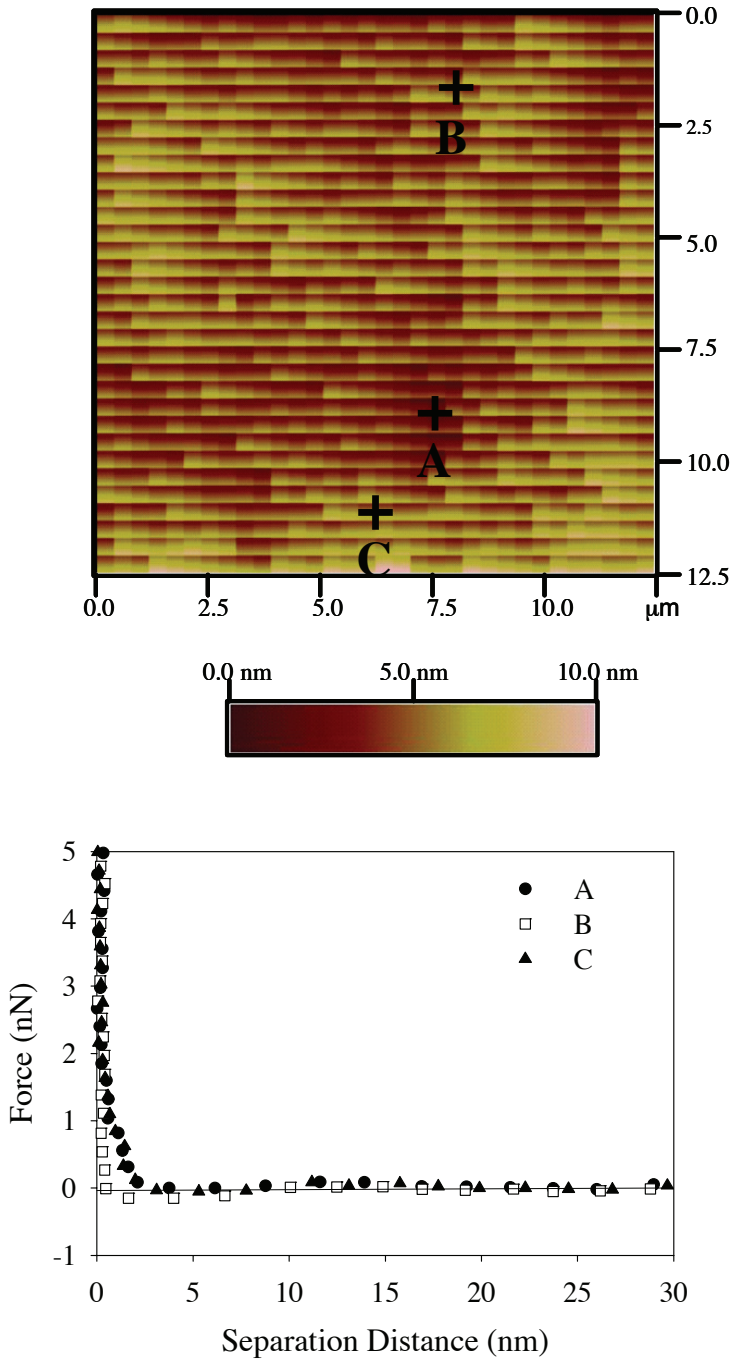

Figure 6.4 Force image and interaction force curves for silica and silicon nitride at pH 4.5, ionic strength of 0.1 M (NaCl used as background electrolyte), and total copper ion concentration of 0.0304 M. *(Taboada-Serrano et al., 2005a)*

Figure 6.4 presents the results for the injection of 0.0304 M total copper ion concentration at pH 4.5. Charge reversal takes place along the whole silica surface; all the forces measured along the surface are repulsive in nature and of varying magnitude. If we assume that copper ion adsorption is responsible for charge reversal, then full coverage of the surface is achieved at this point. Still, there are different shades associated with different regions of the surface, and they appear to be randomly distributed. The darker zones correspond to weak repulsive forces with a range of less than 1 nm and slight attraction (on the order of 0.2 nN depth of the attractive well of the force curve) at 2 to 3 nm of separation distance from the surface. The lighter regions are associated with weak repulsive forces with a range of 3 to 4 nm. The overall force is of a repulsive nature, although regions with interaction forces ranging from barely attractive to net zero at short distances from the surface are present. The surface is nonuniform; however, the difference in the magnitude of the interaction forces is very small.

Figure 6.5 presents the results for the injection into the AFM cell of 0.0016 M total copper ion concentration at pH 5.5. The force image presents zones of very light color with associated repulsive forces that have a range of up to 4 nm. There are also cases of light regions on the surface with associated forces that have a magnitude with oscillatory attraction–repulsion–attraction behavior (at different distances of separation between the surfaces). Darker spots on the surface are associated with attractive forces of up to -1 nN in magnitude. The range of the repulsive forces on the light zones is comparable to the range of repulsive forces measured for total copper ion concentrations of 0.0304 M at pH 4.5. Different degrees of charge reversal have occurred at zones of the surface depicted

with lighter color. The surface is not only nonuniform but is heterogeneously charged in the sense that it contains distinguishable regions bearing a different charge than the background surface.

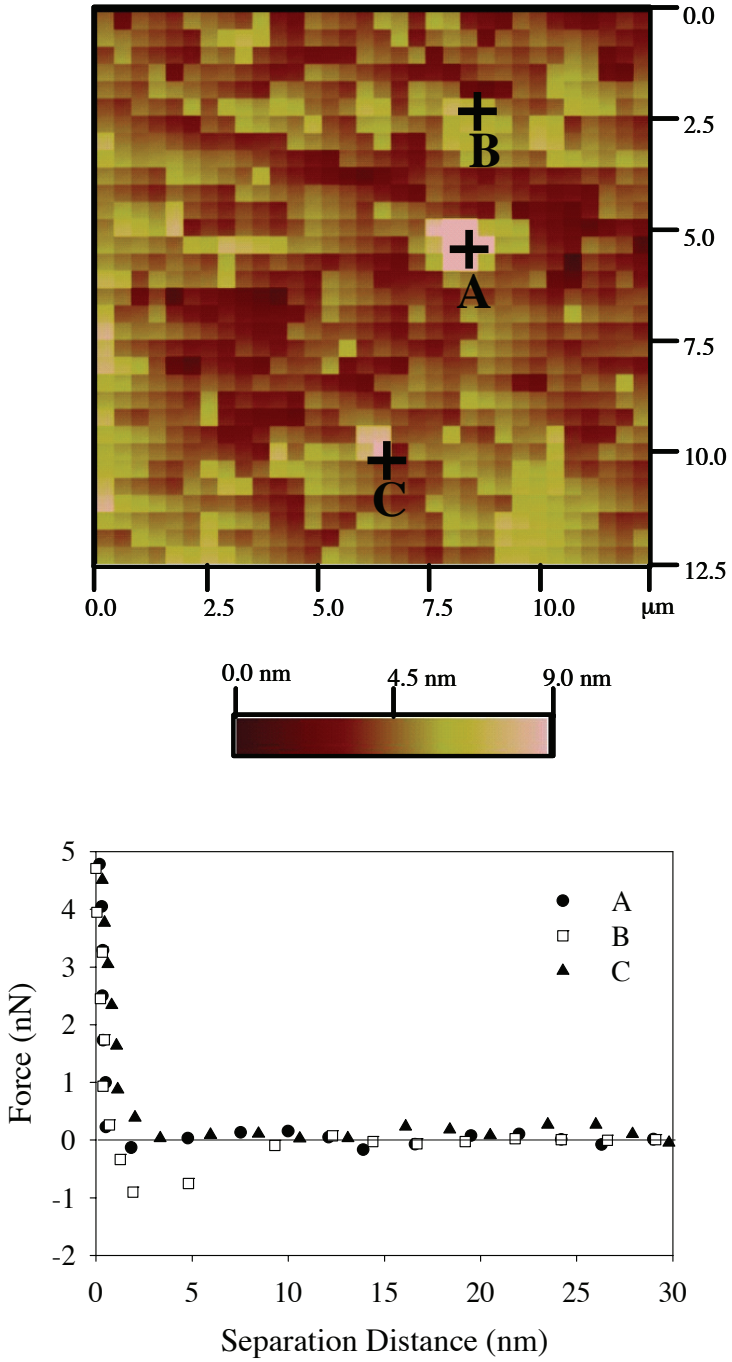

Figure 6.5 Force image and interaction force curves for silica and silicon nitride at pH 5.5, ionic strength of 0.1 M (NaCl used as background electrolyte), and total copper ion concentration of 0.0016 M. *(Taboada-Serrano et al., 2005a)*

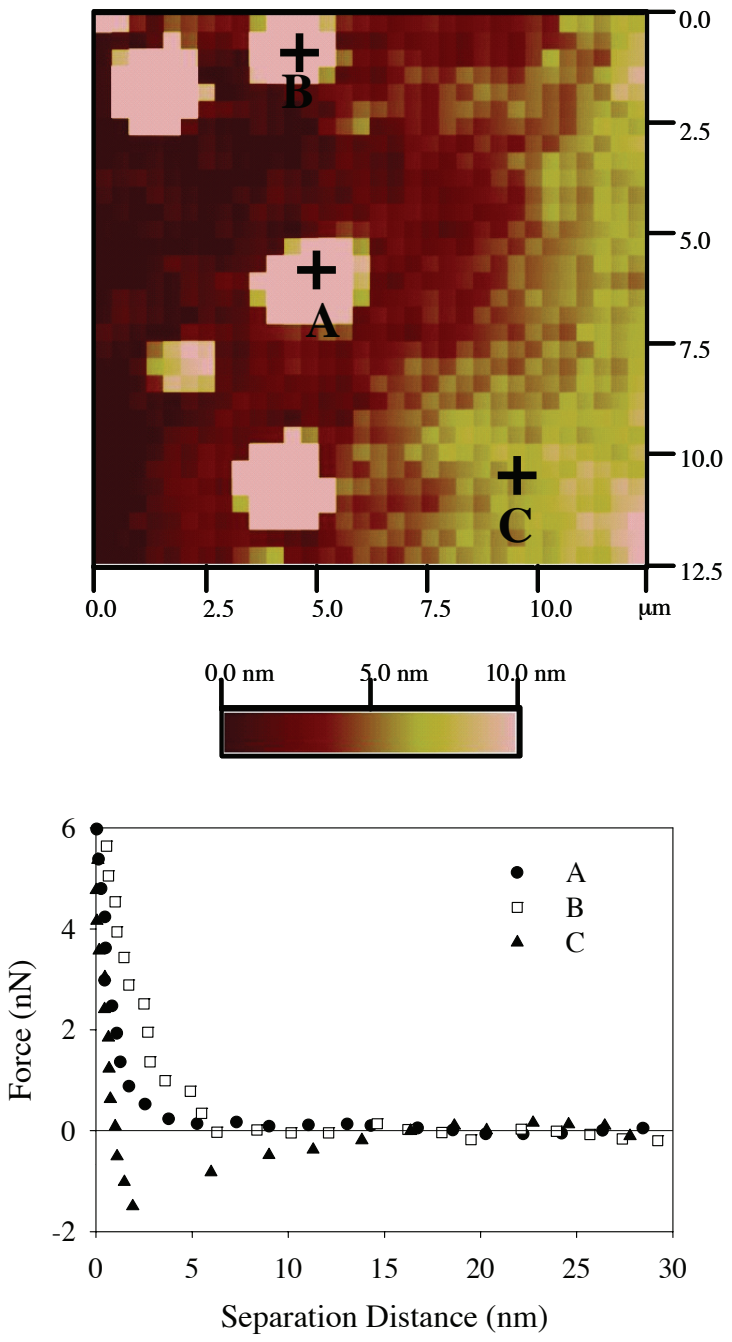

Figure 6.6 Force image and interaction force curves for silica and silicon nitride at pH 5.5, ionic strength of 0.1 M (NaCl used as background electrolyte), and total copper ion concentration of 0.0076 M. *(Taboada-Serrano et al., 2005a)*

Figure 6.6 presents the results for the experiments with 0.0076 M total copper ion concentration at pH 5.5. In this case, the lightest zones on the surface with associated

repulsive forces are larger in size and in number. Strong repulsive forces with a range of up to 7 nm are associated with these light zones. Other zones on the surface depicted in slightly darker shade, present associated attractive forces. The magnitude of these forces varies, reaching values of up to –1.8 nN. The areas surrounding the zones of charge reversal are presented in very dark colors although the magnitude of the attractive forces on them is smaller than the one depicted in force curve C, for example. This behavior might be due to the sudden movement of the sample surface that the control loop system of the AFM is forced to perform when it encounters a strong repulsive force. The set-point value of force for these measurements was set to weak attraction, almost zero force. The dark shades around the zones of charge reversal might be an artifact of the AFM control system logic. However, the zones of charge reversal can clearly be visualized by AFM.

The increase in the number and size of light regions as copper concentration increases supports the idea that copper ions are in fact responsible for charge reversal. This finding also suggests that the association of copper ions with the surface does not occur uniformly at given conditions of pH and concentration but rather preferentially on certain zones of the surface.

Topographic height-imaging of the silica surfaces after copper ion injection (conventional AFM images, not shown) did not reveal clusters or irregularities. The surfaces were relatively smooth with a roughness of 3 nm (as analyzed by the AFM software), before

and after copper ion injection. The zones of charge reversal could be visualized only in force-volume-mode AFM via force imaging.

AFM reproduces the topography of a surface (imaging) or creates a force image based on the information of a control loop that compares height data or deflection data to a fixed set-point value. In the case of normal imaging, a certain height from the surface is chosen as set-point. The upward/downward movements of the sample that aim to keep the separation distance constant are recorded and related to surface features. In the case of force imaging, the set-point value for the control loop is cantilever deflection, i.e., force exerted on the tip. The upward/downward movements of the sample aim to keep the force acting on the tip constant. If the set-point is mild attraction, zones of strong repulsion, for example, result in sudden movements of the sample away from the tip. Therefore, regions with markedly different forces associated to them are clearly identifiable during force imaging. The logic of the AFM control loop leads to the idea that the size of the regions of charge reversal observed in force images depends on the range and magnitude of the electrostatic forces. In order to test this hypothesis, the experiments were repeated at a higher ionic strength.

Figure 6.7 presents the force image and sample force interaction curves for a total copper ion concentration of 0.0076 M and pH 5.5 at approximately five times the value of ionic strength used in the previous measurements. The size and number of light zones of charge reversal are smaller than the ones observed in the experiments with the same concentration of copper ions and pH at lower ionic strength, depicted in Figure 6.6.

Therefore, the AFM force images reflect the range of influence of the electrostatic forces associated with sites of charge reversal rather than the actual size of the heterogeneously charged region. It should be noted that the magnitude of both attractive and repulsive forces detected under higher ionic strength is comparatively lower. The range of the repulsive forces is around 6 nm, while the magnitude of the attractive well of the force curve reaches -0.6 nN.

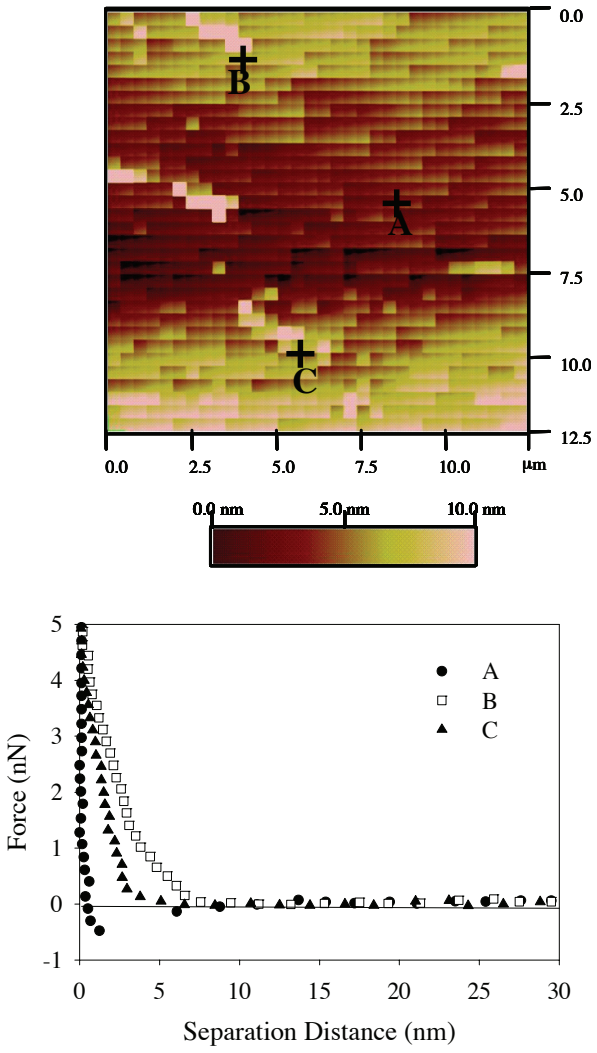

Figure 6.7 Force image and interaction force curves for silica and silicon nitride at pH 5.5, ionic strength of 0.5 M (NaCl used as background electrolyte), and total copper ion concentration of 0.0076 M. *(Taboada-Serrano et al., 2005a)*

Although the dependence on the presence of and the number of regions presenting charge reversal with pH and with total copper ion concentration introduced to the system leads us to conclude that the association of copper ions with silica surfaces is responsible for surface charge heterogeneities, it was necessary to confirm the presence of copper ions on the surface. XPS analyses of the silica surfaces used in AFM experiments, before and after copper ion injection, were performed (results not shown). The presence of copper ions could be detected only on silica surfaces that had been exposed to copper ion solutions. The binding energy of the copper ion on the surface corresponded to Cu 2p3/2. The nature of the binding energy of silicon atoms did not change, and only oxygen atoms, O 1s, could be detected in all the surfaces examined (surfaces not exposed and surfaces exposed to copper ion solutions). Therefore, only oxygen bound to the surface seemed to be present in all the cases (Dambies et al., 2001; Barr, 2004; Sheng et al., 2004). The analysis was not conclusive in terms of the exact chemical nature of the copper associated with the surface or the exact location of adsorption sites. However, the presence of copper on the surface was confirmed. The atomic concentration reached a value of 0.13% at pH 5.5 and 0.0076 M total copper ion concentration introduced to the system.

6.5 Conclusions

The capabilities of force-imaging AFM allow the visualization of zones bearing charges of different magnitudes and even different signs through the mapping of interaction forces of the surface with a silicon nitride tip.

Although the interaction between the silica planar surface and the silicon nitride tip is overall attractive for the conditions of pH and ionic strength selected, the magnitude of the interaction forces is different at different regions of the surface. The discrete nature of the surface charge, a direct consequence of the charging mechanism, results in a non-uniform surface charge distribution with associated forces of different magnitude.

The presence in the electrolyte solution of asymmetric non-indifferent electrolytes does not only modify the electrostatic forces within the domain of the EDL, as discussed in Chapter 5, but foremost results in the modification of the surface charge. As suggested in Chapter 3, the size exclusion effect is overcome through the dehydration of divalent counterions and their subsequent adsorption on the charged groups of the surface. In this case, it is energetically favorable to screen the surface charge at the solid-liquid interface, i.e., beyond the EDL. The dehydration and subsequent adsorption of copper ions on the silica surface generates regions where charged reversal occurs. These regions are randomly distributed on the surface and have associated forces of different direction and magnitude to the overall force expected for the conditions of pH and ionic strength o f the system. As expected, the generation of surface charge heterogeneities depends on the relative concentration of the divalent counterion with respect to the monovalent counterion, i.e., it depends on the concentration of the copper ions. Larger degree of surface charge modification occurs at higher copper ion concentration in the system. The extension of surface charge modification cannot be quantified via AFM, only the effects on the interaction force can be detected. The ionic strength regulates the range of the electrostatic forces. As ionic strength increases, the contribution of the electrostatic

forces to net interaction force diminishes, resulting in increasingly smaller regions of heterogeneous charge on the surface that are detectable via AFM.

The generation of non-uniform and even heterogeneous surface charge through the action of non-indifferent electrolytes implies that real charged surfaces do not comply with the basic assumption of the classical theory of uniformity, within the framework of the mean-field pseudo-one component approximation. A charged surface or colloidal particle might bear an overall charge of certain sign, and still present localized charges of different sign. Therefore, the interactions between charged colloids and surfaces might depend on their orientation and positioning with respect to each other. Theoretical and experimental analysis of nonuniformity of surface charge leads to the conclusion that orientation and positioning of similarly charged surfaces might even result in overall attraction, after a statistical mechanical averaging (Miklavic et al., 1994; Velegol and Thwar, 2001). In our case, whether the net resulting interaction is repulsive or attractive, as well as whether the magnitude of the interaction is weak or strong depends on three factors: the positioning of the colloidal particle with respect to the surface, the size of the colloidal particle (we used a single size of silicon nitride tip in this work), and the range of the electrostatic interactions. The influence of the positioning of the colloidal particle with respect to the planar surface is directly observed in the experimental results. The size of the colloidal particle is important because the net force acting on it depends on the interaction area. While a small particle might experience a strong repulsion in a charge reversal region, a larger particle or tip would experience that force in a smaller magnitude if the surrounding areas exhibit attraction. The effect of the heterogeneously charged

zones would depend on the characteristic distances of the charge heterogeneities with respect to the size of the particle and the interaction distance, because the net force acting on the particle would be a result of a weighted sum of interaction forces on the area of interaction. Therefore, the effect of charge heterogeneities will depend on the relative size of the particle with respect to the relative size of the heterogeneously charged regions. Finally, the ionic strength determines the range and magnitude of the electrostatic forces and their prevalence over other surface forces. The magnitude of the effect of surface charge heterogeneities is expected to decrease at higher ionic strengths.

6.6 Summary

In this part of the work it was demonstrated that the presence of asymmetric non-indifferent electrolytes results in local modification of surface charge, therefore, the effects in this case go beyond the modification of magnitude and range of electrostatic forces due to ion-ion correlations and size effects. Surface charge heterogeneities take place due to the presence of copper ions and their subsequent adsorption on the surface.

Surface charge modifications result in local variations of interaction force on the plane of the charged planar surface, which can explain the occurrence of several deviations between the behavior of solid-liquid interfaces predicted by the classical theory and the one observed in real experimental systems.

CHAPTER 7

CONCLUSIONS

As described in Chapter 1, discrepancies between the classical theory predictions and experimental observations on the behavior of colloidal particles and charged solid-liquid interfaces have been detected in the last decades. Several explanations have been proposed for those differences, for example, the occurrence of secondary minima of interaction potentials due to the large magnitude of Van der Waals interactions in comparison to the electrostatic interactions, still within the framework of the DLVO theory. Surface roughness and surface charge non-uniformity have been also explored as aspects contributing to the deviations of experimental data from the behavior predicted by the classical theory.

The hypothesis of this work is that the mean-field, pseudo-one component approximation used in the derivation of the classical theory might be at least in part responsible for the limited predictive capabilities of this theory when compared to experimental data. Therefore, the charged species involved in the development of surface charge and the EDL are treated as independent species with unique associated charge and size throughout the analysis of the EDL structure and the EDL interactions of charged surfaces. Modeling and experimental techniques at the molecular level are employed for

the EDL analysis and surface force characterization. Fused silica and silicon nitride were selected as models for charged surfaces. Monovalent coions, monovalent, divalent, and trivalent indifferent counterions; and divalent non-indifferent counterions were used in the study with ion size scaled with their valence.

One of the first implications of avoiding the mean-field, pseudo-one-component approximation to deal with the charged groups and with the ions involved in the formation of surface charge and EDL is the discrete nature of the surface charge. Different regions on the surface present different magnitudes of surface charge. Furthermore, counterions and coions are capable of getting closer to the surface in those regions where there are no charged groups present. Therefore, the solid-liquid interface and the EDL are nonisotropic in terms of concentration profiles, and hence, in terms of electrostatic forces exerted on other charged surfaces. This fact was observed during CMC simulations of the EDL and was proved via direct force measurements of the interaction between silica and silicon nitride in 1:1 indifferent electrolytes, which is clearly nonuniform.

Although the dependence of the EDL thickness and, hence, the range and magnitude of EDL forces, on the ionic strength and surface charge density predicted by the classical theory is qualitatively correct, the determinant factors are the size and charge of the counterions present in the solution. The EDL thickness is larger when one takes the size of the ions into account. Therefore, the electrostatic effects, e.g., high local counterion concentrations, low local coion concentrations, and electrostatic interactions, extend for

larger distances from the charged surfaces than the ones predicted by the classical theory. Additionally, the size of the counterions and coions determines their occupancy of different layers of fluid close to the charged surfaces. Layers of fluid with high local concentration of counterions or coions occur at different distances from charged surfaces, in some cases in an ordered manner, and result in some degree of charge neutralization or in net accumulation of charge in certain regions within the EDL.

One of the consequences of the local accumulation of counterions and coions within layers of fluid at different distances of the charged surfaces is the occurrence of long-range attractive forces of electrostatic origin during the interaction of a planar surface and a spherical colloidal particle at low and intermediate values of surface charge density and in electrolyte solutions containing ions of different valence and size. Although not electrostatic in origin, there is also an additional attractive contribution to the interaction force that arises from excluded volume effects, i.e., the consideration of the size of the ions comprising the EDL in all the cases of surface charge and electrostatic coupling examined.

In the case of 1:1 electrolytes and low surface charge densities, the presence of a long-range shallow attractive interaction and a minimum in the interaction force almost at contact of slight repulsive nature can be detected. As surface charge density increases, the long-range electrostatic attraction presents a steep minimum, and the depletion interaction at contact becomes attractive. The occurrence of long-range attractive interactions can explain several phenomena, for example the occurrence of deposition of

colloidal particles under unfavorable conditions (i.e., when electrostatic repulsion is expected for similarly charged surfaces) reported in the literature (Shellenberger and Logan, 2002; Hahn and O'Melia, 2004); or the instability of similarly charged nanoparticles even at low surface charge densities (Kallay and Žalac, 2002). It can also explain the fact that the dependence of attachment efficiencies during deposition of colloidal particles onto charged collectors is not as sensitive to the chemistry of the solution as predicted by the DLVO theory (Ryan and Elimelech, 1996; Krezschmar et al., 1999). Colloidal particles interacting with charged collectors or larger colloidal particles experience long-range attractions in all the cases of charge density examined. Furthermore, at sufficiently high surface charge densities, colloidal particles can become "associated" with other charged surfaces at two separation distances: close to contact due to depletion effects, or at relatively large separations, due to attraction of electrostatic origin. It has been reported that dispersions of highly charged particles in 1:1 electrolytes conserve determined separation distances among them with highly ordered regions of particles in a gel-like structure (Feng and Ruckenstein, 2004).

The gradual increase in surface charge density results not only in a reduction of the thickness EDL, but also in a gradual increase of the interaction force minima at short and long separation distances. Furthermore, increasing surface charge densities result in steeper attractive minima at smaller separation distances, which would explain the gradual increase in instability of colloidal particles with diminishing thickness of the EDL that has been experimentally observed (Behrens et al., 2000).

All the excluded volume and electrostatic effects reported for 1:1 electrolytes are enhanced with increasing electrostatic coupling, i.e., the valence of the counterions present in the electrolyte solutions. High charge asymmetries in mixtures of electrolytes result in an ordering effect: successive layers of fluid depict high local concentrations of counterions and coions at relatively short distances from the charged surfaces. This ordering effect seems to result in a more efficient charge neutralization at larger separation distances than for the case of 1:1 electrolytes and, thus, in the occurrence of enhanced electrostatic attractive effects at shorter separation distances than the ones for 1:1 electrolytes. Additionally, the larger size of higher valence ions assumed in this work results in more marked depletion or excluded volume effects almost at contact.

The results obtained in this work for asymmetric, indifferent electrolytes can explain why the introduction of 2:1 electrolytes, or the replacement of monovalent ions with divalent ions in deposition and aggregation experiments, increases all the differences between classical theory and the experimental observations reported in this work (Elimelech and O'Melia, 1990; Grolimund, 2001). Furthermore, it explains the fact that swelling and contraction of lyotropic lamellar phases and condensation of biopolymers occurs when divalent or higher counterions replace monovalent counterions (Meyer et al., 2001; Angelescu and Linse, 2003) at relatively high surface charge densities. The choice of the valence of counterions present in a solution can modify the behavior of charged solid-liquid interfaces. For example, one should note that potassium or sodium (monovalent ions), and calcium (a divalent ion) are used in living bodies and cells to regulate the

behavior of cellular membranes and biological polymeric molecules that are capable of developing surface charge.

All the phenomena discussed so far involve indifferent electrolytes. In that case, only the behavior of the EDL is affected by charge and size asymmetry of the electrolytes in the system. As discussed in Chapter 3, divalent and trivalent counterions might undergo dehydration so they can counteract the size exclusion effect. Most divalent and trivalent counterions constitute, then, non-indifferent electrolytes.

When non-indifferent asymmetric electrolytes come into play, not only the EDL is modified in the way described in this work, but foremost the surface charge. Local modification of surface charge results from the adsorption of non-indifferent electrolytes onto the charged surface, e.g., surface charge heterogeneities due to copper ion adsorption were detected via direct interaction force measurements by AFM in this work. The occurrence of surface charge heterogeneities, i.e., regions on the surface bearing different magnitudes and even signs, has several implications. For example, two surfaces might bear opposite or similar charge on the average, but the spatial variations of the magnitude of the charge produce spatial variations of the interaction forces. The overall interaction between two similarly charged surfaces might be repulsive, but if non-indifferent electrolytes are present, regions that present strong attraction might be present on the surface. This phenomenon might play a role in processes like directional self-assembly of colloidosomes (Dinsmore et al., 2002). The phenomenon could also be related to the accumulation of proteins and DNA in specific regions of bacteria during

sporulation (Shapiro et al., 2002) and could definitely be related to aggregation and deposition of colloidal particles under unfavorable conditions (Elimelech and O'Melia, 1990; Ryan and Elimelech, 1996; Kretzschmar et al., 1999; Grolimund et al., 2001; Hahn and O'Melia, 2004) if modification of surface charge has occurred. Furthermore, when dealing with environmental systems, there are several additional implications of the action of non-indifferent asymmetric electrolytes on surface charge. Contaminants such as heavy metal ions can be adsorbed onto colloidal and soil particles and modify the surface chemical and charge characteristics. Such surface modification may result in mobilization of the particle, and translocation of the associated contaminants (Ryan and Elimelech, 1996; Kretschmar et al., 1999). Finally, the local character of surface charge heterogeneities enforces the idea that deposition of particles into porous media in engineered and natural systems occurs preferentially onto favorable sites (Ryan and Elimelech, 1996).

In conclusion, the hypothesis of this work has been proved right. The mean-field, pseudo-one-component approximation within the framework of the DLVO theory plays a major role in the differences detected between the classical theory and experimental observations and natural phenomena. The consideration of independent charged groups and ions, i.e., charge and size asymmetry and surface charge discreteness, in the analysis of EDL structure and EDL interactions can explain several of the phenomena observed in experiments and in natural systems dealing with solid-liquid interfaces.

CHAPTER 8

RECOMMENDATIONS

Although the hypothesis of this work was proved right, more work is needed to enforce the arguments behind the proof and, furthermore, provide a deep understanding of the behavior of charged solid-liquid interfaces and colloidal particles.

All the simulation efforts were performed within the framework of a primitive model, i.e. the solvent was accounted for as a continuum with an associated electric permittivity. The role of water molecules in the screening of charge, the structure of the EDL and the electrostatic interactions has to be considered in future work.

The work presented in this dissertation involved simulation and experimental techniques at the molecular level, but they were used independently. The simulations of electrical double layer (EDL) structure and EDL interactions in symmetric and asymmetric electrolytes need experimental validation. The effects of charge and size asymmetry on the EDL structure can be examined via neutron reflectommetry (NR) experiments, for example, in model systems at the same conditions of Canonical Monte Carlo (CMC) simulations. The visualization of concentration profiles via reflectommetry and

scattering techniques is not straightforward, and its success depends on the careful selection of experimental parameters.

The calculations of interaction forces in indifferent, asymmetric electrolytes need experimental validation as well. The experimental validation could be done via direct interaction force measurements, but would require several steps. First, it is necessary to scale the CMC simulation system to depict an atomic force microscopy (AFM) cell. That involves handling several thousands of ions in systems of larger dimensions than the ones used in this work, i.e. dealing with serious computational restrictions. Additionally, a careful selection of experimental conditions has to be performed in order to ensure that the electrolytes will behave as indifferent electrolytes at several values of surface charge density studied, and to ensure that the surface charge on the model surfaces can be unequivocally regulated.

Finally, a protocol for the CMC simulation of non-indifferent electrolytes could be developed in order to explain the microscopic behavior behind the effects of surface charge discreteness, non-uniformity, and heterogeneity through validation of the model.

The fact that the mean-field, pseudo-one-component approximation adopted within the framework of the classical theory can indeed be related to many of the deviations of experimental observations and natural phenomena from the behavior predicted by the theory, leads to more general recommendations. Our understanding of nature and the design of many separation processes relies on the description of the behavior of solid-

liquid interfaces through the Poisson-Boltzmann (PB) equation and the theories based on it, e.g., Derjaguin-Landau-Verwey-Overbeek (DLVO) theory. This classical theory has been used for several decades in the prediction of important parameters in natural and engineered processes involving solid-liquid interfaces. It is important to revise existing or formulate basic statistical mechanical approaches in order to develop a more realistic model for the EDL and the EDL interactions. Methods for the calculation of parameters involved in natural and engineered processes, such as collision efficiencies or attachment efficiencies have to be developed based on those basic statistical mechanical descriptions, and be further implemented in the design of processes and the prediction of the behavior of natural phenomena involving solid-liquid interfaces.

APPENDIX

A.1 Derivation of the classical expression for the calculation of the interaction force between a spherical particle and a planar surface in a 1:1 electrolyte

The interaction potential between two spheres at constant surface charge is given by the expression:

$$V(D)=\frac{2\pi a_1 a_2 n_\infty k_B T}{(a_1+a_2)}\left(\Phi_1^2+\Phi_2^2\right)\left[\frac{2\Phi_1\Phi_2}{\Phi_1^2+\Phi_2^2}\ln\left(\frac{1+\exp(-\kappa D)}{1-\exp(-\kappa D)}\right)-\ln(1-\exp(1-\exp(-2\kappa D)))\right] \quad (A.1)$$

where

$$\Phi_i=\frac{\bar{e}\psi_i}{k_B T} \quad (A.2)$$

corresponds to the reduced potential of the spherical surface *i*.

Considering that the curvature of one of the spheres tends to ∞, i.e., it constitutes a planar surface, and applying a limit to equation A.1:

$$\lim_{a_2\to\infty} V(D)=\frac{2\pi a_1 n_\infty k_B T}{\kappa^2}\left(\Phi_1^2+\Phi_2^2\right)\left[\frac{2\Phi_1\Phi_2}{\Phi_1^2+\Phi_2^2}\ln\left(\frac{1+\exp(-\kappa D)}{1-\exp(-\kappa D)}\right)-\ln(1-\exp(1-\exp(-2\kappa D)))\right] \quad (A.3)$$

Equation A.3 corresponds to interaction potential between a sphere and a planar surface.

Applying the definition of force in terms of interaction potential:

$$F(D)=-\left.\frac{dV}{dz}\right|_{z=D} \quad (A.4)$$

And derivating equation A.3, we obtain the expression for the interaction force between a spherical particle and a planar surface:

$$F(D)=\frac{4\pi a_1 n_\infty k_B T}{\kappa}\frac{\left(\Phi_1^2+\Phi_2^2\right)}{1-\exp(-2\kappa D)}\left[\frac{2\Phi_1\Phi_2}{\left(\Phi_1^2+\Phi_2^2\right)}\exp(-\kappa D)+\exp(-2\kappa D)\right] \quad (A.5)$$

A.2 Program for the CMC simulation of the EDL structure of a planar surface in a mixture of electrolytes

```
MODULE mixdat

! Declaration of global parameters and global variables

    IMPLICIT NONE

    SAVE

    integer,parameter::nstep=1.8E5,nn=324,nw=36
    integer,parameter::npaux1=40,npaux2=100,np=220

    real,parameter::eps=78.5,epso=8.8541E-22,elec=1.60219E-19,pi=3.1415297
    real,parameter::L=30.0,W=600.0,dn=4.25,dw=3.0
    real,parameter::deltaz=5.0
    real,parameter::kb=1.38062E-23,temp=298
    real,parameter::qn=-1.0,qw=-1.0

    integer::nhist

    real,dimension(np)::dp,qp
    real,dimension(np)::xp,yp,zp
    real,dimension(nn)::xn,yn,zn
    real,dimension(nw)::xw,yw,zw
    real dimension(nhist)::zcoord,cpav1,cpav2,cpav3,cnav
    character (len=256):: fout1, fout2, fout3

    END MODULE mixdat

! ----------------------------------------------------------------------

    PROGRAM Predlmix

! Monte Carlo simulation of the EDL formation in mixtures of electrolytes
! NVT Ensemble
! Patricia Taboada Serrano (2004)

    USE mixdat

    IMPLICIT NONE

! Declaration of variables

    integer::step,correc,iprint,icalc,limit,i,j,ihisto,isave
    integer::icount,fcount,index

    real::ovrlap,ovrold,ovrnew
    real::countc,acm,acatma,ratio,cont
    real::drmax,dummy,dummy1,dummy2,dummy3
    real::xiold,yiold,ziold,xinew,yinew,zinew
    real::rminppsq,rminnnsq,rminpnsq,rminpwsq,rminnwsq
    real::rminpmsq,rminnmsq,rminwmsq
    real(kind=8)::avv,acv,consist,vend,vtot
    real(kind=8)::aux,aux1,vold,vnew,deltv

    real:: p1,p2

    namelist /forcein / p1,p2, fout1, fout2, fout3
    read(5,forcein)

! Initialization of variables

    drmax=1.5*dw      !(ion displacement)
    correc=10         !(correction of displacement)
    iprint=1000       !(printout step)
```

```
      icalc=10                !(calculation of force)
      limit=1.7E5             !(equilibration period)

      CALL random_seed()      !Initializing random number generator

      do i=1,npaux1
        dp(i)=9.0
        qp(i)=3.0
      end do

      do i=npaux1+1,npaux2
        dp(i)=6.0
        qp(i)=2.0
      end do

      do i=npaux2+1,np
        dp(i)=4.25
        qp(i)=1.0
      end do

      do i=1,np
        xp(i)=0.0
        yp(i)=0.0
        zp(i)=0.0
      end do

      do i=1,nn
        xn(i)=0.0
        yn(i)=0.0
        zn(i)=0.0
      end do

! Initialization of Z coordinate and conc. Profiles

      nhist=int(W/deltaz)
      zcoord(1)=deltaz
      Do j=2,nhist
           zcoord(j)=zcoord(j-1)+deltaz
      end do

      Do j=1,nhist
          cpav1(j)=0.0
          cpav2(j)=0.0
          cpav3(j)=0.0
          cnav(j)=0.0
       end do

! Equispaced ions uniformly distributed on the surface
! Ions being numbered from left upper corner

      do i=1,nw
        zw(i)=0.0
      end do

      j=1
      do i=1,nw
        xw(i)=-12.5+(j-1)*(dw+(L-6.0*dw)/6.0)
        j=j+1
        if(j>6) then
          j=1
        end if
      end do

      icount=1
      fcount=6

      do j=1,6
        if(j>1) then
          icount=6*j-5
          fcount=icount+6
```

```
      end if
      do i=icount,fcount
        yw(i)=12.5-(j-1)*(dw+(L-6.0*dw)/6.0)
      end do
    end do

! Generation of Initial Configuration

    CALL iniconf(aux)

    CALL writini(aux)

! Initialization of accumulators

    vtot=0.0          !(total potential energy)
    acv=0.0           !(acummulated average potential energy)
    vend=0.0          !(final potential energy)
    acm=0.0           !(total number of attempted moves)
    acatma=0.0        !(total number of accepted moves)
    cont=0.0          !(# of cycles over which average is taken)
    avv=0.0           !(average potential energy)
    ovrlap=0.0        !(overlap criterium)
    ratio=0.0         !(# accepted moves/# total moves)
    countc=0.0        !(# steps over which conc. profiles are averaged)

! Calculation of initial energy

    CALL sumup(ovrlap,vtot)

    write(*,fmt=110)vtot,ovrlap
110  format(1x,E14.6,3x,f10.6)

    if(ovrlap==1.0) then
      goto 100
    end if

! Monte Carlo simulation

    DO step=1,nstep        ! Loop over all cycles

! Movement of positive ions

      DO i=1,np

        index=i
        xiold=xp(i)
        yiold=yp(i)
        ziold=zp(i)
        vold=0.0
        vnew=0.0
        ovrold=0.0
        ovrnew=0.0

! Energy of ion i in the old configuration

        CALL energyp(xiold,yiold,ziold,index,vold,ovrold)

! Move i and generate image ions

        CALL random_number(dummy1)
        xinew=xiold+(2.0*dummy1-1.0)*drmax
        CALL random_number(dummy2)
        yinew=yiold+(2.0*dummy2-1.0)*drmax
        CALL random_number(dummy3)
        zinew=ziold+(2.0*dummy3-1.0)*drmax

        xinew=xinew-L*anint(xinew/L)
        yinew=yinew-L*anint(yinew/L)

! Energy of ion i in the new configuration
```

```
        CALL energyp(xinew,yinew,zinew,index,vnew,ovrnew)

! Check movement acceptance

        deltv=(vnew-vold)/(kb*temp)
        if(ovrnew==0.0) then
          if(deltv<0.0) then
            vtot=vtot+deltv*kb*temp
            xp(i)=xinew
            yp(i)=yinew
            zp(i)=zinew
            acatma=acatma+1.0
          else
            CALL random_number(dummy)
            if((exp(-deltv))>dummy) then
              vtot=vtot+deltv*kb*temp
              xp(i)=xinew
              yp(i)=yinew
              zp(i)=zinew
              acatma=acatma+1.0
            end if
          end if
        end if

        acm=acm+1.0
        ratio=acatma/acm

! Accumulation of average energy

        if(step>limit) then
          acv=acv+vtot
          cont=cont+1.0
          avv=acv/cont
        end if

      end do    ! End cycle over all positive ions

! Movement of negative ions

      do i=1,nn

        index=i
        xiold=xn(i)
        yiold=yn(i)
        ziold=zn(i)
        vold=0.0
        vnew=0.0
        ovrold=0.0
        ovrnew=0.0

! Energy of ion i in the old configuration

        CALL energyneg(xiold,yiold,ziold,index,vold,ovrold)

! Move ion i and generate image ions

        CALL random_number(dummy1)
        xinew=xiold+(2.0*dummy1-1.0)*drmax
        CALL random_number(dummy2)
        yinew=yiold+(2.0*dummy2-1.0)*drmax
        CALL random_number(dummy3)
        zinew=ziold+(2.0*dummy3-1.0)*drmax

        xinew=xinew-L*anint(xinew/L)
        yinew=yinew-L*anint(yinew/L)

! Energy of ion i in the new configuration

        CALL energyneg(xinew,yinew,zinew,index,vnew,ovrnew)
```

```
! Checking for movement acceptance

        deltv=(vnew-vold)/(kb*temp)

        if(ovrnew==0.0) then
          if(deltv<0.0) then
            vtot=vtot+deltv*kb*temp
            xn(i)=xinew
            yn(i)=yinew
            zn(i)=zinew
            acatma=acatma+1.0
          else
            CALL random_number(dummy)
            if((exp(-deltv))>dummy) then
              vtot=vtot+deltv*kb*temp
              xn(i)=xinew
              yn(i)=yinew
              zn(i)=zinew
              acatma=acatma+1.0
            end if
          end if
        end if

        acm=acm+1.0
        ratio=acatma/acm

! Accumulation of average energy

        if(step>limit) then
          acv=acv+vtot
          cont=cont+1.0
          avv=acv/cont
        end if

      end do   ! End of cycle over all negative ions

! Periodic operations

      if(mod(step,iprint)==0) then
        write(*,fmt=150)vtot,acatma,acm,ratio
      end if

 150   format(1x,E14.6,3x,E14.6,3x,E14.6,3x,E14.6)

      if(mod(step,correc)==0) then
        if(ratio>0.3) then
          drmax=drmax*1.05
        else
          drmax=drmax*0.95
        end if
      end if

! Calculating force

      if(step>limit) then
        if(mod(step,icalc)==0) then
          CALL histogram(step)
          countc=countc+1.0
        end if
      end if

    END DO ! End of cycles

! Average concentration profiles

    DO j=1,nhist
        cpav1(j)=cpav1(j)/countc
        cpav2(j)=cpav2(j)/countc
        cpav3(j)=cpav3(j)/countc
```

```
            cnav(j)=cnav(j)/countc
        END DO

! Checking consistency of results

        CALL sumup(ovrlap,vend)

        consist=abs(vtot-vend)

! Writing final and average values

        CALL writfinal(consist,vtot,vend,avv)

 100  STOP

        END PROGRAM

! ------------------------------------------------------------------------

        SUBROUTINE iniconf(overlap)

        USE mixdat

        IMPLICIT NONE

        real,intent(out)::overlap

        integer::j,k
        real::drx,dry,drz,pprsq,pnrsq,pwrsq
        real::nnrsq,nwrsq
        real::dummy1,dummy2,dummy3
        real::rminppsq,rminnnsq,rminpnsq,rminpwsq,rminnwsq

! Initialization of variables

        overlap=0.0
        rminnnsq=dn*dn
        rminnwsq=(dn/2.0+dw/2.0)*(dn/2.0+dw/2.0)
        rminnmsq=(dn/2.0+dm/2.0)*(dn/2.0+dm/2.0)

! Placing positive ions in the box

        do j=1,np

 200    overlap=0.0
         rminpwsq=(dp(j)/2.0+dw/2.0)*(dp(j)/2.0+dw/2.0)
         CALL random_number(dummy1)
         xp(j)=(0.5-dummy1)*L
         CALL random_number(dummy2)
         yp(j)=(0.5-dummy2)*L
         CALL random_number(dummy3)
         zp(j)=dummy3*(W-dp(j)/2.0)

! Checking overlap with previously placed positive ions

          if(j>1) then
            do k=1,j-1
              drx=xp(j)-xp(k)
              dry=yp(j)-yp(k)
              drz=zp(j)-zp(k)
              drx=drx-L*anint(drx/L)
              dry=dry-L*anint(dry/L)
              rminppsq=(dp(j)/2.0+dp(k)/2.0)*(dp(j)/2.0+dp(k)/2.0)
              pprsq=drx*drx+dry*dry+drz*drz
              if(pprsq<rminppsq) then
                overlap=1.0
                goto 200
              end if
            end do
          end if
```

```
! Checking overlap with the walls

      if(zp(j)<(dp(j)/2.0)) then
        overlap=1.0
        goto 200
      else
        if(zp(j)>(W-dp(j)/2.0)) then
          overlap=1.0
          goto 200
        else
          do k=1,nw
            drx=xp(j)-xw(k)
            dry=yp(j)-yw(k)
            drz=zp(j)-zw(k)
            drx=drx-L*anint(drx/L)
            dry=dry-L*anint(dry/L)
            pwrsq=drx*drx+dry*dry+drz*drz
            if(pwrsq<rminpwsq) then
              overlap=1.0
              goto 200
            end if
          end do
        end if
      end if

! Placing negative ions in the box

     do j=1,nn

210   overlap=0.0
      CALL random_number(dummy1)
      xn(j)=(0.5-dummy1)*L
      CALL random_number(dummy2)
      yn(j)=(0.5-dummy2)*L
      CALL random_number(dummy3)
      zn(j)=dummy3*(W-dn/2.0)

! Checking overlap with previously placed negative ions

      if(j>1) then
        do k=1,j-1
          drx=xn(j)-xn(k)
          dry=yn(j)-yn(k)
          drz=zn(j)-zn(k)
          drx=drx-L*anint(drx/L)
          dry=dry-L*anint(dry/L)
          nnrsq=drx*drx+dry*dry+drz*drz
          if(nnrsq<rminnnsq) then
            overlap=1.0
            goto 210
          end if
        end do
      end if

! Checking overlap with positive ions

      do k=1,np
        drx=xn(j)-xp(k)
        dry=yn(j)-yp(k)
        drz=zn(j)-zp(k)
        drx=drx-L*anint(drx/L)
        dry=dry-L*anint(dry/L)
        rminpnsq=(dp(k)/2.0+dn/2.0)*(dp(k)/2.0+dn/2.0)
        pnrsq=drx*drx+dry*dry+drz*drz
        if(pnrsq<rminpnsq) then
          overlap=1.0
          goto 210
        end if
      end do
```

```
! Checking overlap with the walls

        if(zn(j)<(dn/2.0)) then
          overlap=1.0
          goto 210
        else
          if(zn(j)>(W-dn/2.0)) then
            overlap=1.0
            goto 210
          else
            do k=1,nw
              drx=xn(j)-xw(k)
              dry=yn(j)-yw(k)
              drz=zn(j)-zw(k)
              drx=drx-L*anint(drx/L)
              dry=dry-L*anint(dry/L)
              nwrsq=drx*drx+dry*dry+drz*drz
              if(nwrsq<rminnwsq) then
                overlap=1.0
                goto 210
              end if
            end do
          end if
        end if

      end do ! End placing the negative ions

      RETURN

      END SUBROUTINE iniconf

! ----------------------------------------------------------------------------

      SUBROUTINE writini(ovr)

      USE mixdat

      IMPLICIT NONE

      real,intent(in)::ovr

      integer::k

! Opening the file

      open(unit=9,file=fout1,status='unknown',form='formatted')

! Saving the data

      write(unit=9,fmt=310)ovr

      do k=1,npaux1
        write(unit=9,fmt=320)xp(k),yp(k),zp(k)
      end do

      write(unit=9,fmt=310)ovr

      do k=npaux1+1,npaux2
        write(unit=9,fmt=320)xp(k),yp(k),zp(k)
      end do

      write(unit=9,fmt=310)ovr

      do k=npaux2+1,np
        write(unit=9,fmt=320)xp(k),yp(k),zp(k)
      end do

      write(unit=9,fmt=310)ovr
```

```
      do k=1,nn
        write(unit=9,fmt=320)xn(k),yn(k),zn(k)
      end do

      write(unit=9,fmt=310)ovr

      do k=1,nw
        write(unit=9,fmt=320)xw(k),yw(k),zw(k)
      end do


310  format(1x,f10.6)
320  format(1x,E14.6,3x,E14.6,3x,E14.6)

      end file(unit=9)
      close(unit=9)

      RETURN

      END SUBROUTINE writini

! ------------------------------------------------------------------------------------------

      SUBROUTINE sumup(ovr,vint)

      USE mixdat

      IMPLICIT NONE

      real(kind=8),intent(out)::ovr
      real,intent(out)::vint

      integer::i,j,k

      real(kind=8)::vpp,vpps,vpn,vpns,vpw,vpws
      real(kind=8)::vnn,vnps,vnns,vnw,vnws
      real::rxi,ryi,rzi,dri2,dri
      real::xi,yi,zi,zdis
      real::r1,r1aux,r2,r2aux,pos,arctan
      real::EW,aux,fi
      real::qpi,dpi
      real::rminppsq,rminnnsq,rminpnsq,rminpwsq,rminnwsq

! Initialization of variables

      ovr=0.0
      vint=0.0
      vpp=0.0
      vpps=0.0
      vpn=0.0
      vpns=0.0
      vpw=0.0
      vpws=0.0
      vnn=0.0
      vnps=0.0
      vnns=0.0
      vnw=0.0
      vnws=0.0
      vwsm=0.0
      rminnnsq=dn*dn
      rminnwsq=(dn/2.0+dw/2.0)*(dn/2.0+dw/2.0)

! Sum over all positive ions

      do i=1,np

        xi=xp(i)
        yi=yp(i)
        zi=zp(i)
        dpi=dp(i)
```

```
      qpi=qp(i)
      rminpnsq=(dpi/2.0+dn/2.0)*(dpi/2.0+dn/2.0)
      rminpwsq=(dpi/2.0+dw/2.0)*(dpi/2.0+dw/2.0)

! Interaction of positive ions with positive ions

      if(i<np) then
       do k=i+1,np
        rxi=xi-xp(k)
        ryi=yi-yp(k)
        rzi=zi-zp(k)
        rxi=rxi-L*anint(rxi/L)
        ryi=ryi-L*anint(ryi/L)
        rminppsq=(dpi/2.0+dp(k)/2.0)*(dpi/2.0+dp(k)/2.0)
        dri2=rxi*rxi+ryi*ryi+rzi*rzi
        if(dri2>=rminppsq) then
         dri=sqrt(dri2)
         vpp=vpp+(qpi*qp(k)*elec*elec)/(4.0*pi*eps*epso*dri)
        else
         ovr=1.0
        goto 400
        end if
       end do
      end if

! Interaction of positive ions with positively charged sheets

      do k=1,np
       zdis=abs(zi-zp(k))
       r1aux=0.5+(zdis/L)*(zdis/L)
       r1=sqrt(r1aux)
       r2aux=0.25+(zdis/L)*(zdis/L)
       r2=sqrt(r2aux)
       pos=(4.0*zdis*r1)/L
       arctan=atan(pos)
       EW=2.0*pi-4.0*arctan
       aux=log((0.5+r1)/r2)
       fi=-2.0*pi*zdis-4.0*L*aux+zdis*EW
       vpps=vpps+(qpi*qp(k)*elec*elec*fi)/(4.0*pi*eps*epso*L*L)
      end do

! Interaction of positive ions with negative ions

      do k=1,nn
       rxi=xi-xn(k)
       ryi=yi-yn(k)
       rzi=zi-zn(k)
       rxi=rxi-L*anint(rxi/L)
       ryi=ryi-L*anint(ryi/L)
       dri2=rxi*rxi+ryi*ryi+rzi*rzi
       if(dri2>=rminpnsq) then
        dri=sqrt(dri2)
        vpn=vpn+(qpi*qn*elec*elec)/(4.0*pi*eps*epso*dri)
       else
        ovr=1.0
        goto 400
       end if
      end do

! Interaction of positive ions with negatively charged sheets

      do k=1,nn
       zdis=abs(zi-zn(k))
       r1aux=0.5+(zdis/L)*(zdis/L)
       r1=sqrt(r1aux)
       r2aux=0.25+(zdis/L)*(zdis/L)
       r2=sqrt(r2aux)
       pos=(4.0*zdis*r1)/L
       arctan=atan(pos)
       EW=2.0*pi-4.0*arctan
```

```
          aux=log((0.5+r1)/r2)
          fi=-2.0*pi*zdis-4.0*L*aux+zdis*EW
          vpns=vpns+(qpi*qn*elec*elec*fi)/(4.0*pi*eps*epso*L*L)
        end do

! Interaction of positive ions with the walls

        if(zi<(dpi/2.0)) then
          ovr=1.0
          goto 400
        else
          if(zi>(W-dpi/2.0)) then
            ovr=1.0
            goto 400
          else
            do k=1,nw
              rxi=xi-xw(k)
              ryi=yi-yw(k)
              rzi=zi-zw(k)
              rxi=rxi-L*anint(rxi/L)
              ryi=ryi-L*anint(ryi/L)
              dri2=rxi*rxi+ryi*ryi+rzi*rzi
              if(dri2>=rminpwsq) then
                dri=sqrt(dri2)
                vpw=vpw+(qpi*qw*elec*elec)/(4.0*pi*eps*epso*dri)
              else
                ovr=1.0
                goto 400
              end if
            end do
          end if
        end if

! Interaction of positive ions with wall charged sheets

        zdis=abs(zi)
        r1aux=0.5+(zdis/L)*(zdis/L)
        r1=sqrt(r1aux)
        r2aux=0.25+(zdis/L)*(zdis/L)
        r2=sqrt(r2aux)
        pos=(4.0*zdis*r1)/L
        arctan=atan(pos)
        EW=2.0*pi-4.0*arctan
        aux=log((0.5+r1)/r2)
        fi=-2.0*pi*zdis-4.0*L*aux+zdis*EW
        vpws=nw*(qpi*qw*elec*elec*fi)/(4.0*pi*eps*epso*L*L)

      end do  ! Close loop over all positive ions

      write(*,*)'No overlap of positive ions'
      write(*,fmt=410)ovr

! Sum over all negative ions

      do i=1,nn

        xi=xn(i)
        yi=yn(i)
        zi=zn(i)

! Interaction of negative ions with negative ions

        if(i<nn) then
          do k=i+1,nn
            rxi=xi-xn(k)
            ryi=yi-yn(k)
            rzi=zi-zn(k)
            rxi=rxi-L*anint(rxi/L)
            ryi=ryi-L*anint(ryi/L)
            dri2=rxi*rxi+ryi*ryi+rzi*rzi
```

```
          if(dri2>=rminnnsq) then
            dri=sqrt(dri2)
            vnn=vnn+(qn*qn*elec*elec)/(4.0*pi*eps*epso*dri)
          else
            ovr=1.0
            goto 400
          end if
        end do
      end if

! Interaction of negative ions with positively charged sheets

      do k=1,np
        zdis=abs(zi-zp(k))
        r1aux=0.5+(zdis/L)*(zdis/L)
        r1=sqrt(r1aux)
        r2aux=0.25+(zdis/L)*(zdis/L)
        r2=sqrt(r2aux)
        pos=(4.0*zdis*r1)/L
        arctan=atan(pos)
        EW=2.0*pi-4.0*arctan
        aux=log((0.5+r1)/r2)
        fi=-2.0*pi*zdis-4.0*L*aux+zdis*EW
        vnps=vnps+(qp(k)*qn*elec*elec*fi)/(4.0*pi*eps*epso*L*L)
      end do

! Interaction of negative ions with negatively charged sheets

      do k=1,nn
        zdis=abs(zi-zn(k))
        r1aux=0.5+(zdis/L)*(zdis/L)
        r1=sqrt(r1aux)
        r2aux=0.25+(zdis/L)*(zdis/L)
        r2=sqrt(r2aux)
        pos=(4.0*zdis*r1)/L
        arctan=atan(pos)
        EW=2.0*pi-4.0*arctan
        aux=log((0.5+r1)/r2)
        fi=-2.0*pi*zdis-4.0*L*aux+zdis*EW
        vnns=vnns+(qn*qn*elec*elec*fi)/(4.0*pi*eps*epso*L*L)
      end do

! Interaction of negative ions with the walls

      if(zi<(dn/2.0)) then
        ovr=1.0
        goto 400
      else
        if(zi>(W-dn/2.0)) then
          ovr=1.0
          goto 400
        else
          do k=1,nw
            rxi=xi-xw(k)
            ryi=yi-yw(k)
            rzi=zi-zw(k)
            rxi=rxi-L*anint(rxi/L)
            ryi=ryi-L*anint(ryi/L)
            dri2=rxi*rxi+ryi*ryi+rzi*rzi
            if(dri2>=rminnwsq) then
              dri=sqrt(dri2)
              vnw=vnw+(qn*qw*elec*elec)/(4.0*pi*eps*epso*dri)
            else
              ovr=1.0
              goto 400
            end if
          end do
        end if
      end if
```

```
! Interaction of negative ions with wall charged sheets

        zdis=abs(zi)
        r1aux=0.5+(zdis/L)*(zdis/L)
        r1=sqrt(r1aux)
        r2aux=0.25+(zdis/L)*(zdis/L)
        r2=sqrt(r2aux)
        pos=(4.0*zdis*r1)/L
        arctan=atan(pos)
        EW=2.0*pi-4.0*arctan
        aux=log((0.5+r1)/r2)
        fi=-2.0*pi*zdis-4.0*L*aux+zdis*EW
        vnws=nw*(qn*qw*elec*elec*fi)/(4.0*pi*eps*epso*L*L)

      end do  ! Close loop over all negative ions

      write(*,*)'No overlap of negative ions'
      write(*,fmt=410)ovr

      vint=vpp+vpps+vpn+vpns+vpw+vpws+vnn+vnps+vnns+vnw+vnws

      write(*,fmt=420)vint

 410  format(1x,f10.6)
 420  format(1x,E14.6)

 400  RETURN

      END SUBROUTINE sumup

! ------------------------------------------------------------------------------

      SUBROUTINE energyp(dxi,dyi,dzi,ind,vinti,ovr)

      USE mixdat

      IMPLICIT NONE

      integer,intent(in)::ind
      real,intent(in)::dxi,dyi,dzi
      real(kind=8),intent(out)::vinti
      real,intent(out)::ovr

      integer::j,k
      real(kind=8)::vp,vps,vn,vns,vw,vws
      real::xi,yi,zi,zdis
      real::r1,r1aux,r2,r2aux,pos,arctan
      real::EW,aux,fi
      real::rxi,ryi,rzi,dri2,dri
      real::qpi,dpi
      real::rminppsq,rminpnsq,rminnnsq,rminpwsq,rminnwsq

! Initialization of accumulators

      vinti=0.0
      vp=0.0
     vps=0.0
      vn=0.0
      vns=0.0
      vw=0.0
      vws=0.0
      ovr=0.0
      vm=0.0
      xi=dxi
      yi=dyi
      zi=dzi
      qpi=qp(ind)
      dpi=dp(ind)
      rminpnsq=(dpi/2.0+dn/2.0)*(dpi/2.0+dn/2.0)
      rminpwsq=(dpi/2.0+dw/2.0)*(dpi/2.0+dw/2.0)
```

```
! Interaction with positive ions

      do k=1,np
        if(k/=ind) then
          rxi=xi-xp(k)
          ryi=yi-yp(k)
          rzi=zi-zp(k)
          rxi=rxi-L*anint(rxi/L)
          ryi=ryi-L*anint(ryi/L)
          rminppsq=(dpi/2.0+dp(k)/2.0)*(dpi/2.0+dp(k)/2.0)
          dri2=rxi*rxi+ryi*ryi+rzi*rzi
          if(dri2>=rminppsq) then
            dri=sqrt(dri2)
            vp=vp+(qpi*qp(k)*elec*elec)/(4.0*pi*eps*epso*dri)
          else
            ovr=1.0
            goto 500
          end if
        end if
      end do

! Interaction with positively charged sheets

      do k=1,np
        zdis=abs(zi-zp(k))
        r1aux=0.5+(zdis/L)*(zdis/L)
        r1=sqrt(r1aux)
        r2aux=0.25+(zdis/L)*(zdis/L)
        r2=sqrt(r2aux)
        pos=(4.0*zdis*r1)/L
        arctan=atan(pos)
        EW=2.0*pi-4.0*arctan
       aux=log((0.5+r1)/r2)
        fi=-2.0*pi*zdis-4.0*L*aux+zdis*EW
        vps=vps+(qpi*qp(k)*elec*elec*fi)/(4.0*pi*eps*epso*L*L)
      end do

! Interaction with negative ions

      do k=1,nn
        rxi=xi-xn(k)
        ryi=yi-yn(k)
        rzi=zi-zn(k)
        rxi=rxi-L*anint(rxi/L)
        ryi=ryi-L*anint(ryi/L)
        dri2=rxi*rxi+ryi*ryi+rzi*rzi
        if(dri2>=rminpnsq) then
          dri=sqrt(dri2)
          vn=vn+(qpi*qn*elec*elec)/(4.0*pi*eps*epso*dri)
        else
          ovr=1.0
          goto 500
        end if
      end do

! Interaction with negatively charged sheets

      do k=1,nn
        zdis=abs(zi-zn(k))
        r1aux=0.5+(zdis/L)*(zdis/L)
        r1=sqrt(r1aux)
        r2aux=0.25+(zdis/L)*(zdis/L)
        r2=sqrt(r2aux)
        pos=(4.0*zdis*r1)/L
        arctan=atan(pos)
        EW=2.0*pi-4.0*arctan
        aux=log((0.5+r1)/r2)
        fi=-2.0*pi*zdis-4.0*L*aux+zdis*EW
        vns=vns+(qpi*qn*elec*elec*fi)/(4.0*pi*eps*epso*L*L)
```

```
      end do

! Interaction with the walls

      if(zi<(dpi/2.0)) then
        ovr=1.0
        goto 500
      else
        if(zi>(W-dpi/2.0)) then
          ovr=1.0
          goto 500
        else
          do k=1,nw
            rxi=xi-xw(k)
            ryi=yi-yw(k)
            rzi=zi-zw(k)
            rxi=rxi-L*anint(rxi/L)
            ryi=ryi-L*anint(ryi/L)
            dri2=rxi*rxi+ryi*ryi+rzi*rzi
            if(dri2>=rminpwsq) then
              dri=sqrt(dri2)
              vw=vw+(qpi*qw*elec*elec)/(4.0*pi*eps*epso*dri)
            else
              ovr=1.0
              goto 500
            end if
          end do
        end if
      end if

! Interaction with wall charged sheets

      zdis=abs(zi)
      r1aux=0.5+(zdis/L)*(zdis/L)
      r1=sqrt(r1aux)
      r2aux=0.25+(zdis/L)*(zdis/L)
      r2=sqrt(r2aux)
      pos=(4.0*zdis*r1)/L
      arctan=atan(pos)
      EW=2.0*pi-4.0*arctan
      aux=log((0.5+r1)/r2)
      fi=-2.0*pi*zdis-4.0*L*aux+zdis*EW
      vws=nw*(qpi*qw*elec*elec*fi)/(4.0*pi*eps*epso*L*L)

      vinti=vp+vps+vn+vns+vw+vws

 500  RETURN

      END SUBROUTINE energyp

! ------------------------------------------------------------------------

      SUBROUTINE energyneg(lxi,lyi,lzi,ind,vinti,ovr)

      USE mixdat

      IMPLICIT NONE

      integer,intent(in)::ind
      real,intent(in)::lxi,lyi,lzi
      real(kind=8),intent(out)::vinti
      real,intent(out)::ovr

      integer::j,k
      real::xi,yi,zi
      real(kind=8)::vp,vps,vn,vns,vw,vws
      real::r1aux,r1,r2aux,r2,aux,fi,EW,arctan,pos
      real::rxi,ryi,rzi,zdis,dri,dri2
      real::rminppsq,rminnnsq,rminpnsq,rminpwsq,rminnwsq
```

```
! Initialization of accumulators

      vinti=0.0
      vp=0.0
      vps=0.0
      vn=0.0
      vns=0.0
      vw=0.0
      vws=0.0
      ovr=0.0
      vm=0.0
      xi=lxi
      yi=lyi
      zi=lzi
      rminnnsq=dn*dn
      rminnwsq=(dn/2.0+dw/2.0)*(dn/2.0+dw/2.0)

! Interaction with positive ions

      do k=1,np
        rxi=xi-xp(k)
        ryi=yi-yp(k)
        rzi=zi-zp(k)
        rxi=rxi-L*anint(rxi/L)
        ryi=ryi-L*anint(ryi/L)
        rminpnsq=(dp(k)/2.0+dn/2.0)*(dp(k)/2.0+dn/2.0)
        dri2=rxi*rxi+ryi*ryi+rzi*rzi
        if(dri2>=rminpnsq) then
          dri=sqrt(dri2)
          vp=vp+(qn*qp(k)*elec*elec)/(4.0*pi*eps*epso*dri)
        else
          ovr=1.0
          goto 600
        end if
      end do

! Interaction with positively charged sheets

      do k=1,np
        zdis=abs(zi-zp(k))
        r1aux=0.5+(zdis/L)*(zdis/L)
        r1=sqrt(r1aux)
        r2aux=0.25+(zdis/L)*(zdis/L)
        r2=sqrt(r2aux)
        pos=(4.0*zdis*r1)/L
        arctan=atan(pos)
        EW=2.0*pi-4.0*arctan
        aux=log((0.5+r1)/r2)
        fi=-2.0*pi*zdis-4.0*L*aux+zdis*EW
        vps=vps+(qn*qp(k)*elec*elec*fi)/(4.0*pi*eps*epso*L*L)
      end do

! Interaction with negative ions

      do k=1,nn
        if(k/=ind) then
          rxi=xi-xn(k)
          ryi=yi-yn(k)
          rzi=zi-zn(k)
          rxi=rxi-L*anint(rxi/L)
          ryi=ryi-L*anint(ryi/L)
          dri2=rxi*rxi+ryi*ryi+rzi*rzi
          if(dri2>=rminnnsq) then
            dri=sqrt(dri2)
            vn=vn+(qn*qn*elec*elec)/(4.0*pi*eps*epso*dri)
          else
            ovr=1.0
            goto 600
          end if
        end if
```

```
      end do

! Interaction with negatively charged sheets

      do k=1,nn
        zdis=abs(zi-zn(k))
        r1aux=0.5+(zdis/L)*(zdis/L)
        r1=sqrt(r1aux)
        r2aux=0.25+(zdis/L)*(zdis/L)
        r2=sqrt(r2aux)
        pos=(4.0*zdis*r1)/L
        arctan=atan(pos)
        EW=2.0*pi-4.0*arctan
        aux=log((0.5+r1)/r2)
        fi=-2.0*pi*zdis-4.0*L*aux+zdis*EW
        vns=vns+(qn*qn*elec*elec*fi)/(4.0*pi*eps*epso*L*L)
      end do

! Interaction with the walls

      if(zi<(dn/2.0)) then
        ovr=1.0
        goto 600
      else
        if(zi>(W-dn/2.0)) then
          ovr=1.0
          goto 600
        else
          do k=1,nw
            rxi=xi-xw(k)
            ryi=yi-yw(k)
            rzi=zi-zw(k)
            rxi=rxi-L*anint(rxi/L)
            ryi=ryi-L*anint(ryi/L)
            dri2=rxi*rxi+ryi*ryi+rzi*rzi
            if(dri2>=rminnwsq) then
              dri=sqrt(dri2)
              vw=vw+(qn*qw*elec*elec)/(4.0*pi*eps*epso*dri)
            else
              ovr=1.0
              goto 600
            end if
          end do
        end if
      end if

! Interaction with wall charged sheets


      zdis=abs(zi)
      r1aux=0.5+(zdis/L)*(zdis/L)
      r1=sqrt(r1aux)
      r2aux=0.25+(zdis/L)*(zdis/L)
      r2=sqrt(r2aux)
      pos=(4.0*zdis*r1)/L
      arctan=atan(pos)
      EW=2.0*pi-4.0*arctan
      aux=log((0.5+r1)/r2)
      fi=-2.0*pi*zdis-4.0*L*aux+zdis*EW
      vws=nw*(qn*qw*elec*elec*fi)/(4.0*pi*eps*epso*L*L)

       vinti=vp+vps+vn+vns+vw+vws

 600  RETURN

      END SUBROUTINE energyneg

! ------------------------------------------------------------------------

      SUBROUTINE writfinal(consist,vtot,vend,avv)
```

```
      USE mixdat

      IMPLICIT NONE

      real(kind=8),intent(in)::consist,vtot,vend,avv

      integer::j

! Opening the file

      open(unit=8,file=fout2,status='unknown',form='formatted')

! Saving the data

      write(unit=8,fmt=700)consist,vtot,vend,avv

      do j=1,npaux1
        write(unit=8,fmt=710)xp(j),yp(j),zp(j)
      end do

      write(unit=8,fmt=720)avv

      do j=npaux1+1,npaux2
         write(unit=8,fmt=710)xp(j),yp(j),zp(j)
      end do

      write(unit=8,fmt=720)avv

      do j=npaux1+2,np
        write(unit=8,fmt=710)xp(j),yp(j),zp(j)
      end do

      write(unit=8,fmt=720)avv

      do j=1,nn
        write(unit=8,fmt=710)xn(j),yn(j),zn(j)
      end do

      write(unit=8,fmt=720)avv

      do j=1,nw
        write(unit=8,fmt=710)xw(j),yw(j),zw(j)
      end do

      write(unit=8,fmt=720)avv

      do j=1,nhist
          write(unit=8,fmt=730)zcoord(j),cpav1(j),cpav2(j),cpav3(j),cnav(j)
      end do

 700  format(1x,E14.6,3x,E14.6,3x,E14.6,3x,E14.6)
 710  format(1x,E14.6,3x,E14.6,3x,E14.6)
 720  format(1x,E14.6)
 730  format(1x,E14.6,3x,E14.6,3x,E14.6,3x,E14.6,3x,E14.6)

      end file(unit=8)
      close(unit=8)

      RETURN

      END SUBROUTINE writfinal

! ----------------------------------------------------------------------

      SUBROUTINE histogram(printnum)

      USE mixdat

      IMPLICIT NONE
```

```
      integer,intent(in)::printnum

      integer::j,k

      real::aux
      real::indexp(np),indexn(nn)
      real(kind=8)::concp1(nhist),concp2(nhist),concp3(nhist)
      real(kind=8)::concn(nhist)

! Opening a file

      open(unit=7,file=fout3,status='unknown',form='formatted')

! Initializing variables

      Do j=1,nhist
         concp1(j)=0.0
         concp2(j)=0.0
         concp3(j)=0.0
         concn(j)=0.0
      end do

      Do j=1,np
         indexp(j)=0.0
      End do

      Do j=1,nn
         indexn(j)=0.0
      End do

      Do k=1,nhist              !Z coordinate

         Do j=1,npaux1              ! First kind of counterions
            If(indexp(j)==0.0) then
               aux=aint(zp(j)/deltaz)
               if(aux<=k) then
                  indexp(j)=real(k)
                  concp1(k)=concp1(k)+1.0
               end if
            end if
         end do

         Do j=1,npaux1              ! First kind of counterions
            If(indexp(j)==0.0) then
               aux=aint(zp(j)/deltaz)
               if(aux<=k) then
                  indexp(j)=real(k)
                  concp1(k)=concp1(k)+1.0
               end if
            end if
         end do

         Do j=npaux1+1,npaux2             ! Second kind of counterions
            If(indexp(j)==0.0) then
               aux=aint(zp(j)/deltaz)
               if(aux<=k) then
                  indexp(j)=real(k)
                  concp2(k)=concp2(k)+1.0
               end if
            end if
         end do

         Do j=npaux2+1,np              ! Third kind of counterions
            If(indexp(j)==0.0) then
               aux=aint(zp(j)/deltaz)
               if(aux<=k) then
                  indexp(j)=real(k)
                  concp3(k)=concp3(k)+1.0
               end if
```

```
            end if
        end do

        Do j=1,nn               ! Coions
            If(indexn(j)==0.0) then
              aux=aint(zp(j)/deltaz)
               if(aux<=k) then
                 indexn(j)=real(k)
                 concn(k)=concn(k)+1.0
               end if
            end if
        end do

    end do

! Accumulating average concentrations

    Do k=1,nhist
        cpav1(k)=cpav1(k)+concp1(k)
        cpav2(k)=cpav2(k)+concp2(k)
        cpav3(k)=cpav3(k)+concp3(k)
        cnav(k)=cnav(k)+concn(k)
    End do

! Saving the data

    If(mod(printnum,1000==0) then
      write(unit=7,fmt=800)printnum

      Do k=1,nhist
         write(unit=7,fmt=810)zcoord(k),concp1(k), concp2(k), concp3(k), concn(k)
      End do
    End if

800 format(1x,I8)
810 format(1x,E14.6,3x, E14.6,3x, E14.6,3x, E14.6,3x, E14.6)

     if(printnum==nstep) then
       end file (unit=7)
       close(unit=7)
     end if

     RETURN

     END SUBROUTINE histogram
```

REFERENCES

Allen, M.P.; Tildesley, D.J. *Computer Simulation of Liquids*, Oxford: Clarendon Press; 1990.

Angelescu, D.G.; Linse, P.. Monte Carlo simulation of the mean force between two like-charged macroions with simple 1:3 salt added, *Langmuir* **2003,** 19:9661–9668.

Behrens, S.H.; Christl, D.I.; Emmerzael, R.; Schurtenberger, P.; Borkovec, M. Charging and aggregation properties of carboxyl latex particles: experiments vs DLVO theory, *Langmuir* **2000**, 16:2566–2575.

Belloni, L. Colloidal interactions, *Journal of Physics: Condensed Matter* **2000**, 12:R549–R587.

Bester, M.; Vlachy, V. Monte Carlo study of mixed electrolytes, *J. Chem. Phys.* **1992,** 96:7656–7661.

Binnig, G.M.; Quate, C.F.; Gerber, Ch. Atomic force microscope, *Phys. Rev. Lett.* **1986**, 56:930–933.

Blum, L. Theory of electrified interfaces, *J. Phys. Chem.* **1977**, 81:136–167.

Boda, D.; Chan, K.-Y.; Henderson, D. Monte Carlo simulation of an ion-dipole mixture as a model of an electrical double layer, *J. Chem. Phys.* **1998,** 109:7362–7371.

Boda, D.; Henderson, D.; Plaschko, P.; Fawcett, R. Monte Carlo and Density Functional Theory study of the electrical double layer: the dependence of the charge/voltage relation on the diameter of the ions, *Molecular Simulation* **2004,** 30:137–141.

Bohinc, K.; Kralj-Iglič, V.; Iglič, A. Thickness of electrical double layer. Effect of ion size, *Electrochimica Acta* **2001,** 46:3030–3040.

Boyle, E.J.; Scriven, L.E.; Davis, H.T. The generalized van der Waals theory applied to the electrical double layer, *J. Chem. Phys.* **1987**, 86:2309–2318.

Butt, H.-J. Electrostatic interaction in atomic force microscopy, *Biophys. J.* **1991**, 60:777–785.

Butt, H.-J. Measuring local surface charge densities in electrolyte solutions with a scanning force microscope, *Biophys. J.* **1992**, 63:578–582.

Camesano, T.A.; Logan, B.E. Probing bacterial electrostatic interactions using atomic force microscopy, *Environ. Sci. Technol.* **2000**, 34:3354–3362.

Carrera, J.; Manzanares, J.A.; Mafé, S. Ion size effects on the streaming potential of narrow charged pores, *PCCP* **2001,** 3:2493–2496.

Chan, D.Y.C. A simple algorithm for calculating electrical double layer interactions in asymmetric electrolytes – Poisson-Boltzmann theory, *J. Colloid Interface Sci.* **2002**, 245:307–310.

Chin, C.-J.; Yiacoumi, S.; Tsouris, C. Probing DLVO forces using interparticle magnetic forces: transition from secondary-minimum to primary-minimum aggregation, *Langmuir* **2001**, 17:6065–6071.

Chin, C.-J.; Yiacoumi, S.; Tsouris, C. Agglomeration of magnetic particles and breakup of magnetic chains in surfactant solutions, *Colloids Surf. A* **2002a**, 204:63–72.

Chin, C.-J.; Yiacoumi, S.; Tsouris, C., Influence of metal ion sorption on colloidal surface forces measured by atomic force microscopy, *Environ. Sci. Technol.* **2002b**, 36:343–348.

Chu, X.; Wasan, D.T. Attractive interaction between similarly charged colloidal particles, *J. Colloid Interface Sci.* **1996**, 184:268–278.

Cleveland, J.P.; Manne, S.; Bocek, D.; Hansma, P.K., A non destructive method for determining spring constant of cantilevers for scanning force microscopy, *Rev. Sci. Instrum.* **1993**, 64:403–405.

Craven, C. *The effects of electrolyte solution composition on silica surface charge development*, Atlanta: Thesis - Georgia Institute of Technology; 2000.

Crocker, J.C.; Grier, D.G., When like charges attract: the effects of geometrical confinement on long-range colloidal interactions, *Phys. Rev. Lett.* **1996**, 77:1897–1900.

D'Amico, I.; Löwen, H. Effective forces between macroions: a Monte Carlo study, *Physica A* **1997**, 237:25–30.

Delville, A. Monte Carlo simulations of the mechanical properties of charged colloids, *Langmuir* **1994**, 10:395–402.

Delville, A.; Pellenq, R.J-M.; Caillol, J.M. A Monte Carlo (N,V,T) study of the stability of charged interfaces: a simulation on a hypersphere, *J. Chem. Phys.* **1997**, 106:7275–7285.

Delville, A. (N,V,T) Monte Carlo simulations of the electrostatic interaction between charged colloids: finite size effects, *J. Phys. Chem.* **1999**, 103:8296–8300.

Derjaguin, B.V.; Landau, L.D. Theory of the stability of strongly charged lyophobic sols and of the adhesion of strongly charged particles in solutions of electrolytes, *Acta Physico URSS* **1941**, 14:733–762.

Elimelech, M.; O'Melia, C.R. Kinetics of deposition of colloidal particles in porous media, *Environ. Sci. Technol.* **1990**, 24:1528–1536.

Elimelech, M.; Gregory, J.; Jia, X.; Williams, R.A. *Particle Deposition & Aggregation: Measurement, Modelling and Simulation*, Oxford: Butterworth-Heinemann Ltd.; **1995**.

Estel, K.; Kramer, G.; Schmitt, F.J., Changes in the interaction characteristics of polyelectrolyte complex covered silica surfaces, *Colloids Surf. A* **2000**, 161:193–202.

Feick, J.D.; Chukwumah, N.; Noel, A.E.; Velegol, D. Altering surface charge non-uniformity on individual colloidal particles, *Langmuir* **2004**, 20:3090–3095.

Feng, J.; Ruckenstein, E. Attractive interactions in dispersions of identical charged colloidal particles: a Monte Carlo simulation, *J. Colloid Interface Sci.* **2004**, 272:430–437.

Forsman, J. A simple correlation-corrected Poisson-Boltzmann theory, *J. Phys. Chem. B* **2004**, 108:9236–9245.

Gavoille, J.; Takadoum, J. Study of surface forces dependence on pH by atomic force microscopy, *J. Colloid Interface Sci.* **2002**, 250:104–107.

Grant, M.L.; Saville, D.A. Electrostatic interaction sbetween a nonuniformly charged sphere and a charged surface, *J. Colloid Interface Sci.* **1995**, 171:35–45.

Greiner, W.; Neise, L.; Stöcker, H. *Thermodynamics and Statistical Mechanics*, New York: Springer; **2000.**

Grolimund, D.; Elimelech, M.; Borkovec, M. Aggregation and deposition kinetics of mobile colloidal particles in natural porous media, *Colloids Surf. A* **2001**, 191:179–188.

Grønbech-Jensen, N.; Beardmore, K.M.; Pincus, P. Interactions between charged spheres in divalent counterion solution, *Physica A* **1998**, 261:74–81.

Grotendorst, J.; Marx, D.; Muramatsu, A. *Quantum Simulation of Complex Many Body Systems: From Theory to Algorithms*, Jülich: John von Neumann Institute of Computing Press, **2002**.

Guldbrand, L.; Jönsson, B.; Wennerström, H.; Linse, P. Electrical double layer forces. A Monte Carlo study, *J. Chem. Phys.* **1984**, 80:2221–2228.

Guzmán, O.; de Pablo, J.J. An effective-colloid pair potential for Lennard-Jones colloid polymer mixtures, *J. Chem. Phys.* **2003**, 118:2392–2397.

Hahn, M.W.; O'Melia, C.R. Deposition and reentrainment of Brownian particles in porous media under unfavorable chemical conditions: some concepts and applications, *Environ. Sci. Technol.* **2004**, 38:210–220.

Hansen, J.P.; McDonald, I.R. *Theory of Simple Liquids*, New York, Academic Press, **1986**.

Hartley, P.; Matsumoto, M.; Mulvaney, P. Determination of the surface potential of two-dimensional crystals of bacteriorhodopsin by AFM, *Langmuir* **1998,** 14:5203–5209.

Haughey, D.; Earnshaw, J.C. The electrostatic interaction between a small colloidal particle and a charged interface, *Colloids and Surfaces A* **1996**, 106:237–242.

Heinz, W.F.; Hoh, J.H. Relative surface charge density mapping with the atomic force microscope, *Biophys. J.* **1999**, 76:528–538.

Hiemenz, P.C.; Rajagopalan, R. *Principles of Colloid Science and Surface Chemistry*, New York: Marcel Dekker; **1997**.

Hillier, A.C.; Kim, S.; Bard, A.J. Measurement of double-layer forces at the electrode/electrolyte interface using the atomic force miscroscope: potential and anion dependent interactions, *J. Phys. Chem.* **1996**, 100:18808–18817.

Hribar, B.; Vlachy, V.; Bhuiyan, L.B.; Outhwaite, C.W. Ion distribution in a cylindrical capillary as seen by the modified Poisson-Boltzmann theory and the Monte Carlo simulations, *J. Phys. Chem. B* **2000,** 104:11522–11527.

Hu, Y.; Dai, J. Hydrophobic aggregation of alumina in surfactant solutions, *Miner. Eng.* **2003**, 16:1167–1172.

Huang, R.; Hebert, K. The electrical double layer in a nanopore in a barrier surface film, *Journal of Electroanalytical Chemistry* **2004,** 565:103–114.

Hunter, R.J. *Foundations of Colloid Science*, 2nd Edition, Oxford: University Press; **2001**.

Hüttl, G.; Beyer, D.; Müller, E. Investigation of electrical double layers on SiO_2 surfaces by means of force vs. distance measurements, *Surface and Interface Analysis* **1997**, 25:543–547.

Ishino, T.; Hieda, H.; Tanaka, K.; Gemma, N. Imaging charged functional groups with the atomic force microscope operated in aqueous solutions, *J. Electroanal. Chem.* **1997**, 438:225–230.

Israelachvili, J. *Intermolecular and Surface Forces*, San Diego: Academic Press; 1998.

Jamnik, B.; Vlachy, V. Monte Carlo and Poisson-Boltzmann study of electrolyte exclusion from charged cylindrical micropores, *J. Am. Chem. Soc.* **1993,** 115:660–666.

Johnson, A.S.; Nehl, C.L.; Mason, M.G.; Hafner, J.H. Fluid electric force microscopy for charge density mapping in biological systems, *Langmuir* **2003**, 19:10007–10010.

Jönnson, B.; Ståhlberg, J. The electrostatic interaction between a charged sphere and an oppositely charged planar surface and its application to protein adsorption, *Colloids and Surfaces B* **1999**, 14:67–75.

Jönsson, B.; Wennerström, H.; Halle, B. Ion distributions in lamellar liquid crystals. A comparison between Monte Carlo simulations and solutions of the Poisson-Boltzmann equation, *J. Phys. Chem.* **1980**, 84**:**2179–2185.

Kallay, N.; Žalac, S. Charged surfaces and interfacial ions, *J. Colloid Interface Sci.* **2000,** 230:1–11.

Kallay, N.; Žalac, S. Stability of nanodispersions: a model for kinetics of aggregation of nanoparticles**,** *J. Colloid Interface Sci.* **2002**, 253:70–76**.**

Keslarek, A.J.; Rodrigues Costa, C.A.; Galembeck, F. Latex film morphology and electrical potential pattern dependence on serum components: a scanning probe microscopy study, *J. Colloid Interface Sci.* **2002,** 255:107–114.

Kjellander, R.; Åkesson, T.; Jönsson, B.; Marčelja, S. Double layer interactions in mono- and divalent electrolytes: a comparison of the anisotropic hypernetted chain theory and Monte Carlo simulations, *J. Chem. Phys.* **1992**, 97:1424–1431.

Kramer, G.; Estel, K.; Schmitt, F.-J.; Jacobasch, H.-J. Laterally resolved measurement of interaction forces between surfaces that are partly covered with electrolytes, *J. Colloid Interface Sci.* **1998**, 208:302–309.

Kretzschmar, R.; Borkovec, M.; Grolimund, D.; Elimelech, M., Mobile subsurface colloids and their role in contaminant transport, *Adv. Agronomy* **1999**, 66:121–193.

Lai, S.K.; Wu, K.L. Liquid-liquid and liquid-solid phase separation and flocculation of a charged colloidal dispersion, *Phys Rev E* **2002**, 66:041403.

Larson, I.; Pugh, R. Qualitative adsorption measurements with an atomic force microscope, *Langmuir* **1998**, 14:5676–5679.

Linse, P.; Lobaskin, V. Electrostatic attraction and phase separation in solutions of like-charged colloidal particles, *J Chem Phys* **2000**, 112:3917–3927.

Lobaskin, V.; Linse, P. Accurate simulation of highly asymmetric electrolytes with charge asymmetry 20:1 and 20:2, *J. Chem. Phys.* **1998**, 109:3530–3541.

Lobaskin, V.; Linse, P. Simulation of an asymmetric electrolyte with charge asymmetry 60:1 using hard-sphere and soft-sphere models, *J. Chem. Phys.* **1999,** 111:4300–4309.

Lobaskin, V. Quamhieh, K. Effective macroion charge and stability of highly asymmetric electrolytes at various salt concentrations, *J. Phys. Chem. B* **2003,** 107:8022–8029.

Martín-Molina, A.; Quesada-Pérez, M.; Galisteo-González, F.; Hidalgo-Álvarez, R. Electrophoretic mobility and primitive models: surface charge density effect, *J. Phys. Chem. B* **2002,** 106:6881–6886.

Messina, R. Spherical colloids: effect of discrete macroion charge distribution and counterion valence, *Physica A* **2002,** 308:59–79.

Meyer, S.; Levitz, P.; Delville, A. A (N,V,T) Monte Carlo study of the long-range electrostatic coupling between a large collection of charged colloidal platelets, *J. Phys. Chem. B* **2001**, 105:9595–9602.

Miklavic, S.J.; Chan, D.Y.C.; White, L.R.; Healy, T.W. Double layer forces between heterogeneous charged surfaces, *J. Phys. Chem.* **1994**, 98:9022–9032.

Murthy, C.S.; Bacqet, R.J.; Rossky, P.J. Ionic distributions near polyelectrolytes. A comparison of theoretical approaches, *J. Phys. Chem.* **1985,** 89:701–710.

Nguyen, A.V.; Evans, G.M.; Jameson, G.J. Simple approximate expressions for electrical double-layer interaction at constant moderate potentials, *J. Colloid Interface Sci.* **2000,** 230:205–209.

Oettel, M. Depletion force between two large spheres suspended in a bath of small spheres: onset of the Derjaguin limit, *Phys. Rev.* **2004**, 69:041404.

Ohshima, H. Electrostatic interaction between two spherical colloidal particles, *Adv. Colloid Interface Sci.* **1994**, 53:77–102.

Ohshima, H. Electrostatic interaction between a sphere and a planar surface: generalization of point-charge/surface image interaction to particle/surface image interaction, *J. Colloid Interface Sci.* **1998**, 198:42–52.

Pang, T. *An Introduction to Computational Physics*, Cambridge: University Press, 1997.

Patey, G.N. The interaction of two spherical colloidal particles in electrolyte solution – an application of the Hypernetted-chain approximation, *J. Chem. Phys.* **1980**, 72:5763–5771.

Rotsch, C.; Radmacher, M. Mapping electrostatic forces with the atomic force microscope, *Langmuir* **1997**, 13:2825–2832.

Runkana, V.; Somasundaran, P.; Kapur, P. Reaction-limited aggregation in presence of short-range structural forces, *AICHE J* **2005**, 51:1233–1245.

Ryan, J.N.; Elimelech, M. Colloid mobilization and transport in groundwater, *Colloids Surf. A* **1996**, 107, 1–56.

Shellenberger, K.; Logan, B.E. Effect of molecular scale roughness of glass beads on colloidal and bacterial deposition, *Environ. Sci. Technol.* **2002**, 36:184–189.

Snoswell, D.R.E.; Duan, J.; Fornasiero, D.; Ralston, J. Colloid stability of synthetic titania and the influence of surface roughness, *J. Colloid Interface Sci.* **2005**, 286:526–535.

Stankovich, J.; Carnie, S.L. Electrical double layer interaction between dissimilar spherical colloidal particles and between a sphere and a plate: non-linear Poisson-Bolztmann theory, *Langmuir* **1996**, 12:1453–1461.

Stevens, M.J.; Falk, M.L.; Robbins, M.O., Interactions between charged spherical macroions, *J. Chem. Phys.* **1996**, 104:5209–5219.

Striolo, A.; Bratko, D.; Wu, J.Z.; Elvassore, N.; Blanch, H.W.; Prausnitz, J.M. Forces between aqueous nonuniformly charged colloids from molecular simulation, *J. Chem. Phys.* **2002**, 116:7733–7743.

Suresh, L.; Walz, J.Y. Effect of surface roughness on the interaction energy between a colloidal sphere and a flat plate, *J. Colloid Interface Sci.* **1996**, 183:199–213.

Taboada-Serrano, P., Vithayaveroj, V., Yiacoumi, S., and Tsouris, C. Surface charge heterogeneities measured by atomic force microscopy, *Environ. Sci. Technol.* **2005a,** 39:6352–6360.

Taboada-Serrano, P.; Yiacoumi, S.; Tsouris, C. Behavior of symmetric and asymmetric electrolytes near discretely charged planar surfaces: a Monte Carlo study, *J. Chem. Phys.* **2005b**, 123:054703.

Taboada-Serrano, P.; Chin, C.-J.; Yiacoumi, S.; Tsouris, C. Modeling aggregation of colloidal particles, *COCIS* **2005c** (in press).

Tavares, F.W.; Bratko, D.; Prausnitz, J.M. The role of salt-macroion Van der Waals interactions in the colloid-colloid potential of mean force, *COCIS* **2004**, 9:81–86.

Teran Arce, F.; Avci, R.; Beech, I.; Cooksey, K.; Wigglesworth-Cooksey, B., Microelastic properties of minimally adhesive surfaces: a comparative study of RTV 11 and intersleek elastomers, *J. Chem. Phys.* **2003**, 119:1671–1682.

Terao, T.; Nakayama, T., Interparticle force between like-charged colloidal systems: a numerical study, *Colloids & Surf. A* **2001**, 182:299–304.

Torrie, G.M.; Valleau, J.P. Electrical double layers. I. Monte Carlo study of a uniformly charged surface, *J. Chem. Phys.* **1980,** 73:5807–5816.

Torrie, G.M.; Valleau, J.P. Electrical double layers. 4. Limitations of the Gouy-Chapman theory, *J. Phys. Chem.* **1982,** 86:3251–3257.

Torrie, G.M.; Valleau, J.P.; Patey, G.N. Electrical double layers. II. Monte Carlo and HNC studies of image effects, *J. Chem. Phys.* **1982,** 76:4615–4622.

Torrie, G.M.; Kusalik, P.G.; Patey, G.N. Theory of the electrical double layer: ion size effects in a molecular solvent, *J. Chem. Phys.* **1989,** 91:6367–6375.

Tsouris, C.; Yiacoumi, S.; Scott, T.C. Kinetics of heterogeneous magnetic flocculation using a bivariate population-balance equation, *Chem Eng Commun* **1995**, 137:147–159.

Usui, S. Interaction of electrical double layers at constant surface charge, *J. Colloid Interface Sci.* **1973**, 44:107–113.

Valiskó, M.; Henderson, D.; Boda, D. Competition between the effects of asymmetries in ion diameters and charges in an electrical double layer studiend by Monte Carlo simulations and theories, *J. Phys. Chem. B* **2004,** 108:16548–16555.

Valleau, J.P.; Cohen, K.L. Primitive model electrolytes. I. Grand canonical Monte Carlo computations, *J. Chem. Phys.* **1980,**72:5935–5941.

Valleau, J.P.; Cohen, K.L.; Card, D.N. Primitive model electrolytes. II. The symmetrical electrolyte, *J. Chem. Phys.* **1980,** 72:5942–5954.

Valleau, J.P.; Torrie, G.M. The EDL III. Modified Gouy-Chapman theory with unequal ion sizes, *J. Chem. Phys.* **1982**, 76:4623–4630.

Valleau, J.P.; Ivkov, R.; Torrie, G.M. Colloid stability: the forces between charged surfaces in an electrolyte, *J. Chem. Phys.* **1991,** 95:520–532

Van Megen, W.; Snook, I. The grand canonical Monte Carlo method applied to the electrical double layer, *J. Chem. Phys.* **1980,** 73:4656–4662.

VEECO *Command Reference Manual AFM*, Santa Barbara: Digital Instruments; **2002**.

Veeramasuneni, S.; Yalamanchili, M.R.; Miller, J.D. Measurement of interaction forces between silica and α-alumina by atomic force microscopy, *J. Colloid Interface Sci.* **1996**, 184:594–600.

Verwey, E.J.W.; Overbeek, J.Th.G. *Theory of the Stability of Lyophobic Colloids*, Amsterdam: Elsevier; **1948**.

Vithayaveroj, V.; Yiacoumi, S.; Tsouris, C., Modification of surface forces by metal ion adsorption, *J. Disp. Sci. Technol.* **2003**, 24:517–525.

Vlachy, V.; Marshall, C.H.; Haymet, A.D.J. Highly asymmetric electrolytes – a comparison of Monte Carlo simulations and the HNC – integral equation, *J. Am. Chem. Soc.* 1989, 111:4160–4166.

Vlachy, V.; Haymet, A.D.J. Adsorption of the screened Coulomb liquid between hard walls, *Chem. Phys. Lett.* **1988**, 146:32–36.

Waite, T.D.; Cleaver, J.K.; Beattie, J.K. Aggregation kinetics and fractal structure of γ-alumina assemblages, *J Colloid Interface Sci* **2001**, 241:333–339.

Wiese, G.R.; Healy, T.W. Effect of particle size on colloid stability, *Trans. Faraday Soc.* **1970**, 66:490–500.

Wu, J.Z.; Bratko, D.; Blanch, H.W.; Prausnitz, J.M., Monte Carlo simulation for the potential of mean force between ionic colloids in solutions of asymmetric salts, *J. Chem. Phys.* **1999**, 111:7084–7094.

Ying, T.Y.; Yang, K.-L.; Yiacoumi, S.; Tsouris, C. Electrosorption of ions from aqueous solutions, *J. Interface Colloid Sci.* **2002**, 250:18–27.

Yang, K.-L.; Yiacoumi, S.; Tsouris, C. (N,V,T) MC simulations of the fluctuating-charge molecular water between charged surfaces, *J. Chem. Phys.* **2002a,** 117:337–345.

Yang, K.-L.; Yiacoumi, S.; Tsouris, C. Monte Carlo simulations of electrical double layer formation in nanopores, *J. Chem. Phys.* **2002b,** 117:8499–8507.

Zauscher, S.; Klingenberg, D.J. Normal forces between cellulose surfaces measured by colloidal probe microscopy, *J. Colloid Interface Sci.* **2000**, 229:497–510.

VITA

The author, Patricia Larisse Taboada-Serrano, was born in Sao Paulo, Brasil. She grew up in Bolivia, where she obtained her Bachelors Degree in Chemical Engineering from the University Mayor de San Andrés, in 1996. She worked at the "Centro de Investigación en Ciencias Aplicadas – CICA" (Applied Sciences Research Center) during three years before moving to Caracas, Venezuela. She obtained her Masters Degree in Chemical Engineering from the University Simón Bolívar in Caracas, Venezuela, in June 2001. In July 2001, she moved to Atlanta, Georgia, in order to pursue a PhD degree in Environmental Engineering at the Georgia Institute of Technology. She completed her PhD degree in December, 2005. While working on her PhD degree, the author married Dr. Ketan M. Patel, in an exercise of carefully "juggling" PhD work and personal life. The author belongs to different professional and non-profit organizations, for example the Bolivian Engineering Society and the American Institute of Chemical Engineers. Her interests are in physical chemistry, thermodynamics, colloids and surface science, and processes at the nanoscale.